UNIVERSITÀ
DEGLI STUDI
FIRENZE

PhD in Biomedical Sciences
CYCLE XXXVIII

Intercellular Interactions in Paraganglioma Microenvironment: Drivers of Tumour Growth and Progression

COORDINATOR
Prof. Fabrizio Chiti

Academic Discipline (SSD) MED/05

Tutor:
Prof. Mario Maggi

Co-Tutor:
Prof. Elena Rapizzi

Candidate:
Dr. Francesca Amore

Academic year 2024/2025

Index

1. Introduction

1.1 Definition of Paraganglioma

Paragangliomas (PGLs) are rare tumours that arise from the neural crest-derived cells in the adrenal medulla or in the parasympathetic or sympathetic paraganglia located in the head, neck, thorax, abdomen, and pelvis.

The fourth edition of the World Health Organization (WHO) classification of Endocrine Tumours published in 2017 contains substantial modification in the topics of adrenal tumours when compared with the third edition that was published in 2004. In particular, the initial motion replaced the term ‘malignant’ with the term ‘metastatic’ [1]. The terms “malignant pheochromocytoma” and “benign pheochromocytoma” were combined into a single section "Pheochromocytoma” in the new 2017 WHO classification. This is because there are no histological features able to predict metastatic behaviour. Thus, all pheochromocytomas are considered malignant tumours with variable metastatic potential. Historically [1], tumours belonging to this category were divided into pheochromocytomas (PHEO) and paragangliomas (PGLs), respectively based on their intra- or extra-adrenal location. PGLs were further subdivided, based on their location, into thoraco-abdominal PGLs and head and neck PGLs (HNPGLs). This distinction was overcome with the publication of the new 2022 WHO classification [2], which emphasizes the histological homogeneity of the lesions by grouping them all under the term of Paraganglioma, specifying however their location and secretory capacity: while thoracic and abdominal and intra-adrenal PGLs are tumours of sympathetic origin capable of secreting catecholamines, HNPGLs are usually non-secretory tumours.

1.2 Epidemiology

PGLs are rare tumours. Their prevalence varies, from 0.2% to 0.6% in hypertensive patients to less than 0.05% in the general population [3]. The incidence of PGLs is about 0.6 cases per 100.000 person-years [4]. These tumours may occur at all ages, with a peak incidence between 40 and 50 years [4]. PGLs present sporadically, or in the context of a hereditary syndrome. Significant advancements in genetic research since the 1990s have revealed that approximately 40% of these patients carry a germline mutation in one of the more than 20 susceptibility genes so far reported, establishing PGLs as having the highest degree of heritability among all human neoplasms [5]. Furthermore, more than 30% of these tumours are associated with a

somatic mutation [6]. Increasing numbers of individuals and family members in whom germline mutations for one of the PGLs susceptibility genes are now also being routinely screened for PGLs, thereby also influencing the reported incidence of genetic mutations [7]. As regards the prevalence in the sexes, no differences were highlighted in the past. However, the latest epidemiological studies seem to show a higher incidence [8] and prevalence [9] in the female sex. From the point of view of localization, 75-85% of these lesions are located within the adrenal gland, while the remaining part originates from the paravertebral ganglion structures (thorax and abdomen) or the vagus nerve (head and neck area)[10].

1.3 Biochemistry

Catecholamines are synthesized inside the adrenal medulla (Figure 1). The biosynthesis of catecholamines starts with uptake of the amino acid tyrosine by the chromaffin cell. Tyrosine is obtained from dietary sources (such as cheese, chicken, and nuts) and from the amino acid phenylalanine through the activity of phenylalanine hydroxylase. The subsequent steps in the biosynthesis of catecholamines involve the activity of the following enzymes: tyrosine hydroxylase (TH), aromatic L-amino acid decarboxylase (AADC), dopamine ß-hydroxylase (DBH), and PNMT. All these enzymes are located in the cytoplasm of the chromaffin cell, except for DBH, which is located in the cell vesicles. Tyrosine is converted to L-3,4-dihydroxyphenylalanine (L-DOPA) by TH, which is the rate limiting step in this biosynthesis. Subsequently, AADC converts L-DOPA to dopamine. Dopamine is then transported into granulated vesicles to be hydroxylated to norepinephrine by DBH. PNMT converts cytosolic leaked norepinephrine to epinephrine. The transcription of PNMT is stimulated by high cortisol concentrations, explaining why the production of epinephrine is mainly produced by the adrenomedullary chromaffin cells (>95%) and functions as a hormone released directly into the bloodstream. In contrast, circulating norepinephrine is mainly derived from overflow of the neurotransmitter from sympathetic nerve endings with adrenomedullary chromaffin cell production providing usually a less than 10% contribution[11]. Catecholamines are metabolized by the enzyme Catechol-O-Methyl-Transferase (COMT) into metanephrine (MN), normetanephrine (NMN), and 3-methoxytyramine (3-MT). Vanillylmandelic acid (VMA) is the metabolic end-product of epinephrine and norepinephrine, while homovanillic acid (HVA) is the metabolic end-product of dopamine.

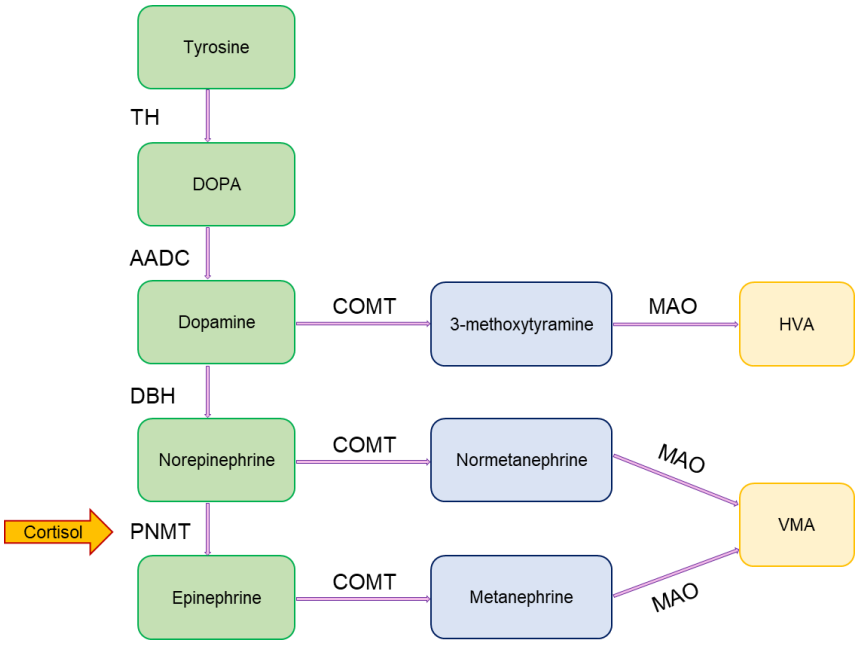

Figure 1. Pathway of synthesis and metabolism of catecholamines. Tyrosine is converted to 3,4-di-hydroxyphenylalanine (dopa) by tyrosine hydroxylase (TH); Aromatic L-amino acid decarboxylase (AADC) converts dopa to dopamine. Dopamine is actively transported into granulated vesicles to be hydroxylated to norepinephrine by dopamine b-hydroxylase (DBH). Norepinephrine is converted to epinephrine by phenylethanolamine N-methyltransferase (PNMT); cortisol serves as a cofactor for PNMT. Abbreviations: COMT: catechol-O-methyl transferase; MAO: monoamine oxidase; VMA: vanillyl mandelic acid; HVA: homovanillic acid.

1.4 Classification of Paraganglioma

PGLs, basing on their location, can be divided in different groups (Figure 2):

1. Adrenal PGL: tumours arising from the adrenal medulla, historically named Pheochromocytoma (PHEO).
2. Extra-adrenal PGL: tumours arising from extra-adrenal chromaffin tissue. These can be further classified in: thoracic paragangliomas, abdominal paragangliomas and head and neck paragangliomas (HNPGL).

   Thoracic paragangliomas arise from sympathetic ganglia (Mediastinal paragangliomas: near the aortopulmonary window or posterior mediastinum and Paravertebral paragangliomas: along the sympathetic chain in the thorax). Abdominal paragangliomas [12] are found at the level of Zuckerkandl's organ - near the aortic bifurcation, at the retroperitoneal/paraaortic level - along the abdominal sympathetic chain and at the perirenal or renal level - adjacent to the kidneys. Abdominal paragangliomas can be located also in the pelvic area, especially near the bladder. This may cause symptoms during micturition. Head and neck paragangliomas are mostly non-functional and can be divided in [13]: Carotid body tumour - at the carotid bifurcation, Glomus jugulare - in the jugular

foramen, Glomus tympanicum – in the middle ear cavity, Glomus vagale - along the vagus nerve and Laryngeal paraganglioma - very rare and located in the larynx.

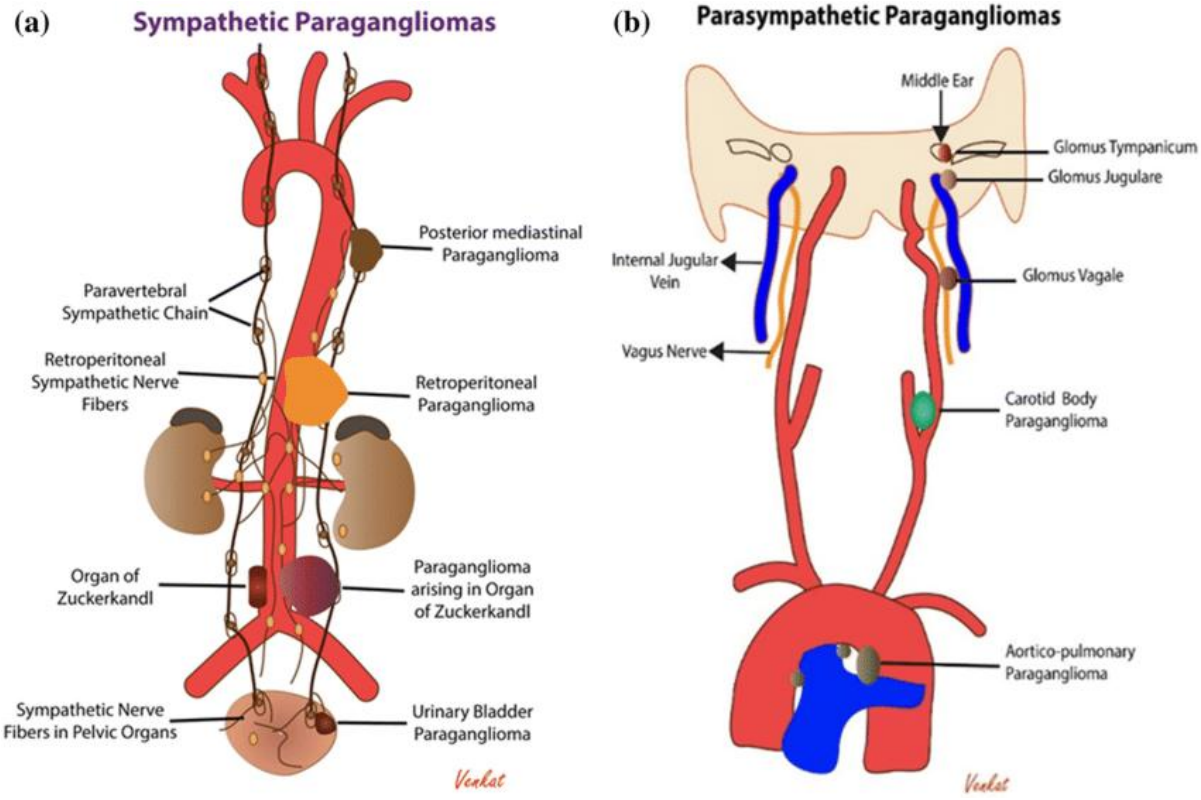

Figure 2: Sympathetic and parasympathetic paragangliomas. A) Drawing of sympathetic paragangliomas originating from the organ of Zuckerkandl, paravertebral sympathetic chain, and sympathetic nerve fibers in the pelvic and retroperitoneal organs. B) Drawing of parasympathetic paragangliomas originating from carotid body and along the cervical and thoracic branches of the vagus and glossopharyngeal nerves. [14]

PGLs can also be classified by their secreting activity in [15-17]:

1. Adrenergic phenotype: secretes mainly adrenaline, identified by an increase in urinary MN values greater than 5% of the sum of the increases in urinary MN, NMN and 3-MT.
2. Noradrenergic phenotype: secretes mainly NA, identified by increased metanephrine values but not to the extent to be included in one of the other phenotypes
3. Dopaminergic phenotype: mainly secretes DA, identified by an increase in urinary 3-MT values greater than 10% of the sum of the increases in urinary MN, NMN and 3-MT.

Recently, in order to facilitate scientific communication and consistent interpretation, Constantinescu and colleagues [15] proposed definitions for the various types of "silent" PGLs (Figure3):

- "Clinically silent" PGLs are those characterized by the absence of signs and symptoms associated with catecholamine excess.
- "Non-secretory" tumours are those with absence of clear catecholamine secretory activity, often adrenergic and presenting with normal plasma and/or urinary catecholamines over multiple sampling time points.
- "Biochemically negative" PGLs are those characterized by plasma or urinary metanephrines below the upper cut-offs of reference intervals. If only catecholamines are measured the same term may be used with clarification
- "Non-functional" tumours are those with absent catecholamine synthesis as determined from measurements of catecholamines in the tumour tissue, assessments of tumours tissue tyrosine hydroxylase or large size in association with negative results for plasma or urinary metanephrines.

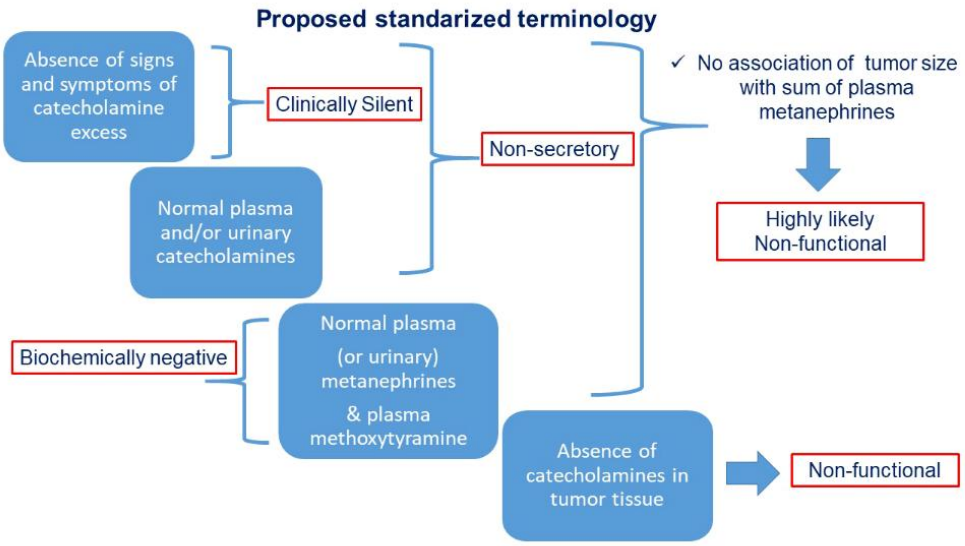

Figure 3: Chart flow with proposed standardized terminology for various types of "silent" PGLs.

1.5 Pathogenesis

As previously stated, PGLs have the highest reported degree of heritability among all tumours. When currently known germline mutations are taken into account, around 30% to 35% of patients with PGLs are affected by germline mutations in various susceptibility genes, and a further 35% to 40% show somatic driver mutations [18-23]. However, these numbers only apply to Caucasians, since among the Chinese population current evidence indicates a lower prevalence of germline mutations

(21%) and a higher proportion of somatic mutations (46%) [18]. In combination, germline and somatic mutations in more than 20 PGL driver genes have been identified in approximately 70% of all patients with PGLs, and these are divided into 3 main molecular clusters: Pseudohypoxia Cluster 1 (1A and 1B), Kinase-signalling Cluster 2, and Wnt-Signalling Cluster 3. Assignment to a specific molecular cluster is associated with differences in biochemical phenotype, clinical behaviour, and long-term prognosis. This expanding genetic knowledge over the past few years has led to significant progress in personalized management and outcomes.

1.5.1 Cluster 1

Cluster 1, termed the “Pseudo-hypoxic cluster”, is characterized by the activation of pathways that mimic hypoxia signalling. Currently, this cluster is divided into 2 sub-clusters, Cluster 1A and 1B, based on whether the gene mutation involves the Krebs cycle (Cluster 1A) or the hypoxia-signalling pathway (Cluster 1B) (Figure 4). Cluster 1A Krebs cycle-related genes (nearly exclusively germline mutations, accounting for 4%-12% of sporadic PGLs) include succinate dehydrogenase subunits (*SDHx* [*SDHA, SDHB, SDHC, SDHD*]) (germline), succinate dehydrogenase complex assembly factor-2 (*SDHAF2*) (germline), fumarate hydratase (*FH*) (germline), malate dehydrogenase 2 (*MDH2*) (germline), mitochondrial glutamic-oxaloacetic transaminase (*GOT2)* (germline), 2-oxoglutarate-malate carrier *(SLC25A11)* (germline), dihydrolipoamide S-succinyl-transferase (*DLST*) (germline), and isocitrate dehydrogenase 1 (*IDH1*) (somatic). Cluster 1B VHL/EPAS1-related genes (about 25% are germline mutations) comprise Egl-9 prolyl hydroxylase-1 and -2 (*EGLN1/2* encoding PHD1/2) (germline), von Hippel–Lindau (*VHL*) tumour suppressor (germline/somatic), hypoxia-inducible factor 2α (*HIF2A*/*EPAS1*) (somatic) (Figure 3), and iron regulatory protein 1 (*IRP1*) (1 case report) [21-26]. Cluster 1A mutations (*SDHA[AF2]*/*B*/*C*/*D, FH, MDH2*, *IDH*, *GOT2*, *SLC25A11* and *DLST*) disrupt the Krebs cycle resulting in severe impairment of mitochondrial oxidative phosphorylation [27]. Consequently, ATP production is severely affected and becomes dependent on increased cellular glycolysis (Warburg effect). Although glycolysis is less efficient in ATP production than oxidative phosphorylation, it is a fast reaction that can be increased 30-fold. This compensates for lost ATP production from cluster 1A mutation–related impairments in the electron transport chain and oxidative phosphorylation. The impairment of the Krebs cycle genes leads to the accumulation of the oncometabolites succinate, fumarate, or 2-hydroxyglutarate. This, in turn,

promotes DNA hypermethylation, inactivation of tumour suppressor genes (including *PHD1*/*2*), resulting in less hypoxia-inducible factor (HIF)-α hydroxylation and significantly lower HIF-α ubiquitination/degradation. This ultimately causes HIF-α stabilization, mitochondrial DNA impairment, collagen instability, and likely an abnormal immune microenvironment [28]. HIF-α ubiquitination is VHL-dependent. Therefore, loss of function mutations in *VHL* that result in impaired binding of the VHL protein to HIF-α therefore stabilize HIF-α and lead to its accumulation. Through HIF-α stabilization, cluster 1 mutations promote angiogenesis (ig, vascular endothelial growth factor (VEGF)/PDGF transcription), tumour extravasation, migration, invasion, metastasis, and other cellular processes [29, 30].

1.5.2 Cluster 2

Molecular cluster 2 includes pathogenetic variants affecting genes involved in tyrosine kinase (TK)-linked signalling pathways (Figure 4) [22-24]. Cluster 2 comprises mutations in the rearranged-during-transfection (RET) proto-oncogene (encoding a receptor TK) (germline/somatic) and genes encoding for neurofibromin 1 (NF1) tumour suppressor (germline/somatic), HRAS (somatic), transmembrane protein 127 (TMEM127) (germline), MYC-associated factor X (MAX) (germline/somatic) and fibroblast growth factor receptor 1 (FGFR1) (somatic) [23]. Furthermore, rare cases with mutations in genes encoding the receptor TKs Met (germline/somatic) and MERTK (germline), encoding B-Raf (somatic) and the nerve growth factor receptor (NGFR, though not yet supported by other studies) have been described [23]. These mutations are linked to overactivation of the phosphatidylinositol-3-kinase (PI3K)/AKT, mechanistic target of rapamycin (mTORC1)/p70S6 kinase (p70S6K), and RAS/RAF/ERK signalling pathways; the resulting cellular impacts include promotion of sustained cell growth, survival, proliferation, chromatin remodelling, angiogenesis, and a metabolic switch to glycolysis and glutaminolysis [23]. Most patients with these tumours show a more favourable clinical outcome compared to patients with cluster 1.

1.5.3 Cluster 3

In contrast to clusters 1 and 2, cluster 3 remains mostly unexplored, but appears to involve Wnt signalling (Figure 4). Wnt signalling–related cluster 3 comprises the “mastermind-like” transcriptional coactivator 3 (*MAML3*) fusion gene (gain-of-function event) and somatic driver mutations (no reported germline mutations) in the cold shock domain-containing E1 (*CSDE1*) gene [23]. MAML3 fusion genes lead to

overactivation of Wnt/Hedgehog signalling. A gain-of-function mutation in *CSDE1* leads to overactivation of ß-catenin, a target of Wnt signalling. Both events, in turn, lead to increased angiogenesis, cell proliferation, survival, invasion, metastasis, and deregulation of metabolism.

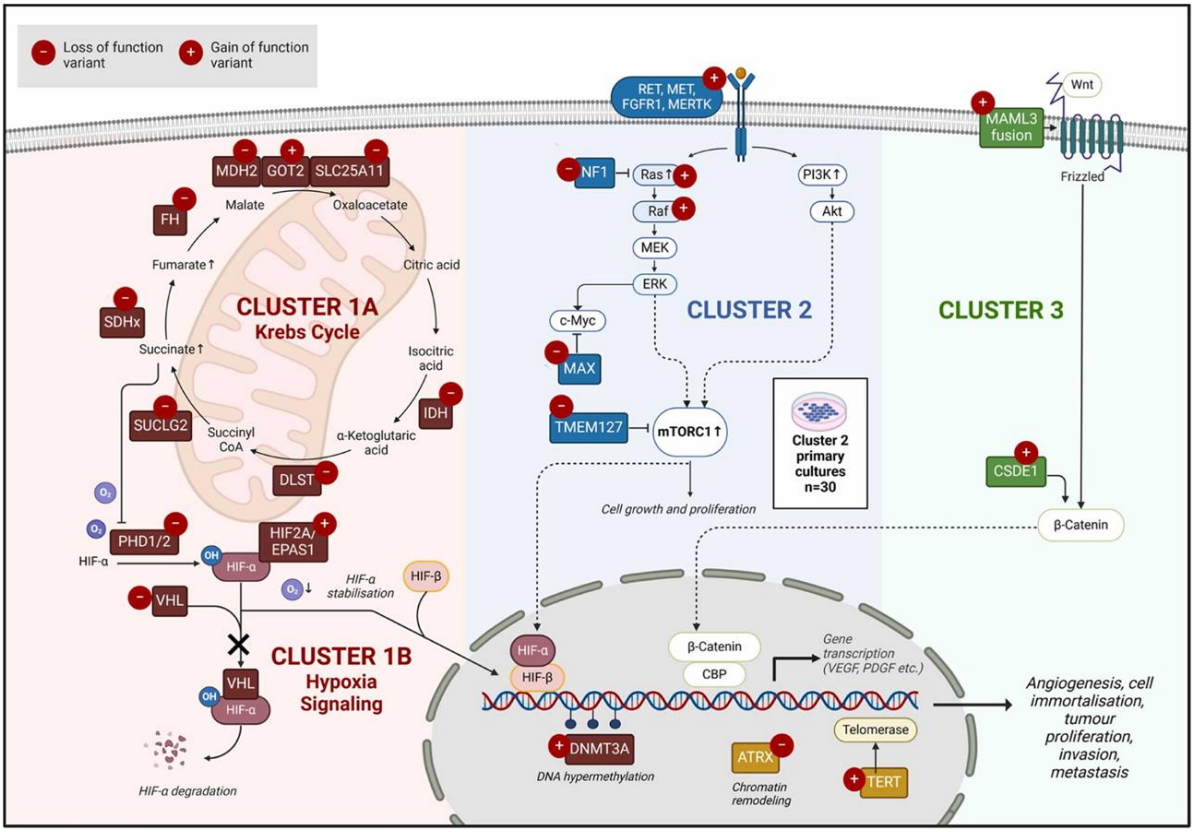

Figure 4. The 3 main molecular clusters of PPGL, cluster 1 A/B (red), cluster 2 (blue), cluster 3 (green), and their associated loss or gain of function pathogenic variants (PVs). Cluster 1A comprises mutations in the Krebs cycle-associated genes: SDHA[AF2]/B/C/D, FH, MDH2, IDH, GOT2, SLC25A11 and DLST. Cluster 1B includes mutations in VHL/EPAS1-related genes: PHD1/2, VHL, HIF2A/EPAS1, IRP1. These mutations lead to stabilization of HIF-2 α and thus, among other actions, promote angiogenesis, tumour progression, migration, invasion, and metastasis. Cluster 3 comprises the MAML3 fusion gene and somatic mutations in CSDE1 associated with overactivation of Wnt- and s-catenin signalling leading, among others, to angiogenesis, proliferation, survival, invasion, metastasis, and deregulation of metabolism [31].

1.6 Clinical presentations

Signs and symptoms of PGLs are usually caused by catecholamine excess, exhibit significant variability, leading to these tumours being referred to “the great mime”. Classic symptoms are recurring episodes of headache, palpitations, perspiration, pallor, and anxiety [32]. However, up to 10% of patients have only minor or no symptoms, and an increasing number of PGLs are found incidentally, during imaging studies [33]. Metabolic effects of catecholamine excess include hyperglycemia, lactic acidosis, and weight loss [32]. Massive catecholamine release can be provoked by several stimuli, including warmth, exercise, increased intra-abdominal pressure,

medication (e.g., metoclopramide), stress, alcohol, and certain foods (e.g., tyramine in some cheeses) [3]. If left untreated, PGLs can present with life-threatening cardiovascular conditions like hypertensive crisis, myocardial infarction, stroke, pulmonary edema, Takotsubo cardiomyopathy, acute heart failure, and high mortality [32]. HNPGLs commonly present as painless, slowly enlarging masses located in the upper part of the neck. Depending on their location these tumours may, due to compression of surrounding tissue, cause symptoms such as tinnitus, hearing loss, dysphagia, vertigo, and hoarseness [13]. Carotid body tumours are the most common HNPGLs, representing 60% of HNPGLs.

In hereditary PGLs, the clinical picture depends on the gene involved. Tumour localization, penetrance, biochemical phenotype, and metastatic risk differ according to genotype. Furthermore, mutations in some of the susceptibility genes are also associated with the development of other neoplasms, including gastrointestinal stromal tumours (GISTs), renal cell carcinoma, pituitary adenomas, and leiomyosarcomas.

PGLs are usually benign; however, there is a risk of malignant transformation in 10-15% of adrenal PGLs, and significantly higher (35-40%) in sympathetic PGLs [34]. HNPGLs are rarely metastatic [35]. There are currently no definite prognostic markers that can accurately predict malignant behaviour in primary tumours. The WHO classifies malignant disease as the presence of chromaffin tissue at locations where chromaffin tissue is normally physiologically absent [1]. Metastases can be found in the lymph nodes, skeleton, liver, and lungs. Current evaluation of the metastatic risk of a PGL is based on a multifactorial assessment, including tumour size (>5cm), extra-adrenal location, the presence of a *SDHB* mutation, a less differentiated biochemic phenotype (noradrenergic, dopaminergic or biochemically negative), and a high Ki-67 index [3]. Metastatic PGLs behave in a variable manner; some initially present with metastases and some develop metastases years after the initial diagnosis.

1.7 Diagnosis

The diagnosis of PGL requires both proof of excessive production of catecholamines and anatomical localization of the tumour. Biochemical proof is required before the next diagnostic step of imaging, except for seriously ill patients in the intensive care unit in whom biochemical testing is insufficiently reliable [7]. Notably, HNPGLs rarely produce epinephrine or norepinephrine, though dopamine is detected in

approximately one-third of these tumours; consequently, their diagnosis frequently relies on imaging techniques.

1.7.1 Biochemical diagnosis

The first step for patient suspected for PGL is the proof of excessive release of catecholamines or their metabolites. Measuring plasma free metanephrines is currently the most accurate method to diagnose a PGL; this method has a sensitivity of 97-99% and specificity of 85-89% [7]. For first-line screening, urinary fractionated metanephrines are also recommended, with a sensitivity of 85-97% and specificity of 68-95% [7]. The high diagnostic accuracy of plasma free and urinary fractionated metanephrines can be attributed to the tumour's continuous metabolic degradation of catecholamines, since the tumour itself contains the enzyme COMT [36]. This process takes place continuously, and is independent of the highly variable release of catecholamines, thereby providing diagnostic advantages for metanephrines above catecholamines. Different assays can measure metanephrines, including liquid chromatography with electrochemical or fluorometric detection (LC-ECD), liquid chromatography with tandem mass spectrometry (LC-MS/MS), or immunoassay methods. Currently, LC-MS/MS is the preferred assay because of its optimal analytical accuracy, cost-effectiveness, and minimal analytical interference from drugs [37, 38]. The challenge of measuring plasma and/or urinary metanephrines lies in the fact that levels of plasma and urinary metanephrines can be influenced by several factors, including age, gender, medication, acute illness, diet, caffeine, smoking, and posture during blood sampling; these factors can lead to false-positive results [7, 39-41]. Metanephrines can also be measured in saliva, using LS-MS/MS [42]. As collecting saliva is non-invasive and less cumbersome than plasma sampling or 24-hour urine collection, it is a promising novel diagnostic tool.

1.7.2 Anatomical imaging diagnosis

Radiologic evaluation is the next step after biochemical confirmation of a suspected PGL, and the first step when suspecting an HNPGL. Anatomical imaging can be performed with Computed Tomography (CT) or Magnetic Resonance Imaging (MRI) and is usually sufficient to locate the tumour and proceed to surgery. Performing CT is usually the first method to locate the PGLs. The non-ionic contrast media is considered safe in patients who have not undergone adrenergic receptor blockade. MRI is the preferred imaging modality for patients with metastatic disease, HNPGL, iodine contrast allergy, or those requiring reduced radiation exposure, such as

children, pregnant women, and individuals with germline genetic defects [7]. Nuclear imaging serves as a valuable adjunct to morphological imaging in the diagnosis and staging of diseases [43]. It has the added advantage in accurately predicting tumour response to eventual treatment with radiolabelled nuclear analogues in patients with avidity for the tracer. Radiopharmaceuticals, distinct from contrast agents, offer specificity to the PPGL lesions, thus facilitating the detection of diminutive lesions in scenarios of multifocal or metastatic disease [44]. These techniques include ^{123}I-metaiodobenzylguanine (^{123}I-MIBG) scintigraphy, ^{111}In-Octreotide scintigraphy, Position Emission Tomography (PET) with F-fluor-2-deoxy-D-glucose (FDG) or L-6-fluor-3,4-dihydroxyphenylalanine (^{18}F-DOPA) as tracers, and more recently, PET/CT using ^{68}Ga-labeled somatostatin analogues such as DOTA-SSA [43]. MIBG functions as a functional analogue of norepinephrine, being incorporated into secretory granules for storage and subsequent exocytosis [45]. ^{68}Ga-DOTA-SSA studies have shown excellent lesion-based sensitivity in detecting PGLs, often more than 92% [46]. A metanalysis comparing the sensitivity of ^{18}F-FDG and ^{68}Ga-DOTA-SSA found that the sensitivity of ^{68}Ga-DOTA-SSA (95%) was superior to that of ^{18}F-FDG (85%) [46]. An additional metanalysis demonstrated that the sensitivity of ^{68}Ga-DOTA-SSA (93%) was superior to ^{18}F-FDOPA (80%), ^{18}F-FDG (74%), and ^{123}I/^{131}I-MIBG (38%) [47]. The European Association of Nuclear Medicine Practice Guideline recently proposed a clinical algorithm for nuclear imaging, based on genetic status and biology, such as tumour localization, size, and secretion profile [43]. According to the most recently published guideline for radionuclide (functional) imaging of PGLs, the most sensitive imaging method for cluster 1A SDHx-related disease is ^{68}Ga-DOTA-SSA PET/CT with a sensitivity of 94% to 100% [43]. In contrast, for VHL-, EPAS1(HIF2A) and PHD1/2-, (cluster 1B) and FH-related disease, ^{18}F-FDOPA PET/CT is likely to be the most sensitive functional imaging method. the most sensitive functional imaging method for cluster 2–related PGLs is ^{18}F-FDOPA PET/CT. The second most sensitive one is most likely ^{68}Ga-DOTA-SSA PET/CT). For anatomic imaging of cluster 3–related PGLs, the same applies as for the other clusters; however, the most sensitive functional imaging modality is unknown [34].

1.8 Therapy

Individualized therapy decisions, particularly for metastatic patients, should be made in a multidisciplinary tumour board, preferably in a specialized centre [7]. Surgical resection is the only curative treatment for PGL. However, surgery is considered a

high-risk procedure. Induction of anesthesia and manipulating of the tumour can lead to a massive release of catecholamines, causing a hypertensive crisis and hemodynamic instability (i.e., cardiac arrhythmia, respiratory edema, and ischemic heart disease). Moreover, hypotension and shock may occur immediately after surgical resection of the tumour, due to the acute withdrawal of catecholamines. Therefore, in functional PGLs, alpha-adrenoreceptor blockade is usually indicated for 7 to 14 days before any treatment intervention, surgical or otherwise, and should be continued for at least 3 days after ablative or systemic therapies [7]. Moreover, alpha-adrenoreceptor blockade should be considered in each patient with metastatic disease with catecholamine-related signs and symptoms. Adrenal-sparing surgery can be an option in patients with a high risk of developing bilateral PCC, such as patients with MEN2. Adrenal-sparing surgery is not preferred for most cluster 1 tumours, since these tumours have a high risk of recurrence and metastases, particularly *SDHB*-mutant tumours [48]. Although adrenal-sparing surgery is associated with development of recurrent disease in about 13% of patients with a germline mutation in *RET* and *VHL,* this is not associated with diminished survival, and can be considered for less aggressive PGLs [49, 50]. Treatment options for metastatic PGL are limited, and these patients require an individualized approach. In patients with rapidly progressive disease, chemotherapy (cyclophosphamide, vincristine, dacarbazine (CVD)) is recommended, and may be especially effective for patients harboring a *SDHx* mutation [3, 51, 52]. For slowly to moderate growing PGL, radionuclide therapy (^{131}MIBG, ^{177}Lutetium-DOTA-TATE) is considered as first line therapy by the guideline of the Working Group on Endocrine Hypertension [3]. Other treatment options include temozolomide, tyrosine kinase inhibitors (sunitinib), mTOR inhibitors (everolimus), immune checkpoint inhibitors (pembrolizumab), and local ablative treatment of metastases [53]. However, many of these treatment options are still being tested in clinical trials. Knowledge of the specific pathways of tumourigenesis is required in order to develop new potential therapeutic targets for metastatic PGL. Moreover, these pathways differ per cluster, suggesting that for particular clusters some therapeutics may be more effective than others.

1.9 Tumour Microenvironment (TME)

Tumours are complex and dynamic entities that extend beyond a mere collection of malignant cells. Increasing evidence highlights that cancer development, progression, and therapy resistance are profoundly influenced by the tumour

microenvironment (TME) - a heterogeneous and interactive milieu characterized by high cellular heterogeneity, which includes cancerous cells, non-cancerous cells, and non-cellular components, giving origin to TME (Figure 5) [54]. The interplay between tumour cells and their surrounding microenvironment orchestrates critical processes such as angiogenesis, immune evasion, metabolic reprogramming, and epithelial-to-mesenchymal transition (EMT), thereby shaping tumour behaviour and treatment outcomes [55, 56]. These insights underscore the necessity of studying tumours not as isolated cell populations but as complex tissues with reciprocal signalling between malignant and non-malignant compartments.

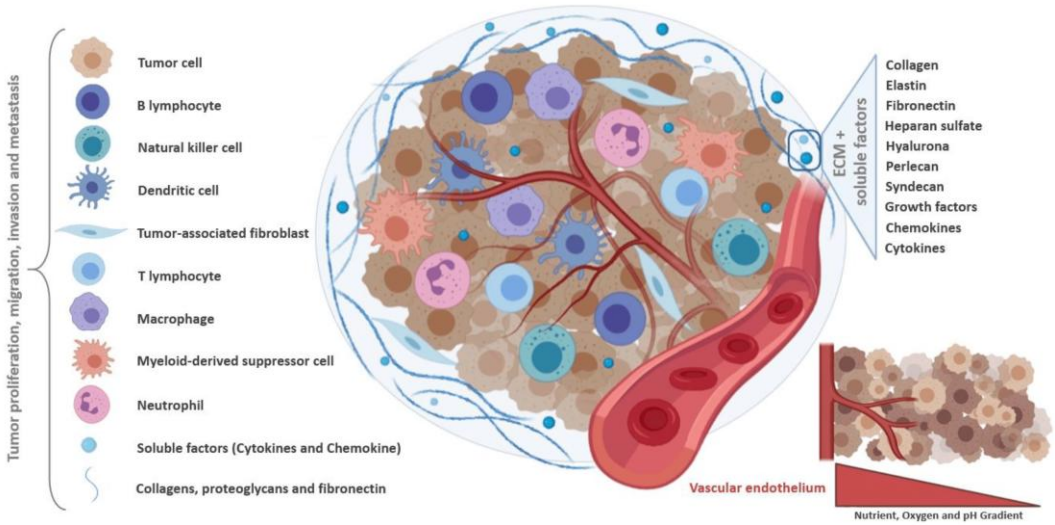

Figure 5: Schematic representation of all the components of the tumour microenvironment.

1.9.1 Cellular components of the TME

The cellular components of TME are represented by fibroblasts, endothelial cells, macrophages as well as immune cells [57].

1.9.1.1 Cancer Associated Fibroblasts (CAFs)

Cancer-associated fibroblasts (CAFs) are a major and functionally diverse component of the TME, playing pivotal roles in nearly every stage of cancer progression. Unlike their quiescent counterparts in normal tissues, CAFs are persistently activated fibroblasts that acquire a pro-tumourigenic phenotype through interactions with cancer cells and other stromal components [1,2]. Quiescent fibroblasts in the interstitial space are the major producers of ECM under normal physiological conditions and can be reversibly activated to facilitate repair and regeneration in response to tissue damage. Preceding their functioning in the regeneration stage, quiescent fibroblasts are activated into myofibroblasts and then accumulate at the sites of repair for wound

healing. The transition into CAFs is not a transient activation but a stable reprogramming of fibroblasts, often maintained even in the absence of direct cancer cell stimuli. The irreversibility of this process is thought to be driven by a combination of sustained paracrine signalling, epigenetic reprogramming, and metabolic shifts. Key factors involved include transforming growth factor-β (TGF-β), interleukin-1 (IL-1), platelet-derived growth factor (PDGF), and other soluble mediators secreted by tumour and immune cells in the microenvironment [58]. In addition, persistent activation of intracellular signalling pathways such as JAK/STAT, SMAD, and NF-κB contributes to the stabilization of the CAF phenotype [59]. Epigenetic modifications, such as DNA methylation, histone acetylation, and chromatin remodelling, further lock fibroblasts into a pro-tumourigenic state, making the transition largely irreversible [60, 61]. These changes underpin the acquisition of CAF-specific traits, including enhanced secretion of extracellular matrix components, pro-inflammatory cytokines, and growth factors that support tumour growth, immune evasion, and metastasis [62]. Exosomes can also play essential role in promoting fibroblasts activation. Tumour-derived exosomes (TDEs) carry a variety of bioactive molecules, such as proteins, lipids, mRNAs, and non-coding RNAs (including microRNAs and lncRNAs), that influence modify cell behaviour. Different studies have shown that exosomes released by cancer cells can induce fibroblast activation by transferring oncogenic content that reprograms their gene expression and epigenetic landscape. For example, exosomal TGF-β and miR-21 have been shown to promote the differentiation of normal fibroblasts into myofibroblast-like CAFs characterized by the expression of α-smooth muscle actin (α-SMA) and enhanced secretion of extracellular matrix components [63, 64]. Moreover, exosomal miR-1247-3p from cancer cells has been implicated in modulating fibroblast phenotype, that can further promote cancer progression by secreting pro-inflammatory cytokines, including IL-6 and IL-8 [65]. Also, a shift in energy metabolism such as aerobic glycolysis is potentially considered as a priming event in the conversion of CAFs. For instance, the downregulation of caveolin-1 (CAV-1), a structural protein critical for maintaining cellular metabolic homeostasis, has been associated with increased glycolysis, oxidative stress, and autophagy, all of which facilitate a pro-tumourigenic phenotype and correlate with poor clinical

outcomes in breast cancer [66-68]. In addition to CAV-1 downregulation, direct mitochondrial transfer from cancer cells to fibroblasts has emerged as another mechanism of stromal reprogramming. Tumour cells can deliver intact mitochondria or mitochondrial components via tunnelling nanotubes or extracellular vesicles, enabling fibroblasts to increase their bioenergetic capacity and promote a supportive microenvironment [69, 70].

CAFs are believed to have multiple cellular origins, including resident fibroblasts, bone marrow–derived mesenchymal stem cells, epithelial or endothelial cells via epithelial-to-mesenchymal transition (EMT) or endothelial-to-mesenchymal transition (EndoMT), and pericytes [71]. This cellular heterogeneity contributes to the functional complexity of CAF populations.

CAFs are typically identified through the expression of different biomarkers, which are expressed at low levels or not expressed in NFs, including but not limited to α-smooth muscle actin (α-SMA, also known as ACTC2), platelet-derived growth factor receptorα/β (PDGFRα/β), fibroblast-specific protein 1 (FSP-1, also known as S100A4), fibroblast activation protein (FAP) [5]. CAFs have been extensively explored and are known to be involved in diverse cellular processes, including cell differentiation, proliferation and extracellular matrix (ECM) remodelling (Figure 6).

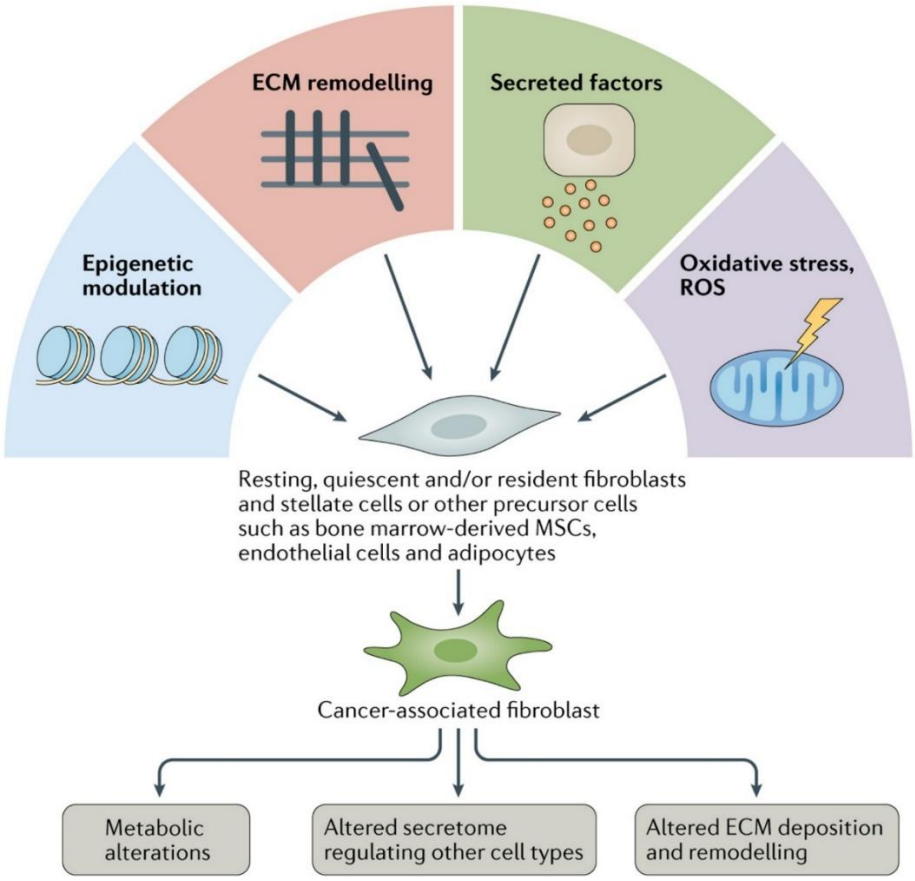

Figure 6: Schematic illustration of various mechanisms involved in cancer-associated fibroblast (CAF) activation. Potential cellular origins of CAFs include quiescent, resting or specific tissue-resident fibroblasts (stellate cells), bone marrow-derived mesenchymal stem cells (MSCs), endothelial cells and other cell types. ECM, extracellular matrix; ROS, reactive oxygen species [72].

Indeed, CAFs secrete a wide range of cytokines, chemokines, growth factors, and extracellular matrix (ECM) components that collectively shape the biochemical and mechanical landscape of the tumour. In particular, key CAF-secreted factors such as transforming growth factor-β (TGF-β), interleukin-6 (IL-6), stromal cell–derived factor-1 (SDF-1/CXCL12), and vascular endothelial growth factor (VEGF) promote tumour cell proliferation, angiogenesis, invasion, and metastasis [62, 73]. Through the production of matrix metalloproteinases (MMPs), CAFs actively remodel the ECM to facilitate cancer cell migration. Importantly, CAFs also influence immune responses by recruiting immunosuppressive cell populations, including regulatory T cells (Tregs) and myeloid-derived suppressor cells (MDSCs), and by expressing immune checkpoint molecules such as PD-L1 [74]. This immunomodulatory capacity contributes to an immunosuppressive microenvironment that supports tumour immune evasion. Furthermore, CAFs have been shown to drive therapeutic resistance by creating physical barriers to drug delivery,

secreting survival factors, and altering tumour metabolism. In particular, CAFs have an increased glycolysis and produce high-energy nutrients that facilitate biogenesis in malignant cells, a process referred to as the “reverse Warburg effect”. The Reverse Warburg Effect describes when glycolysis in the cancer-associated stroma metabolically supports adjacent cancer cells. This catabolite transfer allows cancer cells to generate ATP, increase proliferation, and reduce cell death [75, 76].

1.9.1.2 Endothelial cell (ECs)

Endothelial cells (ECs), which line the inner surface of blood and lymph vessels, play a central role in cancer progression. In fact, tumour development and survival are strictly dependent on an adequate supply of oxygen and nutrients [77, 78]. This is made possible by angiogenesis, a process by which new blood vessels develop from an established vasculature, thus ensuring the growth and hematogenous dissemination of tumour cells [79].

This process is regulated by several pro-angiogenic and anti-angiogenic molecules [80], such as vascular endothelial growth factor (VEGF), fibroblast growth factors (FGFs), and Angiopoietins secreted by tumour cells and stromal components. Among them, VEGF-A is the most well-characterized angiogenic factor [81]. VEGF-A primarily signals through VEGF receptor 1 (VEGFR-1) and VEGF receptor 2 (VEGFR-2) on endothelial cells, thus resulting in the activation of downstream proteins, including mitogen-activated protein kinase (MAPK) and phosphatidylinositol 3-kinase (PI3K) pathways [82, 83]. Several studies have demonstrated that VEGF-A mRNA is upregulated in different human tumours, including prostate [84], lung [85], gastrointestinal tract [86] and kidney [87]. Furthermore, VEGF-A expression has been associated with poor prognosis in human tumours [88].

Fibroblast Growth Factors (FGFs) are a family of heparin-binding proteins that play essential roles in development, tissue repair, and angiogenesis. Among the 22 identified FGF members, FGF1 (acidic FGF) and FGF2 (basic FGF) are most prominently associated with tumour angiogenesis. These ligands exert their pro-angiogenic functions primarily through binding to FGF receptors (FGFR1–4), which activate downstream signalling pathways such as MAPK/ERK, PI3K/AKT, and PLCγ, promoting endothelial cell proliferation, migration, and survival [89]. FGF2, in particular, is one of the most potent

angiogenic factors and can act independently or synergistically with VEGF-A to stimulate aberrant blood vessel formation [90].

The angiopoietin (Ang) family consists of Angiopoietin-1 (Ang-1), Angiopoietin-2 (Ang-2), Ang-3, and Ang-4. These ligands mainly act through the Tie2 receptor tyrosine kinase, which is expressed on endothelial cells and some hematopoietic cells [91]. Ang-1 acts as a vascular stabilizer, promoting endothelial cell survival, vessel maturation and quiescence through the activation of the PI3K-AKT signalling pathway [92]. In contrast, Ang-2 act as an antagonist or partial agonist of Tie2: under basal conditions, Ang-2 disrupts Ang-1-mediated signalling, leading to vascular destabilization, increased endothelial permeability, and sensitization of blood vessels to pro-angiogenic factors such as VEGF-A [93]. In the tumour microenvironment, Ang-2 is often upregulated in both endothelial and tumour cells and is associated with angiogenic sprouting, vessel regression, and metastasis, particularly under conditions of hypoxia or inflammation [94].

1.9.1.3 Tumour Associated Macrophages (TAMs)

Although there are many different types of immune cells infiltrating the tumour, macrophages are the most abundant inflammatory cells in human cancers such as bowel, breast, stomach, bladder and lung cancers. Macrophages are versatile immunocytes that execute a broad spectrum of functions that range from governing tissue homeostasis, defending against pathogens, and helping wound healing [95, 96]. Depending on the physiological micro-environments in which they are embedded, macrophages have distinct presentations and exhibit opposing phenotypes. In particular, macrophages can be divided in two different subpopulations (Figure 7). The first subset is M1 macrophages or “activated” macrophages that are associated with the responses of type I helper T (Th1) cells to pathogens. They are activated by interferon-gamma (IFNγ) and the engagement of Toll-like receptors (TLR) by exhibiting increased expression of major histocompatibility complex (MHC) class II, interleukin (IL-12), and tumour necrosis factor α (TNFα); generate reactive oxygen species (ROS) and nitric oxide (NO); and have the ability to kill pathogens [97, 98]. The second subset is M2 macrophages or “alternatively activated”, also recognise as TAMs, which show a different response to IL-4 and IL-13 and are involved in Th2-type responses, including humoral immunity and wound healing [99].

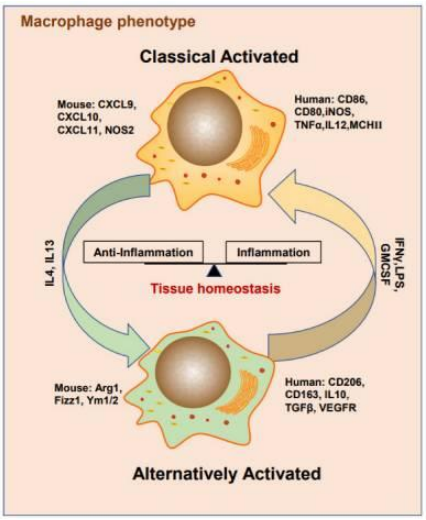

Figure 7: Macrophage M1/M2 polarization status maintains organizational stability. IFN-γ, LPS, GMCSF are the key stimulators of classically activated macrophages (recognized as M1). During the acute inflammation phase, M1 macrophage induces inflammatory responses by expressing cell surface markers to attract immune cells and releasing inflammatory factors. On the other hand, IL4 and IL13 are inducers of alternatively activated macrophages (recognized as M2), which switch the inflammatory response to anti-inflammatory to carry out tissue remodelling function [100].

A large number of studies suggests that M2 macrophages exert a direct effect on promoting metastasis via directly producing soluble factors [101]. Indeed, M2 macrophages can destroy matrix membrane of endothelial cells by secreting matrix metalloproteinases (MMPs), serine proteases, cathepsins, and decompose various collagen and other components of extracellular matrix, thereby helping the migration of tumour cells and tumour stromal cells. In cancers, high macrophage infiltration often associates with a poor prognosis or with tumour progression in many types of solid tumours, including breast [102], bladder [103], head and neck [104], glioma [105], melanoma [106], and prostate cancer [107].

1.9.2 No-cellular components of the TME

In addition to cellular components, there are many pro-tumourigenic non-cellular elements that play important roles in tumour maintenance and progression. The autocrine and the paracrine signalling between TME and cancer cells leads to the production and remodelling of the extracellular matrix (ECM), induces the production of extracellular vesicles (EVs), the secretion of growth factors, cytokines, chemokines, and metabolites, and stimulates blood and lymph vessel networks formation [108]. In addition to the crosstalk between the diverse cells of the TME, the situation of the TME is even more complicated because of the interaction between cellular and the non-cellular components, such as pH conditions, hypoxia, or soluble

factors which could indeed change the conditions of TME that in turn support the tumour progression and metabolism [109].

1.9.2.1 Extracellular Matrix

The ECM is the non-cellular component present within all tissues. The ECM not only provides structural support for resident cells but also critical biochemical and biomechanical cues that drive morphogenesis and tissue-specific differentiation and maintain tissue homeostasis [110]. The ECM interacts with cells to regulate diverse functions, including proliferation, migration and differentiation [111]. ECM is composed by fibrillar collagens, fibronectin, elastin, keratins and laminins [112]. In addition, some cancers, are particularly rich in hyaluronan [113]. The ECM is a highly dynamic structure that is constantly being remodelled through enzymatic and non-enzymatic post-translational modifications that alter its instructive capacity. Functionally discrete tissues are thus defined by unique ECM compositions and topology that are achieved through dynamic and reciprocal biochemical and biomechanical dialogues between the various cellular constituents of the tissue.

1.9.2.2 Extracellular Vesicles (EVs)

Apart from the release of secretory vesicles by specialized cells, which carry, for example, hormones or neuro transmitters, all cells are capable of secreting various types of membrane vesicles, known as extracellular vesicles (EVs).

EVs are important mediators of intercellular communication; they transfer biologically active molecules and genetic material (mRNA, microRNA, siRNA, DNA, protein and lipid) through paracrine mechanisms, which facilitate tumour dissemination [114], e.g., establishment of a premetastatic niche [115], promotion of angiogenesis [116], destruction of the peritoneum [117] or the blood-brain barrier [118], induction of drug resistance [119], and formation of the heterogeneity of cancer-associated fibroblasts [120]. Even though the generic term extracellular vesicles are currently in use to refer to all these secreted membrane vesicles, they are in fact highly heterogeneous. However, EVs can be generally classified according to their size and origin: exosomes (50 –200 nm) [121], micro-vesicles (100 –1,000 nm) [122], apoptotic bodies (50 – 4,000 nm) (9), and prostasomes (40 –500 nm) [123] (Figure 8).

Exosomes originate from the inward budding of the endosomal membrane and are secreted when multivesicular bodies (MVBs) fuse with the plasma membrane [124]. Exosomes have been reported to contain several types of specific surface markers, such as tetraspanins (CD9, CD63, and CD81), heat shock proteins (Hsp70 and Hsp90), MVB synthesis proteins [ALG-2-interacting protein X (Alix) and tumour susceptibility gene 101 (Tsg101)], and membrane transporters and fusion proteins (annexins and flotillin) [125, 126]. Micro-vesicles, which are larger than exosomes, are directly secreted from the plasma membrane via shedding or budding under normal circumstances or in response to stimuli [124]. Several proteins have been identified as micro-vesicle specific, including CD40, ADP-ribosylation factor 6 (ARF6), selectins, phosphatidylserine, and Rho family members [127-129]. Apoptotic bodies are released from the plasma membrane via indiscriminate blebbing when programmed cell death is induced and contain DNA fragments, noncoding RNAs, and cell organelles [130, 131]. Annexin V and histone are reported as specific proteins of apoptotic bodies [132-134]. Prostasomes, which are well-known EVs in reproduction and urology, are released from prostate epithelial cells in human seminal fluid and are reported to play decisive roles in the process of fertilization [135].

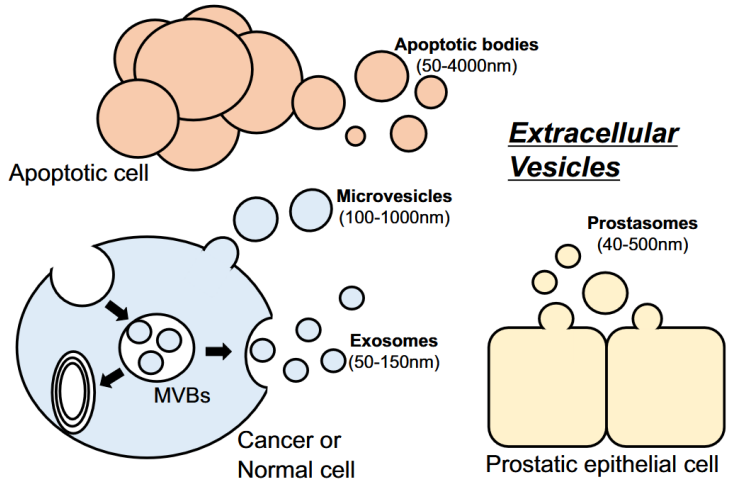

Figure 8: Various kinds of extracellular vesicles (EVs) [136].

EVs are secreted from all type of cells in physiological and pathological conditions and higher amount of EVs have been evaluated from cancerous cells [88].

Another interesting feature in the use of exosomes is their capacity for carrying a payload of proteins or nucleic acids to target cells that may be effective in developing novel cancer therapies that are less harmful than chemotherapy. For most drugs, only a relatively small amount reaches the lesion to exert a therapeutic effect. This reduces the efficacy and can cause toxicity and adverse side effects to the patient. Moreover, exosomes have many advantages, such as small size, natural molecular transport properties, and good biocompatibility [137]. Tumour therapy based on exosomes may become an important part of personalized medicine, because they can be loaded with different types of compounds, such as small-molecule chemical drugs, proteins and nucleic acids [138].

1.9.2.3 Succinate

Succinate is a molecule formed from succinyl-CoA synthetase and converted by succinate dehydrogenase (SDH) to fumarate in the Krebs Cycle. PGL that harbour a SDHx mutation are characterized by dysfunction of the SDH enzyme. As the conversion to fumarate is impaired, a substantial accumulation of succinate occurs. The accumulation of succinate is shuttled from the mitochondrial matrix to reach the cytoplasm where it mediates different oncogenic effects such as the inhibition of prolyl hydroxylase (PHD), which is responsible for hydroxylation of HIF1α. Blocking PHD prevents HIF1a degradation and induces expression of several HIF-target genes that are known to be involved in angiogenesis [139]. Pollard and colleagues described the same phenomenon in SDH- and fumarate hydratase (FH)-mutated PGLs [140], that indeed, are characterized by 25-fold higher succinate levels than tumours mutated in the other susceptibility genes [141]. Alongside PHD inhibition, accumulation of succinate inhibits jumonji-domain histone demethylases (JmjC) and the ten-eleven translocation (TET) family of DNA methylase [142, 143]. This leads to hypermethylation of promotor regions (CpG islands) of several genes involved in tumourigenesis [144, 145]. In PGL, SDHx mutations were shown to promote a massive hypermethylation phenotype. In addition to its role as an oncometabolite, succinate can also act as a ligand for the G protein-coupled receptor 1 (SUCNR1) [146], which has been shown to be expressed in many tissues [147-150]. Depending on cell type, this receptor could be couple to different G-proteins, so the effect of its

stimulation involves different mechanisms [151]. In kidney cells, coupling to Gαq- and/or Gαi-proteins has been proposed, leading to activation of extracellular-signal-regulated-kinases (ERK1/2), generation of inositol triphosphate, augmentation of intracellular calcium, and decrease of cyclic adenosine monophosphate (cAMP). In cardiomyocytes, SUCNR1 stimulation has been shown to increase cAMP concentration, thus coupling to Gαs is also possible [148]. Moreover, it has been demonstrated that succinate promotes hMSC migration through PKCζ/p38-induced DRP1 phosphorylation [152]. In addition, in a study conducted on cardiomyocites, Lu and colleagues showed that in response to cardiac ischemia, succinate activates SUCNR1 and induces mitochondrial fission via regulation of PKC-δ and ERK1/2 signalling [153]. In recent years, several studies have highlighted the role of succinate and SUCNR1 in tumourigenesis [152, 154, 155]. Moreover, succinate treatment as well as SDHB-silencing has been shown to induce SUCNR1 mRNA and protein expression in human hepatoma cells [156], suggesting a positive feedback of inappropriate succinate accumulation on expression of this receptor. Recently, Matlac and colleagues showed that mRNA expression of SUCNR1 was higher in SDHx mutated PGLs compared to cluster 2 tumours. Moreover, they confirmed elevated SUCNR1 protein expression levels in SDHB mutated PGLs compared to VHL (Von Hippel-Lindau) mutated Pheo [157]. However, little is known about the effects of succinate and its receptor on TME cells. Only very recently, it has been demonstrated that lung cancer-derived succinate, released into the TME, induces macrophage polarization and cancer metastasis by activating SUCNR1 [158]. In dendritic cells, succinate enhances the capacity to act as antigen-presenting cells, to migrate towards draining lymph nodes and to produce cytokine in synergy with Toll-like receptor ligands [147, 159, 160].

1.10 Inter-organelle communication: how mitochondria interact with the nucleus

Mitochondria are widely recognized for their role in energy production, but their function extends far beyond ATP synthesis. These dynamic organelles are deeply integrated into a complex network of inter-organelle communication that supports essential processes such as calcium homeostasis, lipid metabolism, apoptosis, and stress responses [161]. Far from being isolated units, mitochondria physically and

functionally interact with nearly every major organelle within the cell, forming contact sites that facilitate the exchange of metabolites, signalling molecules, and structural information. One of the most well-characterized interactions is between mitochondria and the endoplasmic reticulum (ER) [162], forming specialized regions known as mitochondria-associated ER membranes (MAMs) or ER-mitochondria contact sites (MERCs). These structures are crucial for the transfer of calcium from the ER to mitochondria, which regulates metabolic activity, reactive oxygen species (ROS) production, and apoptosis. In addition to calcium signalling, ER-mitochondria contacts are involved in the synthesis and exchange of lipids, helping to maintain mitochondrial membrane composition and function. Proteins such as IP_3 receptors, voltage-dependent anion channels (VDAC), mitofusin-2, and the chaperone GRP75 play central roles in maintaining these interactions. Mitochondria also interact with lipid droplets, enabling direct communication that regulates lipid storage, mobilization, and β-oxidation [163]. This interplay is vital for cellular energy balance, especially under metabolic stress. In parallel, mitochondria maintain close functional relationships with lysosomes [164], which are central to mitochondrial quality control. Through processes like mitophagy, damaged mitochondria are selectively degraded, preserving cellular health and preventing the accumulation of dysfunctional organelles. These processes depend on tightly regulated contact sites and signalling cascades that sense mitochondrial damage and initiate clearance. Additionally, mitochondria share metabolic and functional crosstalk with peroxisomes [165], particularly in the context of fatty acid oxidation and reactive oxygen species metabolism. The machinery that controls mitochondrial fission and fusion is often shared or coordinated with peroxisomes, underscoring the interdependence of these two organelles in maintaining redox balance and metabolic flexibility. Recent studies have also highlighted a more direct connection between mitochondria and the nucleus, leading to the identification of structures known as nucleus-associated mitochondria (NAMs) [166]. These physical contacts may serve as sites for efficient communication during stress adaptation, coordinating mitochondrial signals such as ROS, calcium, and metabolic intermediates with nuclear transcriptional responses.

Growing evidence suggests that the formation of physical contact sites between mitochondria and the nucleus is a regulated process involving multiple proteins that either directly tether these organelles or modulate their functional interaction. In this context, a central player is the Translocator Protein (TSPO), a conserved outer

mitochondrial membrane protein traditionally known for its role in cholesterol transport, ROS regulation, and apoptosis, but more recently shown to be essential for NAM formation by promoting mitochondrial anchoring to the nuclear envelope, possibly through interactions with cytoskeletal or scaffolding components [166]. TSPO is well studied in the context of mitochondrial function. It modulates mitochondrial Ca^{2+} homeostasis and redox signalling [167], for example by limiting mitochondrial Ca^{2+} uptake and thereby influencing cytosolic NADPH oxidase activity and ROS production. In addition, TSPO is also implicated in suppressing mitophagy under stress conditions, linking mitochondrial quality control and disease processes [168]. In steroidogenic and mitochondrial-active cells, TSPO has been associated with regulation of fatty acid oxidation and mitochondrial metabolism [169]. ACBD3 (Acyl-CoA Binding Domain Containing 3), a Golgi- and mitochondria-associated protein, has been implicated in the recruitment of TSPO into multimolecular complexes that span the mitochondrial and nuclear membranes, facilitating physical proximity and functional communication. In addition, AKAP95, a nuclear A-kinase anchoring protein, has been proposed to participate in mitochondria-nucleus contact formation by linking nuclear structures to cytoplasmic elements that are themselves connected to mitochondria, thus indirectly stabilizing the interface.

The Protein Kinase A (PKA) is recruited into the TSPO/ACBD3 complex; contributes to phosphorylation events and signalling involved in maintaining the contact and functional communication. These protein interactions are dynamically regulated in response to cellular stress, metabolic demands, or mitochondrial dysfunction, allowing mitochondria to relay signals directly to the nucleus, thereby influencing transcriptional programs and nuclear responses through a mechanism known as Mitochondrial Retrograde Response (MRR).

The integrity of mitochondrial communication with other organelles is essential for maintaining cellular homeostasis. Disruptions in these networks are increasingly implicated in a wide range of diseases, including cancer, neurodegenerative disorders, metabolic syndromes, and aging [170-172]. In cancer, altered ER-mitochondria and mitochondria-nucleus communication may contribute to tumour progression by supporting metabolic reprogramming, evasion of apoptosis, and resistance to stress. In neurodegenerative diseases, impaired mitochondria-nucleus cross-talk and mitochondrial-lysosomal interactions lead to the accumulation of damaged organelles and misfolded proteins, exacerbating cellular dysfunction, as

observed in Alzheimer's disease and Parkinson's disease where disruptions in mitochondrial-nuclear gene expression coordination and lysosomal clearance have been documented [170, 173].

Understanding the molecular basis of these inter-organelle connections, and how they are modulated under physiological and pathological conditions, offers valuable insights into cell biology and provides potential therapeutic targets. In this context, the role of TSPO and NAMs represents a promising frontier in the study of mitochondrial signalling, particularly in diseases where mitochondrial dysfunction is a central feature.

1.11 PGLs Cell Models

1.11.1 Rat pheochromocytoma cells (PC12)

The adrenal rat pheochromocytoma (PC12) cell line, originally isolated from a PCC developed in an irradiated rat in 1976, has been a cornerstone in neuroendocrine tumour research for decades due to its versatile properties and well-characterized molecular profile [174]. Although not derived from human paraganglioma tissue, PC12 cells share key features with chromaffin cells, making them a widely accepted *in vitro* surrogate for mechanistic studies related to pheochromocytoma and, by extension, paraganglioma. These cells possess the ability to synthesize, store, and release catecholamines - primarily dopamine and norepinephrine - while lacking basal expression of phenylethanolamine N-methyltransferase (PNMT), the enzyme responsible for epinephrine synthesis. However, PNMT can be induced in PC12 cells through glucocorticoid exposure, allowing researchers to model stress-responsive catecholamine regulation [175]. A hallmark feature of PC12 cells is their capacity to undergo phenotypic differentiation. Upon treatment with nerve growth factor (NGF), they adopt a neuronal-like morphology characterized by neurite outgrowth and electrophysiological activity [176, 177], whereas exposure to dexamethasone pushes the cells toward a more endocrine or chromaffin-like state with increased secretory granule formation. This bidirectional differentiation potential enables researchers to dissect signalling pathways involved in both neural and endocrine tumour biology. PC12 cells are important also for PGLs studies. Indeed, they express several of the catecholamine biosynthetic enzymes, including tyrosine hydroxylase (TH) along with the enzymes converting L-DOPA to DA and DA to NA, that is, aromatic l-amino acid decarboxylase (AADC) and DA β-hydroxylase (DBH), respectively. However, the final

enzyme in the catecholamine biosynthetic pathway, PNMT, which produces A from NA, is not expressed in these cells. Despite these advantages, PC12 cells are not without limitations. They are rodent-derived and thus may not fully recapitulate human tumour biology. Moreover, in these cells, functional MAX protein is not expressed. Hopewell and colleagues have identified a homozygous mutation of MAX gene, which is consistent with the aberrant processing of MAX transcripts in these cells. It has been suggested that the loss of MAX expression may have been a selected event either in the development of the rat PCC or during subsequent cell culturing *in vitro* [178].

Nonetheless, due to their ease of culture, robust catecholaminergic phenotype, and high responsiveness to differentiation stimuli and genetic manipulation, PC12 cells remain an indispensable tool in the broader study of neuroendocrine tumourigenesis and paraganglioma pathophysiology, particularly in early-phase mechanistic and drug discovery research.

1.11.2 Mouse Pheochromocytoma Cell line (MPC) and Mouse Tumour Tissue cell (MTT)

The MPC (mouse pheochromocytoma) and its more aggressive derivative MTT (mouse tumour tissue-derived) cell lines are among the most validated and widely utilized *in vitro* models for preclinical studies of paraganglioma. These cells originally derived from adrenal medullary tumours in *Nf1* heterozygous knockout mice [179]. Tischler and colleagues characterised these tumours and isolated cells cultured *in vitro* [180]. A few years later, multiple independent MPC lines - including the well-characterized MPC4/30/PRR - demonstrate chromaffin cell features, such as expression of catecholamine-synthesizing enzymes and susceptibility to neuronal differentiation under favourable culture conditions. Nevertheless, subsequent studies demonstrated that the wild type *Nf1* allele was not present, possibly indicating that the protein produced was functionally defective[181].

The less differentiated MTT line was established by serial passage of MPC-derived xenografts in nude mice, culminating in a model that reliably forms liver metastases within 4 weeks and harbours a distinct gene expression signature associated with high metastatic capacity. Both cell lines express HIF1α but not HIF2α, an important distinction in hypoxia-linked tumour biology.

The MTT cells maintain a PCC phenotype, as confirmed by measuring intracellular catecholamines, by evaluating the expression of TH and PNMT along with monitoring the presence of dense-core secretory granules. Furthermore, gene expression array analysis on MTT revealed genes that may be crucial for the development of an aggressive and more malignant phenotype of PCC[182]. MPC and MTT thus serve complementary roles in research: MPC cells, with intact PNMT expression and relatively slow growth, resemble differentiated, hormone-active tumours, while MTT cells, with enhanced invasiveness and metastatic behaviour, model of aggressive disease states.

Different cell lines were then derived from MPC and MTT to improve and diversify research studies, with a particular interest in *SDHB* mutations, because mutations in this gene represent a high-risk factor for malignancy [183, 184]. To assess possible associations between *SDHB* gene mutations and invasiveness, Richter and colleagues established an MTT *SDHB* knockdown by viral transduction with lentiviral particles [185]. Of note, one of the shortcomings of silencing the *SDHB* subunit in an *Nf1* heterozygous KO mouse is the mixing of the phenotypes of clusters 1 and 2.

1.11.3 Immortalised Chromaffin Cell (imCC)

Developed by Letouzé and colleagues [25], imCCs were derived from mouse adrenal chromaffin cells harboring floxed *Sdhb* alleles and rendered immortal after extended culture, followed by Cre-mediated recombination to achieve complete SDHB knockout. These cells exhibit hallmark features of SDHB-mutant tumours, including total loss of SDHB protein and enzymatic activity, resulting in profound succinate accumulation and pseudo-hypoxic stabilization of HIF2α, thereby faithfully recapitulating the metabolic and transcriptional phenotype of human SDHB-related PGL [25, 186]. Moreover, imCCs demonstrate a hyper-methylator epigenetic landscape, with widespread DNA promoter methylation, and display epithelial-to-mesenchymal transition (EMT)-like characteristics, including upregulation of mesenchymal markers (i.g., *Twist1*, *Snai1*, *N-cadherin*) and downregulation of epithelial genes like *Krt19* [186]. These EMT features are reversible by treatment with demethylating agents such as decitabine, highlighting the interplay between SDH loss, epigenetic plasticity, and invasive tumour behaviour. To date, the imCC line remains a powerful tool for mechanistic studies and therapeutic screening in SDHB-related paraganglioma research, offering critical insights into tumour metabolism, epigenetics, and invasiveness.

1.11.4 RS0: Rat-derived SDHB deficient cell

The RS0 system represents a landmark advance in *in vitro* modelling of SDH-deficient paragangliomas. Originating from a heterozygous Sdhb+/− Sprague–Dawley rat pup exposed to perinatal γ-irradiation, small pheochromocytoma (PC) and carotid body paraganglioma lesions were harvested and used to establish xenografts in NSG (NOD-scid gamma) mice. This process yielded two serially transplantable tumour lines: RS0, which completely lost the wild-type Sdhb allele, and RS1/2, which retained it. RS0 is distinguished by complete absence of SDHB protein and robust accumulation of succinate and lactate, accurately reflecting the metabolic phenotype of human SDHB-mutant tumours [187]. RS1/2 serves either as a control for studies of RS0 or as a potential tool for studying patients' tumours that may be haplo-insufficient for SDH, having undetermined driver mutations.

RS0 closely mirrors SDHB-mutated human paragangliomas at the genome, transcriptome, and metabolome levels, including high expression of hypoxia-inducible (EPAS1/HIF2α) gene networks. These cells express neuroendocrine markers such as TH and chromogranin A. Moreover, in RS0, cytoplasmic vacuoles and sparse, often tiny, secretory granules are present. In contrast, RS1/2 cells have larger secretory granules and lack cytoplasmic vacuoles.

1.11.5 Progenitor cells derived from a human Pheochromocytoma (hPheo1)

The hPheo1 cell line is currently the only well-established human-derived pheochromocytoma precursor model, generated in 2013 by Ghayee et al. through hTERT-mediated immortalization of primary human tumour cells obtained from a sporadic adrenal pheochromocytoma (female donor, age 39) [188]. Exhibiting a stable diploid karyotype with a single deletion at 9p22 (encompassing the tumour suppressor gene *CDKN2A*), hPheo1 cells have undergone more than 300 population doublings without signs of senescence, demonstrating robust proliferative capacity. Although they display a mesenchymal-like morphology in culture, differentiation protocols using BMP4, NGF, and dexamethasone can induce neuroendocrine marker expression - including chromogranin A, PNMT, and NCAM (CD56) - alongside neurite-like outgrowth, indicating retained chromaffin lineage potential. Transcriptomic analyses place hPheo1 close to adrenal medulla and primary pheochromocytoma tissues, although with relatively low baseline expression of catecholamine synthesis enzymes. Functional studies using CRISPR and shRNA to

deplete *SDHB* in hPheo1 cells have revealed metabolic reprogramming toward glutamine oxidation and polyamine pathway upregulation, coupled with reduced adhesion and increased proliferation - mimicking metabolic and behavioural traits seen in SDHB-mutated paragangliomas [189]. Despite limitations such as lack of hormones production, hPheo1 remains a unique and indispensable human cell model for exploring molecular mechanisms, metabolic vulnerabilities, and therapeutic interventions in pheochromocytoma and paraganglioma research.

2. Aims of the study

Initially, the thesis focused on studying the interactions between hPheo1 cell lines (Parental and SDHB-deficient) and human primary fibroblasts. This was a targeted investigation into how these cells communicate or influence each other. The decision to expand my thesis from its initial focus and divide it into five distinct aims was driven by the natural evolution and increased complexity of my PhD research. As my work progressed, we broadened the study to capture a more comprehensive understanding of the system. These additions weren't arbitrary; they built on the foundational work to address emerging questions, test new hypotheses, or integrate interdisciplinary elements, making the research more robust and reflective of *in vivo* tumour biology. By dividing the study into five objectives, we were able to better organise the content, so that each aim could focus on a specific aspect, preventing the thesis from becoming overly complex or disjointed and improving its fluidity.

2.1 Aim 1 - electrophysiological properties of hPheo1

The first aim was to investigated the metabolic, functional and electrophysiological characteristics in two human pheochromocytoma cells, hPheo1 Parental or deficient for the B subunit of the succinate dehydrogenase (SDHB-deficient). Since bioelectrical properties and signalling in cancer are an emerging field and since biophysical properties are key features in neuroendocrine cells, we studied both the membrane passive properties such as Resting Membrane Potential (RMP), Capacitance (Cm) and Resistance (Rm) both the outward potassium currents.

2.2 Aim 2 - succinate role as an oncometabolite

The second aim was to evaluate the role of the oncometabolite succinate in our cell lines. In particular, we aimed to study not only the effect of intracellular succinate accumulation on histone methylation and protein succinylation, but also the intracellular pathways activated by the binding of succinate to its G protein-coupled membrane receptor, namely SUCNR1.

2.3 Aim 3 - mitochondria interaction with the nucleus

The third objective aimed at investigate the role of mitochondrial communication with the nucleus and to further explore the role of the Translocator Protein (TSPO) in NAM formation. We therefore used electron microscopy, western blotting and advanced imaging techniques to study NAMs and to corroborate the role of TSPO in hPheo1 cell lines.

2.4 Aim 4 - crosstalk between hPheo1 and endothelial cells

The next objective of this thesis was to explore the contribution of different components of the tumour microenvironment (TME) to the progression of paragangliomas (PGLs). Specifically, in the fourth objective, we focused on the interaction between tumour cells and endothelial cells by co-culturing Human Umbilical Vein Endothelial Cells (HUVECs) with hPheo1 cells. This experimental setup enabled us to evaluate the reciprocal effects of tumour–endothelial crosstalk on key cellular processes, including proliferation, migration, endothelial permeabilization, and tube formation, all of which are critical for angiogenesis and tumour progression. Importantly, we also investigated the role of tumour-derived Extracellular Vesicles (EVs) to gain deeper insight into how tumour cells may modulate endothelial behaviour through EV-mediated signalling, thereby promoting angiogenesis and contributing to the invasive capacity of PGLs.

2.5 Aim 5 - hPheo1 communication with the stroma

In the fifth aim of this thesis, we investigated the role of fibroblasts as a critical component of the tumour microenvironment (TME). To this end, we utilized Human Primary Cancer-associated Fibroblasts (CAFs) isolated from PGL patients carrying either non-pathogenic variants (NPVs) or SDHx mutations, and co-cultured them with the hPheo1 cell lines. While initial experiments were performed in conventional 2D co-culture systems, we then transitioned to a more physiologically relevant model by adopting a three-dimensional (3D) culture approach. Specifically, we generated tumour spheroids, which better mimic the structural and functional complexity of in vivo tumour architecture, and placed them onto a monolayer of CAFs. This 3D system allowed us to evaluate the impact of fibroblast genotype on tumour cell behaviour, with a particular focus on spheroid migration as an indicator of invasive potential and tumour–stroma interaction.

3. Materials and Methods

Despite the different aims of this thesis, some of the methodologies used were the same but with slightly different experimental conditions. For this reason, we have separated the general materials and methods from those specific to each aim.

3.1 General Material and Methods

3.1.1 Cell lines, tissue samples, primary human cell cultures and materials

hPheo1 cells (Parental and the deficient for the SDHB subunit, hereinafter referred to as Parental and SDHB-deficient, respectively), generated by Ghayee and Matlac [157, 188] and kindly provided by Jiri Neuzil, were maintained at 5% CO2, 37℃ in RPMI supplemented with 10% foetal bovine serum (FBS), with 4.5 g/L glucose, 2 mM l-glutamine, 100 U/mL of penicillin/streptomycin, 2 mM of sodium pyruvate and 50 µg/mL uridine (complete RPMI). HUVEC cells were maintained in Endothelial Basal Medium (EBM) supplemented with 2% foetal bovine serum (FBS), 0.004 ml/ml Endothelial Cell Growth Supplement (ECGS), 0.1 ng/ml human Epidermal Growth Factor (hEGF), 1 ng/ml human basic Fibroblast Growth Factor (hbFGF), 1 µg/ml Hydrocortisone (HC), 2 mM l-glutamine, 100 U/mL of penicillin/streptomycin (complete EBM). For co-culture experiment between HUVECs and tumour cells we used complete EBM supplemented with 4.5 g/L glucose, 2 mM of sodium pyruvate and 50 µg/mL uridine (hereinafter referred to as co-culture medium).

Tumour tissue samples were collected from PGL patients who underwent surgical resection at Careggi Hospital (Florence, Italy), as part of routine clinical care. All procedures were conducted in compliance with institutional and national ethical guidelines, and written informed consent was obtained from each patient prior to sample collection (ENS@T protocol 59/11, version 1.3). The cohort included patients carrying either SDHB-mutations (PAVA and MENI) or non-pathogenic variants (NPVs) (BELO and CALU). Immediately following surgical excision, tumour specimens were either snap-frozen in liquid nitrogen and stored at –80°C for molecular analyses or fixed in formalin and embedded in paraffin (FFPE) for histological and immunohistochemical evaluation. In addition, small fragments (approximately 0.5–1 cm^3) of either tumour tissue or adjacent peritumoural fat were collected under sterile conditions were collected and enzymatically processed to isolate primary fibroblasts within a few h of collection. Specifically, Human primary fibroblasts were obtained following a multi-step process involving enzymatic

digestion, cell seeding, and culture maintenance (Figure 9). After rinsing with sterile warm PBS, tissues were finely minced and subjected to enzymatic digestion using a mix of trypsin 1x and collagenase I (1mg/ml) (Sigma-Aldrich) for 1.5 h at 37 °C to allow the enzymatic digestion. The resulting cell suspensions were filtered using cell strainer (100µm pore size) and plated in 6-well plates and let grow under standard conditions (37°C, 5% CO_2).

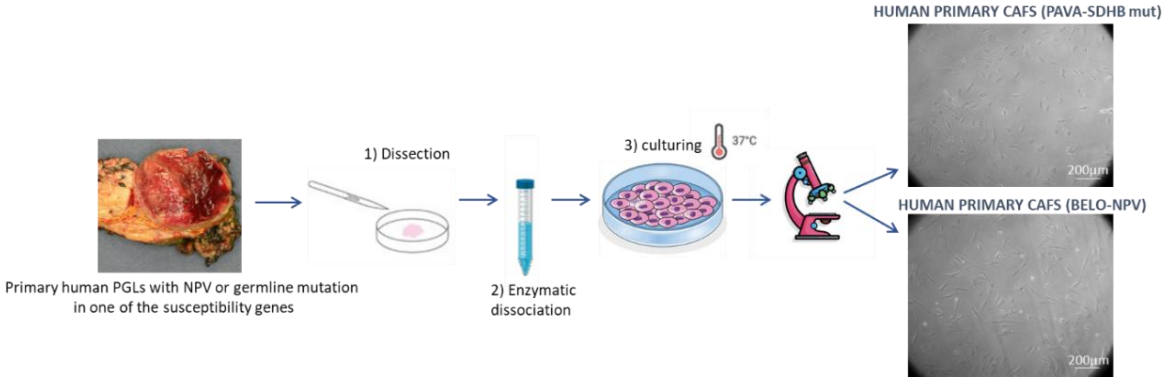

Figure 9: Workflow of the isolation of Human Primary Fibroblast from PGL patients with NPV or germline mutation in one of the susceptibility genes.

Glibenclamide was purchased from Sigma (Sigma-Aldrich) and was dissolved in dimethyl sulfoxide (DMSO). Methyl-succinate (M81101) succinate (224731) were purchased from Sigma (Sigma-Aldrich) and were dissolved in RPMI and ethanol, respectively. SCH772984 (HY-50846) was from MedChemExpress and was dissolved in DMSO.

3.1.2 Co-Culture

To study the *in vitro* effects of the interactions that occur between tumour and TME cells, we used the 2D co-culture technique (Figure 10). This involves one of the two cell lines seeded into the wells of a multi-well, while the other is seeded inside inserts with a porous membrane at the bottom. 24 h h after plating, the inserts are placed inside the wells and, in doing so, although the two cell lines remain physically separated by the porous membrane itself, exchanges of all material produced by both cell lines (molecules and/or vesicles and/or proteins, etc.) are permitted.

The membrane pores can be of different sizes, depending on the purpose of the experiment: for cell proliferation and western blot experiments, we used 3 µm pores while for migration experiments, we used 8 µm pores, so that the cells in the upper insert could pass through it and migrate.

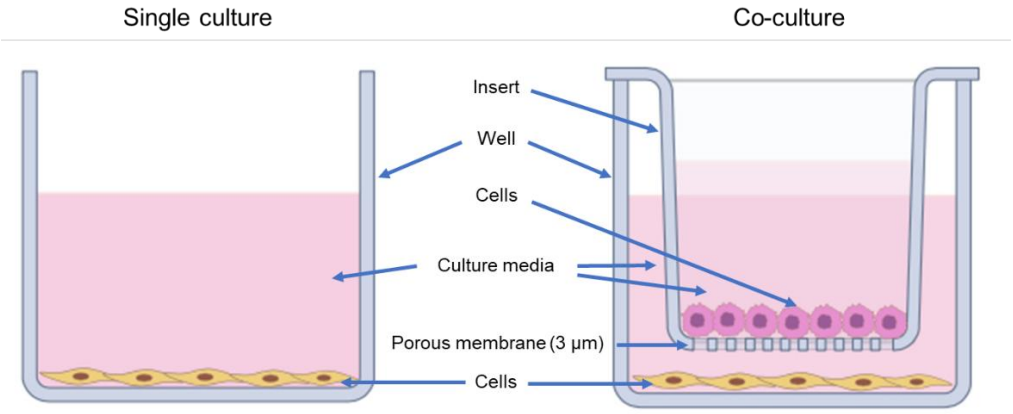

Figure 10: Schematic representation of co-culture

3.1.3 Cell Proliferation

To evaluate proliferation, cells were seeded at different density into 12-well plates, allowed to adhere overnight and then treated or not with increasing doses of different drugs in complete culturing medium and counted at different timepoint.

For co-culture experiment, one cell line was seeded into 3 µm pore size transwell inserts (Greiner Bio-one, Kremsmünster, Austria) while a different cell line was seeded into the 12-well plates below. Cells were allowed to adhere overnight before starting the co-culture and then counted at different timepoints.

3.1.4 2D Migration

Transwell migration assay was performed using 8 µm pore size transwell inserts (Greiner Bio-one, Kremsmünster, Austria). Briefly, cells were seeded in complete medium in inserts and allowed to adhere overnight. The next day, the medium in the inserts was replaced with serum-free medium while in the lower wells, complete medium was used as chemoattractant. After 16 at 37 °C, adherent cells in the upper part of the insert were removed, while cells migrated to the lower side of the inserts were fixed with cold methanol for 10 minutes, stained with 0.1% crystal violet and observed under the microscope. All the images were acquired using a light microscope. To obtain a quantitative analysis, stained cells were eluted with DMSO, and the crystal violet released in the solution was quantified as OD at 560 nm by the spectrophotometer VICTOR^3 1420 Multilabel Counter (Packard Instruments, Perkin-Elmer). Migration was normalized on total cell number.

For co-culture migration experiments, one cell line was seeded into transwell inserts (Greiner Bio-one, Kremsmünster, Austria) while a different cell line was seeded into the 12-well plates below. Cells were allowed to adhere overnight and before starting the co-culture the media was replaced with serum-free media in the inserts and with

complete media in the lower wells. As controls, cells in single culture (without different cell lines in the bottom well), were used.

3.1.5 Western Blot

Cells were lysed in a buffer containing 50 mM Tris–HCl, pH 7.5, 120 mM NaCl, 1 mM EGTA, 6 mM EDTA, 15 mM Na4P2O7, 20 mM NaF, 1% Triton X-100 and protease inhibitor cocktail. Lysates were clarified by centrifugation at 10,000 g for 15 minutes at 4℃, and supernatants were quantified for protein content (Coomassie Blue reagent, Bio-Rad). All passages were carried out on ice as previously described [190]. Proteins (30 µg) were separated using 8%, 10%, 12% or 14% sodium dodecyl sulphate polyacrylamide (SDS-PAGE) gels and transferred to PVDF or Nitrocellulose membranes (Fisher Scientific or Immobilon, Millipore, MA, USA). Proteins with bound antibodies were detected using the ECL reagent (Immobilon Crescendo, Millipore, MA, USA) and analysed with the Bio-Rad Chemi-Doc Imaging System (Quantity One). Band intensity was determined by optical density analysis using the image J software. All the antibodies used in this thesis are shown in Tables 1.

(A) Primary antibodies

Name	Supplier	Catalogue number	Dilution
Anti-ACBD3	Santa Cruz Technology	Sc-101277	1:200 (WB)
Anti-AKAP95	Santa Cruz Technology	Sc-390335	1:500 (WB)
Anti-Actin	Santa Cruz Technology	Sc-1615	1:1000 (WB)
Anti-CD31 (PECAM)	Cell Signaling Technology	#3528	1:1000 (WB) 1:200 (IF)
Anti-Claudin5	Cell Signaling Technology	#49564	1:1000 (WB) 1:100 (IF)
Anti-Collagen type I	Invitrogen	#PA1-26204	1:1000 (WB) 1:100 (IF)
Anti-DRP1	Cell Signaling Technology	#8570	1:1000 (WB)
Anti-ERK1/2	Cell Signaling Technology	#9102	1:1000 (WB)
Anti-FAP	Invitrogen	#PA5-99313	1:100 (IF)
Anti-Fibronectin	Invitrogen	#PA5-29578	1:100 (IF)
Anti-FSP1 (S100A4)	Invitrogen	#PA5-95736	1:100 (IF)
Anti-GAPDH	Cell Signaling Technology	#2118	1:1000 (WB)
Anti-H3	Cell Signaling Technology	#9733	1:1000 (WB)
Anti-H3K9me3	Cell Signaling Technology	#13969	1:1000 (WB)
Anti-Kir6.1	Alomone Labs	APC-105	1:500

Anti-Ksuccinylation	PTM bio	PTM-401	1:500 (WB)
Anti-Lamin B1	Abcam	Ab8982	1:1000 (WB) 1:250 (ICC)
Anti-MCT1	GeneTex	GTX631643	1:1000
Anti-MCT4	Santa Cruz Biotecnology	Sc-50329	1:500
Anti-pDRP1 (SER616)	Cell Signaling Technology	#3455	1:1000 (WB)
Anti-Perk1/2 (SER616)	Cell Signaling Technology	#9106	1:1000 (WB)
Anti-PKA	Abcam	Ab76238	1:1000 (WB)
Anti-SDHA	Abcam	Ab14715	1:1000 (WB)
Anti-SDHB	Atlas Antibodies	HPA002868	1:1500 (WB)
Anti-SDHD	Sigma-aldrich	SAB3500797	1:1000 (WB)
Anti-SUCNR1	Sigma-Aldrich	ab140795	1:1000 (WB)
Anti-Thrombospondin 1	Invitrogen	#MA5-13377	1:100 (IF)
Anti-TSPO	Abcam	Ab109497	1:1000 (WB) 1:1000 (IF)
Anti-TOMM20	Abcam	Ab56789	1:400 (IF)
Anti-Vinculin	Abcam	Ab129002	1:1000 (WB)
Anti-αSMA	Sigma-Aldrich	A2547	1:1000 (WB) 1:100 (IF)
Anti-αTubulin	Cell Signaling Technology	#3873	1:1000 (WB)

(B) Secondary antibodies

Name	Supplier	Catalogue number	Dilution
Goat anti-rabbit	Cell Signaling Technology	#7074	1:5000 (WB)
Horse anti-mouse	Cell Signaling Technology	#7076	1:5000 (WB)
Rabbit anti-mouse Alexa Fluor 488	Thermo Fisher Scientific	A11059	1:200 (IF)
Goat anti-rabbit Alexa Fluor 568	Thermo Fisher Scientific	A11011	1:200 (IF)
Goat anti-mouse Alexa Fluor 568	Thermo Fisher Scientific	A11004	1:200 (IF)
Goat anti-rabbit Alexa Fluor 488	Thermo Fisher Scientific	A11008	1:200 (IF)

Table 1. List of primary (A) and secondary (B) antibodies used in all experiments. IF indicates Immunofluorescence and WB indicates western blot.

3.1.6 Gas Chromatography-Mass Spectrometry (GC-MS)

Tumour cells ($5x10^5$) were collected and subjected to extraction using a mixture of MeOH:H_2O (4:1) containing 1 µg/mL of norvaline, used as internal standard. Samples were sonicated and centrifuged at 15,000 g. for 10 min at 4℃ The supernatant was

collected, and dried polar metabolites were derivatized with 10 µL of methoxyamine hydrochloride in pyridine (40 mg/mL) (Sigma-Aldrich) at 37℃ for 1.5 h.

Then, 50 µL of N-tert-butyldimethylsilyl-N-methyltrifluoroacetamide with 1% tert-butyldimethylchlorosilane (Sigma-Aldrich) were added and samples were incubated at 60°C for 30 min. Samples were acquired on an Intuvo 9000 GC System 5977B MSD (Agilent Technologies). Sample (1 µL) was injected into a HP-5MS UI GC column in splitless mode using an inlet temperature of 240℃. GC runs were performed with helium as carrier gas at 1.1 mL/min. The GC oven temperature ramp was from 70℃ to 280℃. The first temperature ramp was from 70℃ to 140℃ at 3℃/min. The second temperature ramp was from 140℃ to 150℃ at 1°C/min. The third temperature ramp was from 150℃ to 280℃ at 3℃/min. The measurement of metabolites was performed under electron impact ionization at 70 eV using a SIM mode. The ion source and transfer line temperatures were set to 230℃ and 290℃, respectively. For the determination of relative metabolite abundances, the integrated signal of selected ions for each metabolite was normalized by the signal from norvaline and cell protein content.

3.1.7 Immunofluorescence

Cells were cultured into 12-well plates or on 8-well chambered slides (Sigma-Aldrich, C7182). Reached the right confluence, cells were washed twice in warm PBS for 5 minutes and after fixation with PFA 4% for 20 min, cells were permeabilised by incubation in 0.1% Triton X100 (Sigma-Aldrich, T8787) in PBS for 10 minutes at room temperature. The blocking of non-specific binding sites was performed with 2% of bovine serum albumin (BSA) with 0.2% triton X-100 (Sigma-Aldrich, Milan, Italy) added in PBS for 1 h at room temperature. After one wash with PBS, the primary antibodies (diluted in 1% BSA in PBS) were added for overnight incubation at 4 °C. Cells which were not incubated with primary antibodies were used as negative controls. The next day, after 2 washes with PBS for 10 minutes, cells were incubated for 1.5 h at room temperature with secondary (diluted in 1% BSA in PBS) Goat anti-Rabbit IgG secondary antibody AlexaFluor488 (green fluorescence) or Goat anti-Mouse IgG secondary antibody AlexaFluor555 (red fluorescence) (all from ThermoFisher Scientific, Milan, Italy). Nuclei were labelled with Hoechst 33342 (Sigma-Aldrich; blue fluorescence). Slides were then washed with PBS and examined with Leica Stellaris DMi8 confocal microscope. Cell fluorescence intensity was measured using ImageJ.

3.1.8 Electron microscopy

Cells ($7.5x10^5$) were pelleted by centrifugation, washed with PBS and fixed in cold 2.5% glutaraldehyde and 2% formaldehyde in 0.1 M sodium cacodylate buffer (pH 7.4) overnight at 4℃ and post-fixed in cold 1% osmium tetroxide in 0.1 M phosphate buffer (pH 7.4) for 1 h at room temperature. In parallel, small fragments of PGL tumour tissue samples were processed using the same fixation and post-fixation protocol. The samples were then dehydrated in graded acetone, passed through propylene oxide and embedded in epoxy resin (Epon 812). Ultrathin sections were stained with gadolinium acetate and alkaline bismuth sub-nitrate and examined by means of the JEM 1010 electron microscope (Jeol, Tokyo, Japan) at 80 kV. Micrographs were taken with the Veleta Radius (EMSIS, Muenster, Germany) digital camera connected to a personal computer with dedicated software (RADIUS EMSIS, Muenster, Germany).

Computational analysis of mitochondria and mitochondrial cristae areas and perimeters was performed using iTem Soft Imaging System Program. Briefly, the edges of mitochondria and cristae were carefully and faithfully drawn by hand, then values of the areas and perimeters were automatically calculated by the program itself.

Analysis of mitochondria-nucleus Membrane Contact Sites (nmMCSs) was performed with ImageJ by measuring the distance at their closest point between the nucleus (outer membrane) and each perinuclear mitochondrion (outer membrane). NAM were defined as nmMCSs with membrane proximity equal to or lower than 40 nm.

3.1.8 Statistical Analysis

Data analyses were performed by the computer program GraphPad Prism Version 8.3.0 for Windows (GraphPad Software). Metabolic and functional experiments were conducted at least three times independently, with three or four replicates for each experimental condition. Results are expressed as mean ± S.D. The students t-test was used to compare the means between two sets of data. One-way analysis of variance followed by Bonferroni's post hoc-test was used for multiple comparisons.

3.2 Materials and Methods to achieve aim 1 - electrophysiological properties of hPheo1

3.2.1 Cell Proliferation specific for aim 1

Cells were seeded at the density of 2.5×10^4 per well into 12-well plates, allowed to adhere overnight and then treated or not with increasing doses of glibenclamide (30

nM, 300 nM, 100 nM, 1 μM, 3 μM, 10 μM, 33 μM and 100 μM) in complete culturing medium for 6 days.

3.2.2 SDH activity

Cell homogenates (50 μg) were incubated in a phosphate buffer containing sodium azide, 2,6 dichlorophenolindophenol (DCPIP), sodium succinate, and phenazine methosulphate. Complex II specific activity was evaluated by photometry using the Victor3 1420 Multilabel Counter (Packard Instruments, PerkinElmer, Waltham MA, USA) to measure the decrease in absorbance that resulted from the oxidation of DCPIP at 600 nm [191].

3.2.3 Extracellular pH and lactate measurement

Cells were seeded into a 6-well plate with a density of 7.5×10^4 per well in complete RPMI. After 72 h, culture media were harvested, and their pH was immediately assessed by pH meter (Basic 20 pH, Crison, Barcelona, Spain). pH of RPMI medium was used as control (Ctr). For lactate measurements, Lactate Colorimetric/Fluorometric Assay Kit (Abcam, Cambridge, UK) was used, according to the manufacturer's protocol. Briefly, culture media were centrifugated at 4℃, 14,000 g for 15 min, then 2 μL/each sample in triplicates were mixed with 48 μL of Buffer and 50 μL of mix solution in a 96-well plate, and left at RT for 30 min. The absorbance was measured at 570 nm wavelength using a microplate reader VICTOR^3 1420 Multilabel Counter (Packard Instruments, Perkin-Elmer, Waltham, MA, USA) and normalized on cell number.

3.2.4 Intracellular ATP measurement

For intracellular ATP evaluation, we used the CellTiter-Glo luminescent cell viability assay (Promega Corporation, Madison, WI, USA) performed according to the manufacturer's protocol as described [192]. Briefly, tumour cells were seeded into 96-well plates at the density of 2.5 × 104 per well. After 24 h, triplicates for each cell lines were counted and used for normalization. In other three wells for each cell line, cells were washed twice in phosphate-buffered saline (PBS) and 125 μL of CellTiter-Glo and 125 μL of PBS were added into each well. The culture plates were gently shaken and incubated at room temperature for 30 min to stabilize the luminescent signal. Luminescence was measured using the Victor3 1420 Multilabel Counter (Packard Instruments, Perkin-Elmer, Waltham, MA, USA).

3.2.5 Quantitative real time-polymerase chain reaction (qRT)-PCR

The extraction of total RNA from hPheo1 Parental and SDHB-deficient cells was performed with TRIzol reagent (Life Technologies) and RNeasy Mini Kit (Qiagen), both according to the manufacturers' indications. RNA concentration and quality were measured with a Nanodrop ND-1000 (Thermo Fisher Scientific) at 260 and 280 nm. Absorbance ratios were between 2.0 and 2.1 for all samples. cDNA synthesis was carried out with the iScript cDNA Synthesis Kit (Bio-Rad Laboratories) and 100 ng of mRNA in 20-µL reaction volume, in accordance with the following protocol: 5 min at 25°C, 30 min at 42°C and 5 min at 85°C. Semiquantitative RT-PCR amplification and detection were carried out with the SsoAdvanced Universal Probes Supermix and the CFX96 Two-Color Real-Time PCR Detection System (Bio-Rad Laboratories) with the following thermal cycler conditions: 40 cycles at 95°C for 15 s and 60°C for 1 min. Gene expression analysis was performed with predeveloped assays purchased from Life Technologies (in Table 2, we report the assay list and probe IDs). The 18S ribosomal RNA subunit was quantified with a predeveloped assay and used as the housekeeping gene for the relative quantitation of the target gene based on a slight modification of the comparative threshold cycle $2^{-\Delta\Delta Ct}$ method [193].

Human assay	IDs
Snai1	Hs00195591_m1
Snai2	Hs00161904_m1
Twist1	Hs00361186_m1
Vim	Hs001855984_m1
18S	Hs99999901_s1

Table 2: Predeveloped assays and relative IDs. Snai1, Snail family transcriptional repressor 1; Snai2, Snail family transcriptional repressor 2; Twist1, twist-related protein1; Vim, vimentin.

3.2.6 Trypsin sensitivity test and adhesion assay

Cells were plated in a 12-well plate at the density of 2×10^4. After 24 h, cells were treated or not with increasing doses of glibenclamide (30 nM, 1 µM, 3 µM) in a complete culturing medium for 72 h. For trypsin sensitivity, cells were washed twice in PBS and treated with 0.05% w/v trypsin (Euroclone, Milan, Italy) for 1 minute. The detached cells were recovered, counted and normalized to a total cell number [194]. For the adhesion assay, cells were harvested and seeded in 96-well plates at the density of 1 × 104 per well. After 4 h, non-adherent cells were discarded and the remaining cells stained for 5 min with Bengal rose (0.25% in PBS, pH 7.3). After two

washing steps with PBS, cells were lysed with PBS/ethanol (1:1) for 30 min under continuous shaking. Lysates were then transferred in a 96-well plate and absorption was evaluated by Victor^3 1420 Multilabel Counter (Packard Instruments, Perkin-Elmer) at 560 nm. PBS/ethanol (1:1) was used as blank [195].

3.2.7 Electrophysiological records

For electrophysiological records, Parental and SDHB-deficient hPheo1 cells were plated at low density (2×10^4 cells per well) in standard polystyrene-treated culture dishes (35 mm×10 mm, Corning Incorporated, Corning, NY). The electrophysiological properties of the cells were evaluated at room temperature by the whole-cell patch-clamp technique as reported [196] under a Nikon Eclipse TE200 inverted microscope. Patch pipettes were obtained from borosilicate glass capillaries (GC150-7.5, Harvard apparatus LTD, Cambridge, MA, USA) by a two-stage vertical puller (Narishige, Amityville, NY, USA) to get a final tip resistance of 1.5-3 MΩ when filled with the internal solution. The pipette solution contained 130 mM KCl, 10 mM NaH2PO4, 0.2 mM CaCl2, 1 mM EGTA, 5 mM MgATP and 10 mM HEPES. The pH was set to 7.2 with TEA-OH. For SDHB-deficient cells, Mg-free solution (107 mM KCl, 1 mM K2SO4, 10 mM EGTA and 10 mM HEPES) was used (Proks et al. 2010). ATP (1–5 mM) was delivered intracellularly through the patch pipette and added as potassium salt to avoid KATP channel activation (pH maintained at 7.2 with KOH) and the KATP blocker glibenclamide was used at 20 μM. The patch electrode contained a chloride ion-coated silver wire and was held on a CV203BU head-stage (Axon Instruments, Foster City, CA, USA) connected to a three-way coarse manipulator and micro-manipulator (Narishige, Amityville, NY, USA) as well as to the Axopatch 200 B amplifier (Axon Instruments, Foster City, CA, USA). During recordings, cells were superfused at the rate of 1.8 mL/min with a physiological solution comprising 150 mM NaCl, 5 mM KCl, 2.5 mM CaCl2, 1 mM MgCl2, 10 mM d-glucose and 10 mM HEPES. The pH was set to 7.4 with NaOH. Pulse protocol generation and data acquisition were achieved by the A/D-D/A interfaces (Digidata 1200; Axon Instruments, Foster City, CA, USA) and Pclamp 6 software (Axon Instruments, Foster City, CA, USA). The RMP was measured in the current clamp mode of the 200 B amplifier using the current stimulus I = 0nA. The membrane's passive properties were evoked in voltage-clamp mode applying a voltage pulse of ±10mV starting from a holding potential (HP) of −70 mV, as reported [196, 197]. The resulting current responses were analysed by the Clampfit 9 software (Axon Instruments, Foster City, CA, USA). In particular, the

decay of the recorded passive current was fitted by an exponential function and the linear membrane capacitance (Cm) was calculated from the area under the capacitive transient current. The Cm value is used as an index of the cell surface area since the membrane-specific capacitance is assumed to be 1 μF/cm2. Membrane resistance (Rm) was calculated from the steady-state membrane current (Im) as described [197]. Ion currents were evoked from HP = −80 mV by applying step voltage pulses, 1 s long, from −80 to 50 mV, in 10 mV increments. Current–voltage relationships were estimated by measuring the steady-state current obtained in response to the applied voltage steps with on-line leak subtraction (P/4). The currents were low-pass filtered with a Bessel filter at 2 KHz. To compare properly the current amplitudes elicited in cells of different dimensions, we normalized their values to Cm. Thus, the ratio I/Cm is considered as current density.

3.3 Material and Methods to achieve aim 2 - succinate role as an oncometabolite

3.3.1 Cell proliferation, 2D migration and GC-MS specific for aim 2

Cells were seeded at the density of $1.2x10^4$ per well into 12-well plates, allowed to adhere overnight, and then treated or not with 1mM of methyl-succinate or 1mM of extracellular succinate in complete RPMI media and counted at day 2 and 3.

Cells were treated with increased doses of SCH772984 (10, 25, 50, 100 and 200nM) and counted at different time points (data not shown). Doubling times were calculated using the least square fitting method of a time series (Roth V. 2006 Doubling Time Computing).

For 2D migration, tumours cells were treated for 72 h with 1mM of extracellular succinate or 1mM of methyl-succinate, then were counted and seeded in complete RPMI at the density of $3×10^4$ per insert and allowed to adhere overnight. The next day, medium in the inserts was replaced with serum free RPMI, while complete RPMI (plus or not succinate) was used as chemoattractant in the lower wells. After 24h at 37 °C migrated cells were fixed and stained following the protocol described in General Materials and Methods. The same experimental condition was used to perform migration using the specific ERK1/2 inhibitor, namely SCH772984, with only one difference: 24h after seeding, the medium in the lower wells was replaced with complete RPMI with or without 10nM of SCH772984 and with or without succinate.

Gas Chromatography–Mass Spectrometry (GC-MS) was used to evaluate intracellular succinate levels following 1mM of Methyl-succinate treatment for 72h in

hPheo1 Parental and SDHB-deficient cells. For complete protocol see General Materials and Methods.

3.4 Material and Methods to achieve aim 3 - mitochondria interaction with the nucleus

3.4.1 siRNA transfection

Silencing RNA (siRNA) transfection was used to induce downregulation of TSPO (SI02777061, Qiagen; sense: CAUCUUCUUUGGUGCCCGATT; antisense: UCGGGCACCAAAGAAGAUGGG). Cells were seeded with a confluency of 80% for 72h siRNA experiments using Lipofectamine 3000 in OptiMEM according to the manufacturer's protocol. Lipofectamine 3000 and siRNA were separately incubated in OptiMEM and incubated for 5 minutes at room temperature. Both solutions were mixed at a 1:1 ratio and incubated for 15 minutes at room temperature and added to the cells in a dropwise manner. 24 h after siRNA transfection, media was exchanged with complete RPMI. RNA interference protocol was optimised by testing both RNAiMAX and Lipofectamine 3000 transfection reagents; 24, 48 and 72 h incubation. In control conditions, AllStars Negative Control siRNA (Qiagen,1027281) was used.

3.4.2 Cell proliferation, 2D migration and immunofluorescence specific for aim 3

hPheo1 Parental and SDHB-deficient cells were transfected to induce downregulation of TSPO. After 72h of transfection, cells were detached and counted. For proliferation, 2.5×10^4 cells were seeded into 12-well plates, let them adhere overnight and then counted at day 1, 2 and 3. For 2D migration, 3×10^4 cells were seeded into 12-well inserts and migration was analysed as reported in General Materials and Methods.

For analysis of co-localization between TSPO and Lamin B1, Parental and SDHB-deficient cells were seeded on 8-well chambered slides (Sigma-Aldrich, C7182). 24 h after seeding, cells were transfected with siRNA targeting TSPO or left untreated (as previously described). 72 h after transfection, cells were fixed and immunofluorescence was carried out as reported in General Material and Methods.

3.4.3 Perinuclear extraction

For each condition, cells were seeded in eleven 10 cm Petri dishes; after reaching a confluence of 70-80%, cells were scraped in PBS on ice. Cells from the same treatment group were combined and centrifuged at 500 g for 5 min at 4°C. The cell pellet was resuspended in extraction buffer (1M mannitol, 1M sucrose, 200 mM EGTA, 400 mM Hepes-NaOH, pH 7.4) and homogenised with 40 strokes × 3 times

using a Potter homogeniser. The homogenate was centrifuged at 2000 g for 10 min at 4°C, and the pellet was stored as a nuclear fraction. The supernatant was stored as mitochondrial and cytosolic fractions, collectively. The nuclear pellet was then resuspended in Buffer A (200 mM EGTA, 400 mM Hepes-NaOH pH 7.4, 1 M KCl, 5% glycerol, 100 mM β-glycerophosphate with 0.05% NP-40 (approximately 100 µl/plate) and incubated at 4°C for 30 min under constant agitation. The tubes were then centrifuged at 1000 g for 5 min at 4 °C; the supernatant was removed and discarded, whereas the pellet was resuspended in Buffer A without NP-40. The tubes were centrifuged at 1000 g for 5 min at 4 °C; the supernatant was discarded. The pellet was resuspended in Buffer B (1 M KCl, 100 mM Tris-HCl pH 7.4, 2 M LiCl, 25 mM MgCl2, 5% deoxycholate, Triton X-100) and incubated at 4°C for 1 hour under constant agitation. The tubes were centrifuged at 2000 g for 5 min at 4 °C, and the supernatant was collected and stored as a perinuclear fraction.

3.4.4 Proximity ligation assay (PLA)

To visualise and quantify NAM events in intact cells, hPheo1 Parental and SDHB-deficient cells were seeded in 8-well chamber slides, washed with warm PBS and fixed in 4% PFA after 24 h. Transfection with siRNA targeting TSPO or with control siRNA was performed 72 h before fixation. PLA was performed by using the Duolink® PLA Red reagents (DUO92008, Sigma-Aldrich). were permeabilised with 0.1% Triton X-100 in PBS. Blocking was performed with the Duolink® Blocking Solution for 1 hour at 37 °C. Cells were incubated with the primary antibody solution (Duolink® Antibody Diluent) for 2 h at RT and then washed two times in 1x Wash Buffer A for 5 minutes. The following primary antibodies were used: anti anti-Lamin B1 (1:250; Abcam, ab16048) and anti-TOMM20 (1:400, Abcam, ab56783). PLA probes were diluted 1:5 in Duolink® Antibody Diluent. Cells were incubated with the PLA probes for 1 hour at 37 °C and then washed twice in 1x Wash Buffer A for 5 minutes. Ligation was performed for 30 minutes at 37 °C with 1 µl Ligase in 40 µl Duolink® Ligation Solution per reaction, followed by two washes in 1x Wash Buffer A for 5 minutes. 0.5 µl Polymerase was added to 40 µl Duolink® Amplification Buffer per reaction for probe amplification. Coverslips were incubated in a pre-heated humidity chamber for 100 minutes at 37 °C. Amplification was followed by two washes in 1x Wash Buffer B for 10 minutes, followed by one wash with 0.01x Wash Buffer B. A cover glass pre-heated at 37 °C was then mounted using a mounting medium with DAPI (Abcam, ab104139).

3.4.5 Measurement of mitochondrial superoxide (O_2^-) levels

Mitochondrial superoxide levels were detected with mitoSOX™ Red (Life Technologies, M36008); 1.5 x 10^5 cells were seeded in 35 mm imaging dishes. The day after, cells were incubated for 30 minutes at 37˚C, protected from light, with 25nM solution of mitoSOX™ Red. The media is than replaced with a live-cell imaging solution (Thermo Fisher Scientific, A59688DJ) and cell were imaged onto a Zeiss LSM510 confocal microscope.

3.4.6 Measurement of hydrogen peroxide (H_2O_2) levels

To measure intracellular mitochondrial H_2O_2 levels, genetically encoded, ratiometric fluorescent HyPer-dMito was employed. 1.5 x 10^5 cells were seeded in 35 mm imaging dishes. The day after, cells were transfected with the respective construct with Lipofectamine 3000 (following the manufacturer's instruction) and using 1.6 uL Lipofectamine and 1.1 ug construct (HyPer-dMito). The transfection mix was removed after 24 h from transfection and replaced with the warm culturing medium. 36 to 40 h after transfection, the growth medium was replaced with a live-cell imaging solution (Thermo Fisher Scientific, A59688DJ), and the cell culture dish was placed on the stage of a Nikon Eclipse Ti-E inverted fluorescence microscope (Nikon) with a CFI S Fluor 40x/1.30 oil immersion objective. Regions of interest (ROIs) were selected using the Andor iQ2 software to obtain HyPer fluorescence emission values at 420 nm and 500 nm. The plasmids encoding the hydrogen peroxide (H_2O_2) HyPer-dMito was purchased from Evrogen (Moscow, Russia).

3.4.7 Lipid Peroxidation Assay

To measure lipid peroxidation was employed C11BODIPY™ 581/591. Briefly, hPheo1 Parental and SDHB-deficient cells were seeded into 8-well chamber for live cell imaging (Sigma-Aldrich, C7182) at the density of 1x10^4. The day after, cells were loaded with C11-BODIPY (5 μM), and fluorescence was measured after 20 minutes using a Zeiss LSM510 confocal microscope.

3.5 Material and Methods to achieve aim 4 - crosstalk between hPheo1 and endothelial cells

3.5.1 Cell proliferation, 2D migration and immunofluorescence specific for aim 3

hPheo1 Parental or SDHB-deficient cells were seeded (2.5×10^4) into 12-well plate inserts (control single culture) and for co-culture, HUVECs (2.5×10^4) in the well below. After 24 h at 37°C, before starting the co-culture, the medium in the inserts and in the wells below was replaced with co-culture media, and cells were counted after 24 and

72 h. To evaluate hPheo1 Parental and SDHB-deficient 2D migration in the presence or absence of endothelial cells, tumours cells were seeded in complete RPMI at the density of 3×10^4 per insert while HUVECs were seeded into 12-well plates at the same density in complete EBM, and vice-versa. The next day, before starting the co-culture, the medium in the inserts was replaced with serum free co-culture media, while complete co-culture media was used as chemoattractant in the lower wells. After 16 h at 37 °C migrated cells were fixed and stained following the protocol described in General Materials and Methods.

For immunofluorescence experiment, HUVECs were seeded ($3x10^4$ cells) in complete EBM into 24-well plate and incubated in a 5% CO_2 atmosphere at 37 °C. Once they reached confluency, co-culture with hPheo1 Parental and SDHB-deficient cells seeded into 24-well inserts ($3x10^4$ cells/ insert) was performed for 72h.

3.5.2 Conditioned medium

To obtain conditioned medium, tumour cells ($3x10^6$ hPheo1 SDHB-deficient and 2×10^6 hPheo1 Parental) were seeded in a 100cm dish in complete RPMI medium and allowed to adhere overnight. The next day, the culture medium was replaced with fresh co-culture media. After 48 h, the supernatant was collected, centrifuged for 10 min, 4°C at 2600 *rpm* and the supernatant (conditioned medium) used for further experiments.

3.5.3 Extracellular Vesicles (EVs) isolation and Nanoparticle Tracking Analysis (NTA)

Conditioned media from hPheo1 Parental and hPheo1 SDHB-deficient was centrifuge at 100000g, 4°C for 1h using a Beckman Coulter Optima XPN-100 ultracentrifuge. Nanoparticle tracking analysis was performed on a NanoSight NS300 (Malvern Panalytical, Westborough, MA, USA) equipped with a 488 nm excitation laser and an automated syringe sampler (Figure 11). NanoSight technology calculates size and concentration based on the relationship between Brownian motion and hydrodynamic diameter through the Stokes–Einstein equation. Samples were diluted 1:500 in PBS and loaded into 1 ml syringes. CSV files generated by NTA by software v3.2 were used for computational analysis.

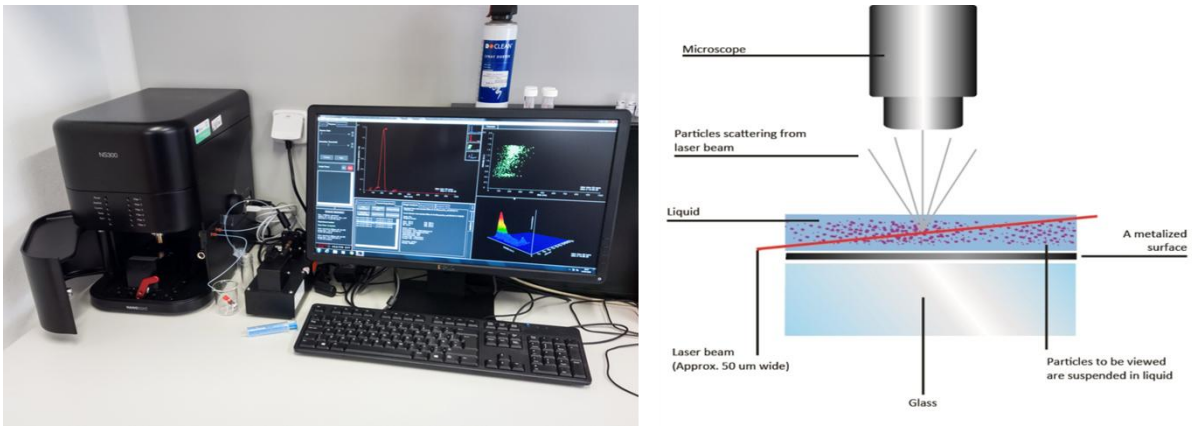

Figure 11: Image of the Nanosight ns300 (left) and magnification of the microfluidic system (right).

3.4.4 *In vitro* capillary morphogenesis assay

In vitro capillary morphogenesis was performed in 96-wells coated with 50µl of Corning Matrigel Basement Membrane Matrix (BD Bio-sciences). HUVECs were plated ($1.5x10^4$/well) in EBM, in conditioned medium or in a culture medium enriched with EVs (EVs secreted by Parental or SDHB-deficient cells) and in the supernatant counterparts. HUVECs were than incubated at 37°C and 5% CO_2. After 6 h pictures were acquired with a Leica AM6000 inverted phase contrast fluorescence microscope. Quantification and statistical analysis were performed using the Angiogenesis Analyzer tool for ImageJ.

3.5.5 FICT-dextran Permeability assay

HUVEC ($1x10^5$ cells) were seeded on top of the 0,4 µm pore size transwell inserts in 300µl of complete EBM while hPheo1 Parental and SDHB-deficient ($1x10^5$ cells) were seeded in each well of a 24-well plate in RPMI complete medium. After 24 h at 37° C, before starting the co-culture, the medium in the inserts and in the wells was replaced with co-culture media. After 72h of co-culture, Hanks' Balanced Salt Solution (HBSS) 600µl was added to the lower chambers of a 24 well plate, and 100µl of HBSS containing Fitc-Dextran (1 µg/mL) was added to the upper chambers. The plate was incubated for 3 h at 37°C. The amount of Fitc-dextran in the lower compartments was quantified at 535 nm by the spectrophotometer VICTOR^3 1420 Multilabel Counter (Packard Instruments, Perkin-Elmer). A standard curve of Fitc-dextran (0-1 µg/mL) was used for the determination of FITC-dextran abundances in each sample (Figure 12).

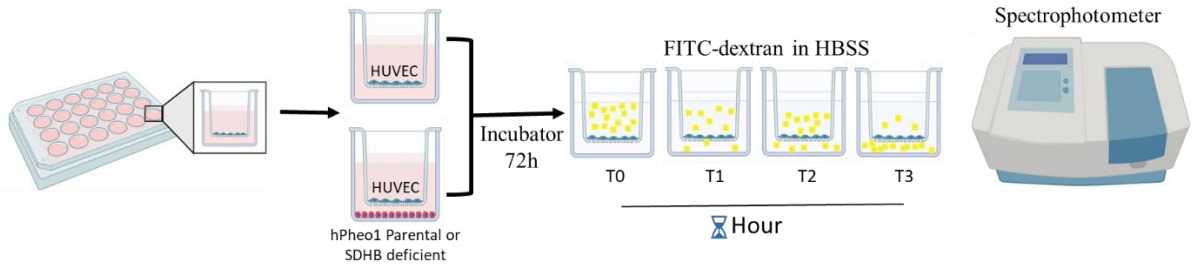

Figure 12: Workflow of the FITC-Dextran permeability assay.

3.6 Material and Methods to achieve aim 5 - hPheo1 communication with the stroma

3.6.1 Cell proliferation and 2D migration specific for aim 4

hPheo1 Parental or SDHB-deficient cells were seeded (3×10^4) into 24-well plate inserts (control single-culture) and for co-culture, Human Primary CAFs (1.2×10^4) in the well below and vice-versa. The next day, the co-culture was performed. The proliferation was assessed by counting the cells seeded in the lower wells. CAFs proliferation was evaluated after 3 days while hPheo1 proliferation was assessed at day 2, 3 and 6.

For 2D migration, Human Primary CAFs were seeded at the density of 1.2×10^4 cells per insert while $3x10^4$ hPheo1 cells per well were seeded into 12-well plate.

For immunofluorescence experiment, $1.2x10^4$ of Human Primary CAFs were seeded in complete RPMI into 12-well plate and incubated in a 5% CO_2 atmosphere at 37 °C until confluent.

3.6.2 Lentiviral transduction

HEK293T cells (7.5–10×10^6) were seeded in 75cm² flasks in 10 ml DMEM supplemented with 10% foetal bovine serum (FBS) and 1% L-glutamine. The following day, when cells reached 50–80% confluence, a plasmid mixture consisting of psPAX2 (packaging plasmid), pMD2.G (envelope plasmid), and the transfer plasmid (pCDH-EF1a-eFFly-mCherry/eGFP) was prepared (Figure 13). The plasmids were diluted in Opti-MEM and combined with polyethyleneimine (PEI) to form transduction complexes. After replacing the medium with fresh DMEM containing 10% FBS, the DNA/PEI mixture was added dropwise to the HEK293T cells, followed by gentle rocking to ensure even distribution. Cells were maintained at 37°C in a humidified incubator with 5% CO_2. After 5 days, the culture supernatant containing lentiviral particles was collected and centrifuged at 1000 rpm for 5 min to remove cells and debris. The clarified supernatant was subsequently filtered through a 0.45 µm filter (Steriflip, Millipore, or syringe filter). Viral titers were determined, and

the resulting lentivirus was stored at −80°C or used immediately for transduction. For transduction, hPheo1 Parental and SDHB-deficient cells were seeded in 6-well plates at a density of 3×10^5 cells per well and allowed to adhere to for at least 3 h. Subsequently, 300µl of the previously produced lentiviral supernatant was added dropwise to each well. Cells were incubated with the viral suspension for 18 h at 37°C in a humidified incubator with 5% CO_2. Following incubation, the medium was replaced with fresh culture medium. Transduced cells were maintained under standard culture conditions until further expansion and subsequently subjected to fluorescence-activated cell sorting (FACS) to isolate successfully transduced populations.

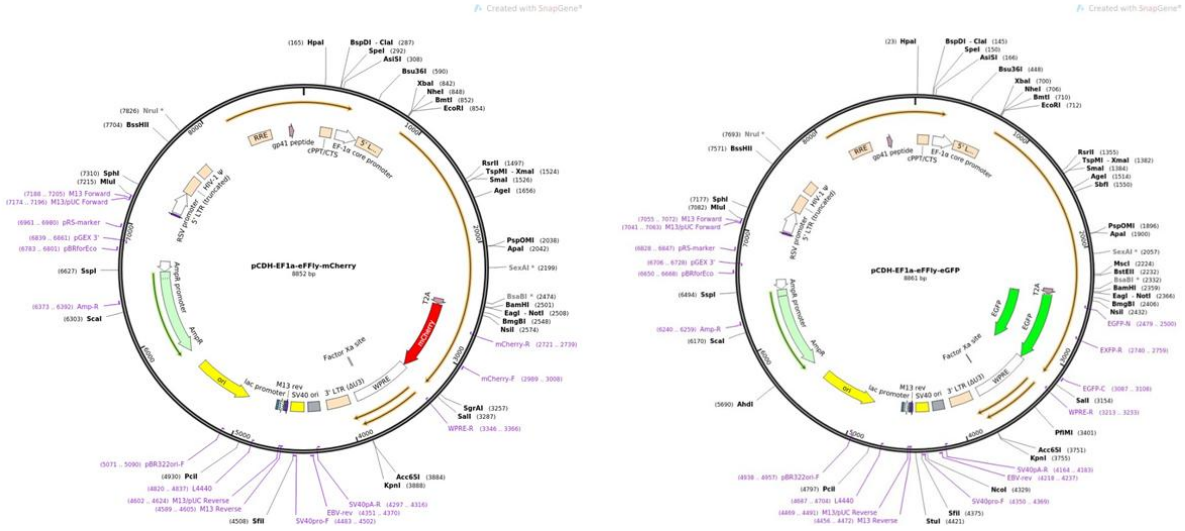

Figure 13: Plasmid maps of lentiviral vectors used for transduction: schematic representations of the plasmids pCDH-EF1α-eFFLy-mCherry and pCDH-EF1α-eFFLy-eGFP.

3.6.3 Spheroid induction

To generate cancer spheroids (Figure 14), 5 × 10^3 tumour cells were added into each well of a round, low adherence, bottomed 96-well plates. Plates were then centrifuged at 300 *g* at room temperature for 10 min to initiate cell-cell interaction, and incubated at 37 °C, 5% CO_2. After 72 h, spheroids were easily handled using a regular pipette without dissociating and were used for experiments [198].

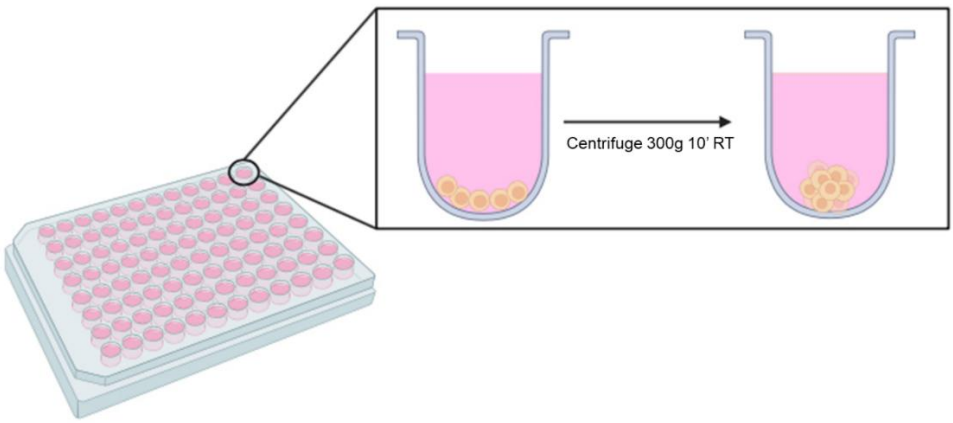

Figure 14: schematic representation of the workflow for spheroids induction.

3.6.4 3D migration

To determine the effects of fibroblasts on spheroids migration, Human Primary CAFs were seeded in 8-well chambers (1×10^4 cells/well). The next day, mCherry SDHB-deficient spheroids were selected and individually laid on the monolayer of Human Primary CAFs. Bright field images of the spheroids were acquired after 4h by an AxioCam MRc digital camera for an inverted microscope Axiovert25 (Zeiss). After 72 h, cell nuclei were stained with Hoechst and images were acquired using Leica Stellaris DMi8 confocal microscope. Using ImageJ software, areas were calculated by drawing circles around the spheroids. Cell migration areas were calculated as the difference between areas at day 0 and days 3.

3.6.5 RNA isolation

Fibroblasts ($3x10^4$ per well) were seeded in a 6-well plate in complete RPMI medium and let them grow until confluence at 37°C and 5% CO_2. Tumour cells ($1.5x10^5$ hPheo1 Parental and SDHB-deficient) were seeded in complete RPMI medium in 3µm pore size transwell inserts (Greiner Bio-one, Kremsmünster, Austria) and allowed to adhere overnight. The next day, co-culture with fibroblasts was performed. After 72h, the extraction of CAF total RNA from each well was performed with TRIzol reagen (Life Technologies) and RNeasy Mini Kit (Qiagen), both according to the manufacturers' indications. RNA concentration and quality were measured with a Nanodrop ND-1000 (Thermo Fisher Scientific) at 260 and 280 nm. Absorbance ratios were between 2.0 and 2.1 for all samples. RNAseq was performed, and differential gene expression was assessed using the DESeq2 R package. Enrichment analyses (GO, GSEA, and EnrichR) were conducted to identify dysregulated pathways. Comparisons across fibroblast batches were used to detect consistent gene expression patterns and shared biological responses to tumour co-culture.

4. Results

4.1 Results aim 1 - electrophysiological properties of hPheo1

The following results has been published on Endocrine-related cancer. doi: 10.1530/ERC-23-0167.

4.1.1 Depletion of SDHB impairs cell metabolism.

The efficiency of knocking out the SDHB subunit in hPheo1 cells was confirmed by Western blotting, which showed very low levels of the SDHB protein, while it did not affect the levels of other subunits such as SDHA or SDHD (Figure 15A). In SDHB-deficient cells, we also observed a functional impairment of SDH enzyme activity that was significantly reduced by approximately 50%, compared to Parental cells (Figure 15B). Moreover, the alteration of SDH function was also demonstrated by a considerable increase in the intracellular succinate/fumarate ratio, coupled with a decrease in the intracellular ATP concentration in SDHB-deficient cells compared to Parental cells (Figure 15C and D, respectively). We also observed a significant accumulation of intracellular lactate in SDHB-deficient cells (Figure 15E), further supporting a marked metabolic shift from oxidative phosphorylation to aerobic glycolysis. This was linked to a significant decrease of pH (6.998 ± 0.04 vs 7.23 ± 05) and to a significant increase of lactate (9.7 ± 0.09 vs 5.3 ± 0.15) in culture media of SDHB-deficient cells compared to that of Parental (Figure 15F and G, respectively). Accordingly, we found increased expression of the MCT4, while MCT1 expression was not affected (Figure 15H).

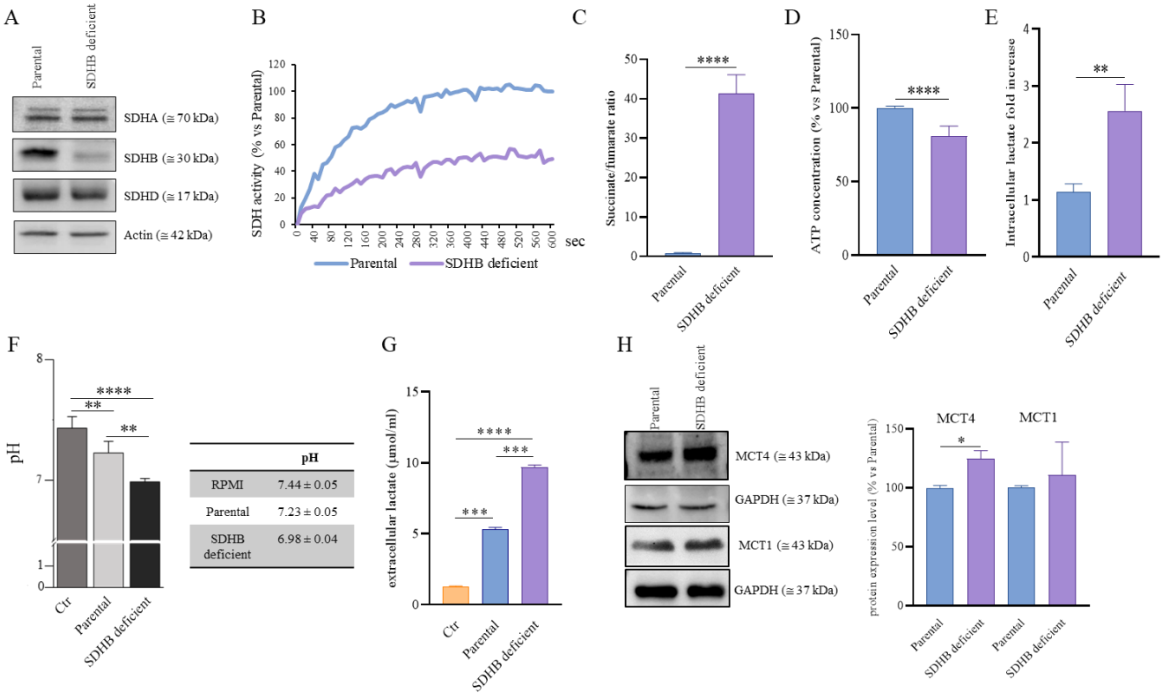

*Figure 15: Effects of SDHB depletion on cell metabolism. (A) Representative blots showed the levels of SDHA, SDHB and SDHD subunits. Actin was used as loading control. (B) Representative traces of SDH enzymatic activity measured in Parental and SDHB-deficient homogenates. The SDHB-deficient cells (dark grey line) showed a decrease in SDH activity of approximately 60% compared with Parental (light grey line). (C) The bar graph shows the significant increase of the intracellular succinate/fumarate ratio, assessed by GC/MS, in SDHB-deficient cells compared with Parental. (D) Intracellular ATP concentration in SDHB-deficient cells was significantly reduced compared to Parental cells. (E) A significant increase in intracellular lactate levels, measured by GC/MS, was observed in SDHB-deficient cells. (F) pH measurement showed acidification of the media of both Parental and SDHB-deficient cells, but the pH of SDHB-deficient cell media was significantly lower than that of Parental cells. (G) Extracellular lactate concentration was significantly higher in SDHB-deficient cells compared to Parental ones. (H) Representative blots and densitometric evaluation of MCT4 expression, which was significantly upregulated in SDHB-deficient cells vs Parental ones, and MCT1 expression, which was unchanged between the two cell populations. GAPDH was used as loading control. Bar graphs are derived from three or four independent experiment, each of them conducted in triplicate, ± s.d. (*P < 0.05, **P < 0.01, ***P < 0.001, ****P < 0.0001.)*

4.1.2 SDHB-deficient cells display mitochondrial cristae disorganization and epithelial – mesenchymal transition (EMT)-like phenotype.

Electron microscopy analysis revealed less compact mitochondrial cristae in SDHB-deficient cells compared to Parental ones (Figure 16A). This observation was demonstrated by the computational analysis of mitochondria and mitochondrial cristae areas and perimeters in our cells (Figure 16B). SDHB-deficient cells showed both mitochondria and cristae areas higher than those of the Parental ones, but interestingly, perimeters did not differ between the two cell populations, confirming that in SDHB-deficient cells, mitochondria were swollen and cristae were less compact. Recently, Tabebi and colleagues [199] found that several genes involved in EMT were upregulated in hPheo1 SDHB-deficient cells compared with controls. By

qRT-PCR, we confirmed that the expression of the main markers of EMT, such as Twist1, Snai1, Snai2 and Vimentin, was significantly increased in SDHB-deficient cells (Figure 16C), suggesting that these cells undergo a transcriptional reprogramming associated with an EMT phenotype.

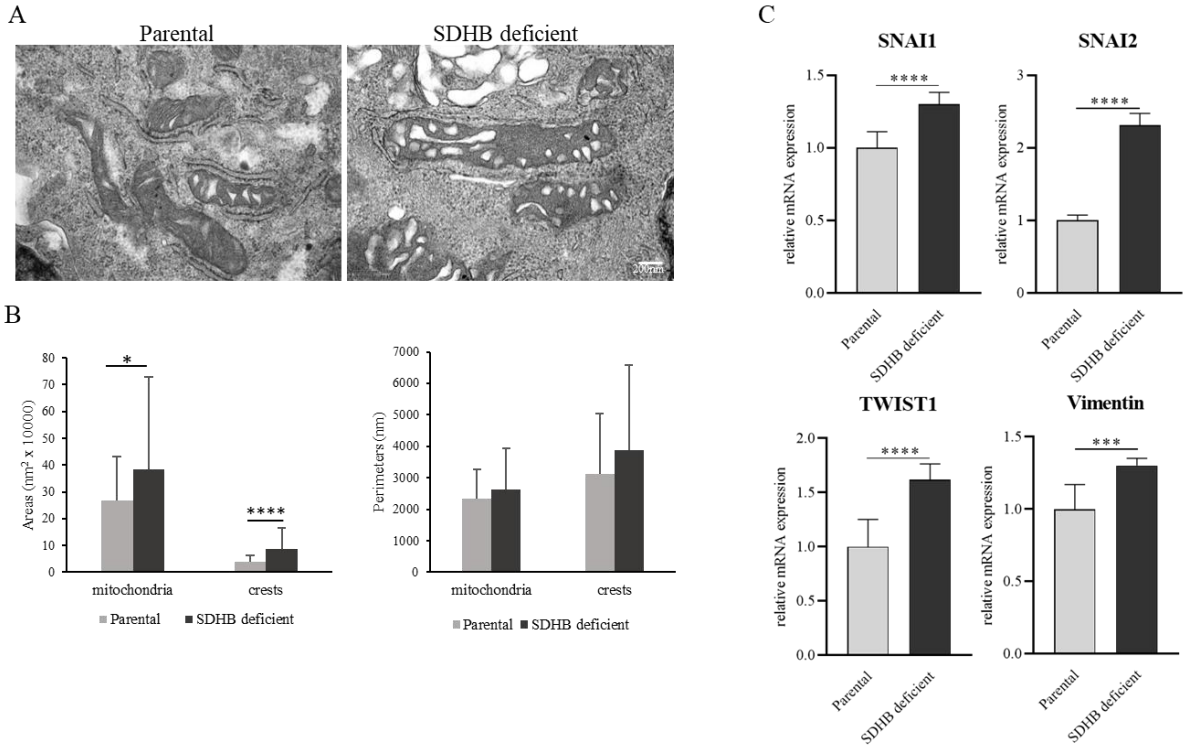

*Figure 16: Characterization of mitochondrial morphology and EMT process. (A) Ultrathin sections of Parental and SDHB-deficient cell were examined under a JEM 1010 electron microscope. Micrographs were taken using a Veleta Radius digital camera (EMSIS, Muenster, Germany). In SDHB-deficient cells, mitochondrial cristae appear slightly less compact than in Parental cells. Scale bar = 200 nm. (B) The bars graph showed the areas and perimeters or mitochondria and mitochondrial cristae in Parental (n = 44) and SDHB-deficient cells (n = 33). In SDHB-deficient cells, the areas of both mitochondria and mitochondrial cristae were significantly increased compared to Parental ones. On the other hands, no significant differences were observed in mitochondria and cristae perimeters. The analysis was obtained using iTem Soft Imaging System program. (C) qRT-PCR analysis demonstrated a significant upregulation of Snai1, Snai2, Twist1 and Vimentin in SDHB-deficient cells compared to the Parental ones. (*P < 0.05, ***P < 0.001, ****P < 0.0001.)*

4.1.3 Membrane electrical features and K+ currents in SDHB-deficient cells: effects of glibenclamide and ATP.

Unlike other pheochromocytoma cell lines, such as the mouse pheochromocytoma cell (MPC) line and the mouse tumour tissue-derived cell (MTT) line, hPheo1 cells do not grow in clusters, allowing us to analyse the electrophysiological properties of single cells by the whole cell patch-clamp technique. We first measured the RMP values of the two cell populations in the current clamp mode. SDHB-deficient cells resulted in being significantly more polarized (−11.9 ± 11.7 mV; n = 23) than Parental cells (−5.8 ± 6.1 mV; n = 20) (Figure 17A). We then analysed the cell passive properties that represent membrane electrical features allowing excitable cells to

conduct electrical impulses without involving voltage-dependent ion channels. They determine the membrane potential changes in response to current across the cell membrane (linearly with a current stimulus application). They are mainly represented by Rm and Cm that herein were estimated from current traces evoked by suitable step voltage pulses, sufficiently negative to avoid the appearance of voltage-dependent currents. The pulse protocol of stimulation and the typical current responses are depicted in Figure 17B. The calculated Cm values, used as an index of cell surface area, were found to be significantly smaller in SDHB-deficient than in Parental cells, being 10.2 ± 8.5 pF (n = 17) and 31.6 ± 28.9 pF (n = 12), respectively (Figure 17C). Rm values in SDHB-deficient (647.05 ± 700.1 MΩ; n = 30) did not show statistically significant differences compared to Parental cells (982.03 ± 1449.1 MΩ, n = 37), suggesting a scarce effect of this condition on membrane-resting permeability (Figure 17D).

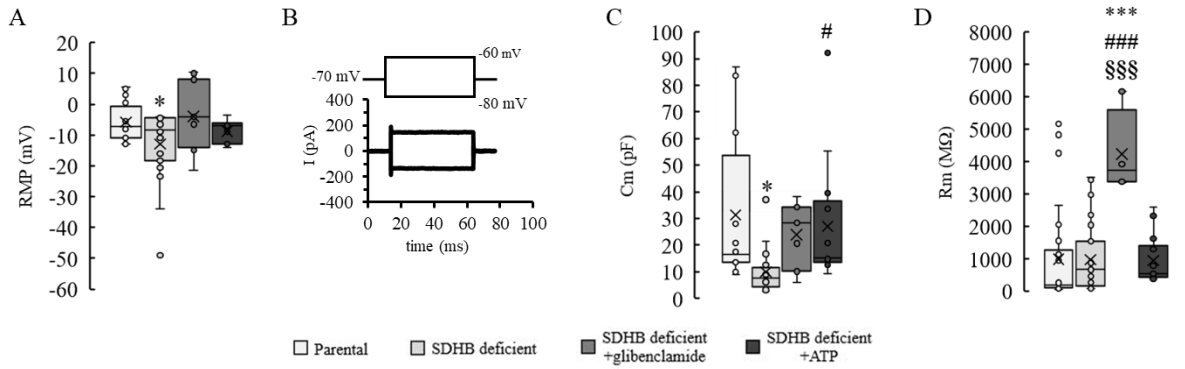

*Figure 17: Analysis of Parental and SDHB-deficient cell membrane passive properties. Data related to all of the conditions have been here plotted together to better highlight differences and similarities. (A) Resting membrane potential, RMP (in mV), evaluated in current-clamp mode with I = 0 nA in Parental cells (n = 20), SDHB-deficient cells (n = 23), SDHB-deficient cells + glibenclamide (n = 11) and SDHB-deficient cells after intracellular delivery of ATP by the patch pipette (n = 11). SDHB-deficient cells showed significantly more hyperpolarized RMP compared to Parental cells, but in the presence of glibenclamide and ATP, RMP was restored. (B) Voltage pulse protocol of stimulation (upper panel) and typical passive currents (lower panel) obtained in response to its application under voltage clamp condition. (C) Cell capacitance, Cm (in pF), estimated in voltage-clamp mode in Parental cells (n = 12), SDHB-deficient cells (n = 17), SDHB-deficient cells + glibenclamide (n = 7) and SDHB-deficient cells after intracellular delivery of ATP by the patch pipette (n = 13). Cm is significantly smaller in SDHB-deficient cells compared to Parental cells. Cm significantly increased after ATP delivery in SDHB-deficient cells compared to SDHB-deficient ones. Cm of SDHB-deficient cells + glibenclamide or + ATP and Parental ones were not significantly different. (D) Membrane resistance, Rm, values (in MΩ) measured in Parental cells (n = 37), SDHB-deficient cells (n = 35), SDHB-deficient cells + glibenclamide (n = 8) and SDHB-deficient cells after intracellular delivery of ATP by the patch pipette (n = 20). Rm values obtained in the presence of glibenclamide resulted significantly bigger compared to any other condition. Data are mean values ± s.d. (*P < 0.05, ***P < 0.001 vs Parental; #P < 0.05, ###P < 0.001 vs SDHB deficient; §P < 0.05; §§§P < 0.001 vs SDHB deficient + ATP. One-way ANOVA, with Bonferroni's correction).*

Analysis of ion currents under voltage clamp condition (pulse protocol depicted in Figure 18A) recorded from Parental cells revealed the occurrence of outward K+

currents with the time course and I–V relation typical of voltage-dependent currents [200], with a voltage activation threshold of about −10 mV (Figure 18B and F, respectively). In contrast, analysis of SDHB-deficient cells revealed a larger mean current amplitude and a lack of voltage threshold significantly different to Parental cells, as shown in Figure 18C and F, respectively. Notably, this greater outward current agrees with the observed resting membrane potential that is more hyperpolarized in SDHB-deficient cells than in Parental cells. Since the related I–V plot brought to mind that reported for ATP-sensitive K+ currents [201], and since these cells showed reduced intracellular ATP content because of SDHB deficiency, to test the occurrence of possible KATP currents, we performed two different sets of experiments. In the first, we used the specific KATP channels inhibitor, glibenclamide [201]. In the second, to overcome the effect of low intracellular concentration of ATP on KATP channels, we carried out experiments in which intracellular ATP content was raised by adding the nucleotide in the form of a K+ salt [202]. Interestingly, both glibenclamide and ATP caused a significant reduction in outward currents compared to those recorded from SDHB-deficient cells (Figure 18D, E and F, with a statistical significance at voltage steps from −30 up to +50 mV and for any voltage step positive to −10 mV, respectively). Moreover, the outward currents recorded in the presence of glibenclamide or ATP resulted not significantly different from those of the Parental cells. Noteworthy, glibenclamide also restored the voltage threshold of appearance at −10 mV, as observed in Parental cells (Figure 18F). These results indicate the presence of the KATP current in the overall currents recorded in these cells. We also evaluated whether the difference in K+ currents might have been associated with a different expression of the KATP channel Kir6.1, but as shown in Figure 18G, Kir6.1 was not differentially expressed in the two cell populations. A similar outcome was observed for passive properties when glibenclamide or ATP was added to the bath solution. In fact, when compared to those measured from untreated SDHB-deficient cells, the RMP values tended to be more depolarized after glibenclamide addition, being −4.02 ± 10.4 mV (n = 11; Figure 17A), Cm values increased to 24.22 ± 12.2 pF (n = 7, Figure 17C) and, as expected, following the use of a channel blocker, Rm significantly increased to 4235.1 ± 1215.8 MΩ (n = 8) (Figure 17D). In ATP-rescued SDHB-deficient cells, RMP value increased to −8.8 ± 3.5 mV (n = 11, Figure 17A), Cm increased to 27.32 ± 23.7 (n = 14, Figure 17C) and Rm increased to 936.7 ± 733.9 MΩ (n = 20) (Figure17D) compared to those recorded from untreated SDHB-

deficient cells. Again, after both treatments, the passive properties of the SDHB-deficient cells were no longer statistically significant from those of Parental cells, suggesting a partial recovery of biophysical properties induced by blocking KATP channels. Overall, these data indicate that one of the main differences between SDHB-deficient and Parental cells' bioelectric profiles is due to KATP channel engagement in the former population.

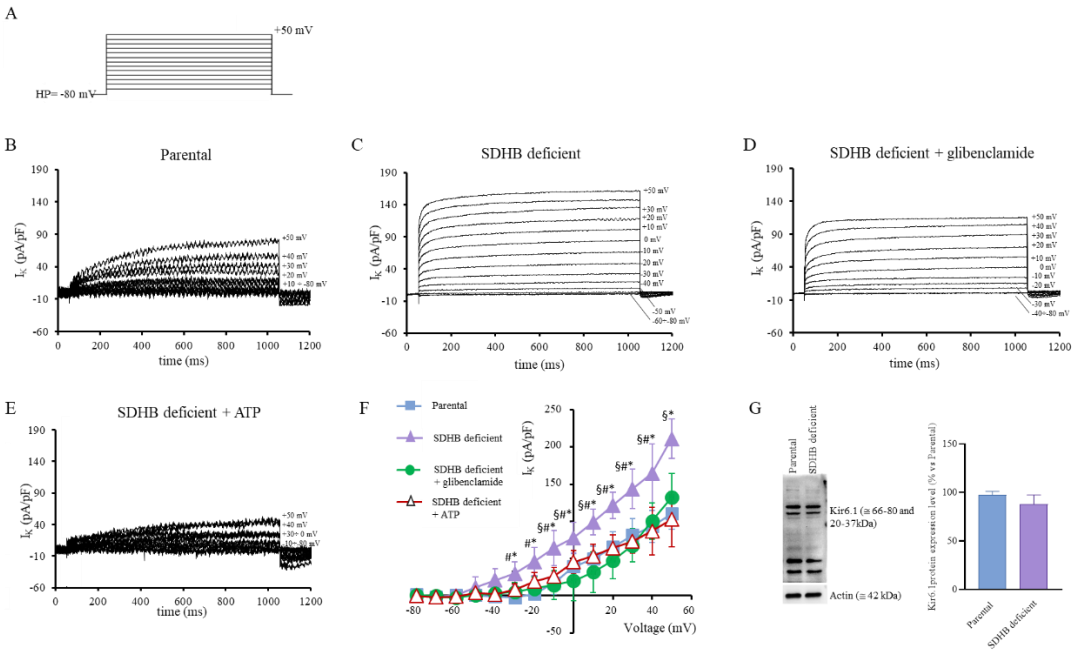

*Figure 18: Analysis of K+ currents in Parental and SDHB-deficient cells: effects of glibenclamide and ATP. (A) Voltage pulse protocol of stimulation (HP = −80 mV) used to evoke the current responses. Representative traces of normalized outward K+ currents (pA/pF) elicited in a Parental (B) and in a SDHB-deficient cell (C). (D) Typical records obtained in the presence of the selective KATP blocker glibenclamide (20 μM) in the same SDHB-deficient cell as reported in B. (E) Representative traces of normalized outward K+ currents (pA/pF) evoked in an SDHB-deficient cell after intracellular delivery ATP by the patch pipette. (B–E) The voltage step pulse evoking each current response is indicated in mV next to the corresponding trace. When current responses are superimposed, this indication is given as a voltage range for clarity. (F) I–V curves related to IK in Parental (n = 4), in SDHB-deficient cells in the absence (n = 4) and in the presence of glibenclamide 20 μM (n = 4) and in ATP-rescued SDHB-deficient cells (n = 4), here plotted together to better highlight differences and similarity. Data from SDHB-deficient cells are significantly different from those obtained in Parental cells starting from voltages more depolarized than −30 mV (*P < 0.05). Results from SDHB-deficient cells + glibenclamide and from ATP-rescued SDHB-deficient cells are not significantly different neither between them (P > 0.05) nor compared to Parental cells (P > 0.05) for any voltage step applied. In contrast, statistically significant differences were observed for SDHB-deficient cells + glibenclamide vs SDHB-deficient cells starting from −30 mV up to +50 mV (#P < 0.05) and for ATP-rescued SDHB-deficient cells vs SDHB-deficient cells for any voltage step positive to −10 mV (§P < 0.05). Data are mean values ± s.d. One-way ANOVA, with Bonferroni's correction. (G) Representative blots (left) and densitometric evaluation (right) of Kir6.1 expression level, which did not differ between Parental and SDHB-deficient cells. Actin was used as a loading control.*

4.1.4 Functional characteristics of SDHB-deficient cells are related to their bioelectrical features.

We next investigated whether Parental and SDHB- deficient cells showed differences in their functional characteristics and whether, by restoring the electrophysiological

properties of SDHB-deficient cells by glibenclamide, the differences in functional features could also be eventually re-established. First of all, when we analysed cell growth, we found that SDHB-deficient cells had a reduced proliferation rate compared to Parental cells (Figure 19A). Interestingly, we observed that the number of SDHB-deficient cells was significantly increased after 6 days of glibenclamide (1 and 3μM) treatment compared to the untreated counterpart. In contrast, the treatment with the same doses of the KATP channel inhibitor on Parental cells did not have the same effect. The treatment with glibenclamide 30nM did not influence either Parental or SDHB-deficient cell proliferation (all the doses tested are reported in figure 19F. On the original paper, see Supplementary Figure 1). We next tested whether SDHB-deficient and Parental cells were sensitive to detachment after trypsinization for 1 min. This test is used to distinguish differentially adherent cell types [203]. We found that the number of SDHB-deficient cells detached after trypsin treatment was significantly higher compared to Parental cells. Interestingly, glibenclamide treatment, at all the doses tested, was able to reduce the number of SDHB-deficient cells detached (Figure 19B). In another experiment, we investigated the adhesion potential of both Parental and SDHB-deficient cells in the presence or not of glibenclamide. After 4h of plating, non-adherent cells were removed while adherent ones have been quantified using Bengal rose staining. By this assay, we showed that SDHB-deficient cells had a significantly lower adhesion capacity compared to Parental cells (Figure 19C), but glibenclamide addition induced a significant increase in adhesion in these cells. In contrast, glibenclamide did not cause appreciable effects in Parental cells. To further explore the migration abilities of the two cell lines, we used the transwell assay technique, in which we stained the migrated cells (Figure 19D) and quantified the eluted dye by optical density (Figure 19E). We found that SDHB-deficient cells showed a significantly higher migration ability compared to Parental cells, regardless the absence or presence of the chemoattractant, represented by the serum, in the lower wells. Moreover, we observed a significant reduction of SDHB-deficient cell migration only after the administration of 1μM glibenclamide for 16 h. On the contrary, glibenclamide did not have any effects on Parental cell migration.

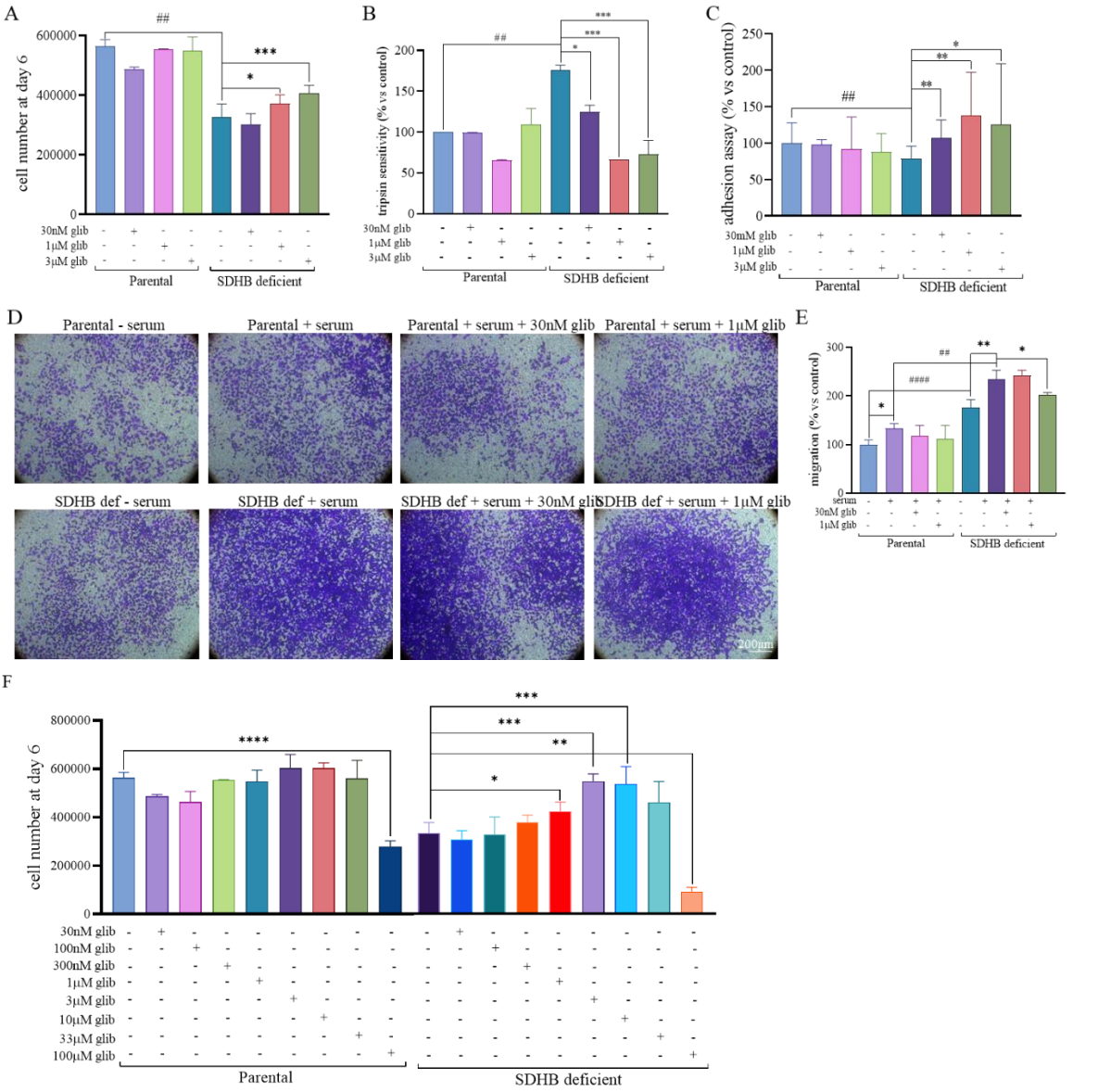

Figure 19: Analysis of functional properties and role of glibenclamide in their modulation. (A) Cell number at day 6 in the absence (black bars) or in the presence of 30 nM (white bars), 1 µM (dark grey bars) and 3 µM (light grey bars) of glibenclamide (abbreviation: Glib). SDHB-deficient cells significantly increased their growth capacity after 1 µM and 3 µM of glibenclamide treatment. The administration of 30 nM of glibenclamide did not affect the proliferation of both cell populations. (B) SDHB-deficient cells displayed higher sensitivity to trypsin treatment compared to Parental cells. This sensitivity was significantly reduced by glibenclamide at all doses. (C) Adhesion capacity was assessed using the Bengal rose assay. SDHB-deficient cells showed a significantly less efficient adhesion capability compared to Parental cells. All doses of glibenclamide tested caused a significant increase in SDHB-deficient adhesion capacity. (D) Parental and SDHB-deficient cell migration through 8 µm porous transwell membranes in the presence or absence of serum with or without 30 nM or 1 µM of glibenclamide for 16 h. Images are representative of migrating cells of three independent experiments, each performed in duplicate. Scale bar = 200 µm. Migration was normalized on total cell number (migrated and not), and no differences was observed in SDHB-deficient and Parental cell number (3.2 × 104 ± 0.01 and 3.1 × 104 ± 0.01, respectively). (E) Quantification of Parental and SDHB-deficient cell migration reported as percentages. In the presence (white bars) or in the absence (dark grey bars) of serum, SDHB-deficient cells migrated significantly more compared with Parental cells. Addition of 30 nM of glibenclamide did not affect either Parental either SDHB-deficient cell migration (dark grey bars). In contrast, treatment with 1 µM of glibenclamide (light grey bars) induced a significant reduction of migration only in SDHB-deficient cells. (F) Parental and SDHB deficient cells were counted after 6 days of treatment or not with increasing doses of glibenclamide (abbreviation: glib). Hashtags indicate

*the statistic of values between parental and SDHB deficient (##p<0.01), while asterisks indicated the statistical differences between parental or SDHB deficient treated or not glibenclamide. All data are the mean values of three independent experiments, each conducted in triplicates, ± S.D. Hashtags indicate the statistic of values between Parental and SDHB deficient (##P < 0.01, ####P < 0.0001), while asterisks indicate the statistical differences between Parental or SDHB-deficient treated or not glibenclamide (*P < 0.05, **P < 0.01, ***P < 0.001).*

4.2 Results aim 2

4.2.1 Intracellular succinate accumulation drives hyper-methylation and hyper-succinylation.

In this study, we used two forms of succinate, one that is permeable to cell membranes (methyl-succinate), which allowed us to study the effects of its accumulation, and one that is not permeable (succinate), which acts by binding its membrane receptor SUCNR1. Indeed, methyl-succinate was able to increase intracellular succinate levels in both hPheo1 cells after 72 h treatment (Figure 20A). As expected and in line with our previous results [204], SDHB-deficient cells showed higher basal levels of succinate accumulation, due to the impairment of SDH activity, compared to Parental cells. Not surprisingly, and according with the literature [25], only methyl-succinate treatment was able to increase histone 3 lysine 9 methylation in both cell lines (Figure 20B). Furthermore, basal methylation levels were higher in SDHB-deficient cells. Moreover, succinate has been shown to post-translationally modify (PTM) proteins by lysine succinylation [205]. In this regard, we used western blot to analyse the total level of lysine succinylation in our cell lines, both under basal conditions and after increasing intracellular succinate levels using the permeable form of succinate. We found not only that SDHB-deficient cells showed a significantly increased expression of total lysine succinylation compared to Parental cells, but also that methyl-succinate treatment significantly increased lysine succinylation levels in both hPheo1 cell types compared to their untreated counterparts (Figure 20C).

4.2.2 Migration of hPheo1 cells is positively influenced only after non-permeable succinate treatment.

To assess whether treatment with the two forms of succinate had the same or different effects on functional properties, we analysed both proliferation and migration. As we already published, the proliferation rate of SDHB-deficient cells was significantly lower compared with Parental cells, but migration was significantly higher [204]. Interestingly, proliferation of Parental and SDHB-deficient cells was not affected by either methyl-succinate or succinate compared to their untreated counterparts (Figure 20D). For the migration experiment, we used the 2D transwell

assay in which we stained the migrated cells with crystal violet (Figure 20E) and quantified the eluted dye by optical density. We observed that only succinate treatment was able to increase hPheo1 migration, whereas methyl-succinate treatment was unable to influence migration.

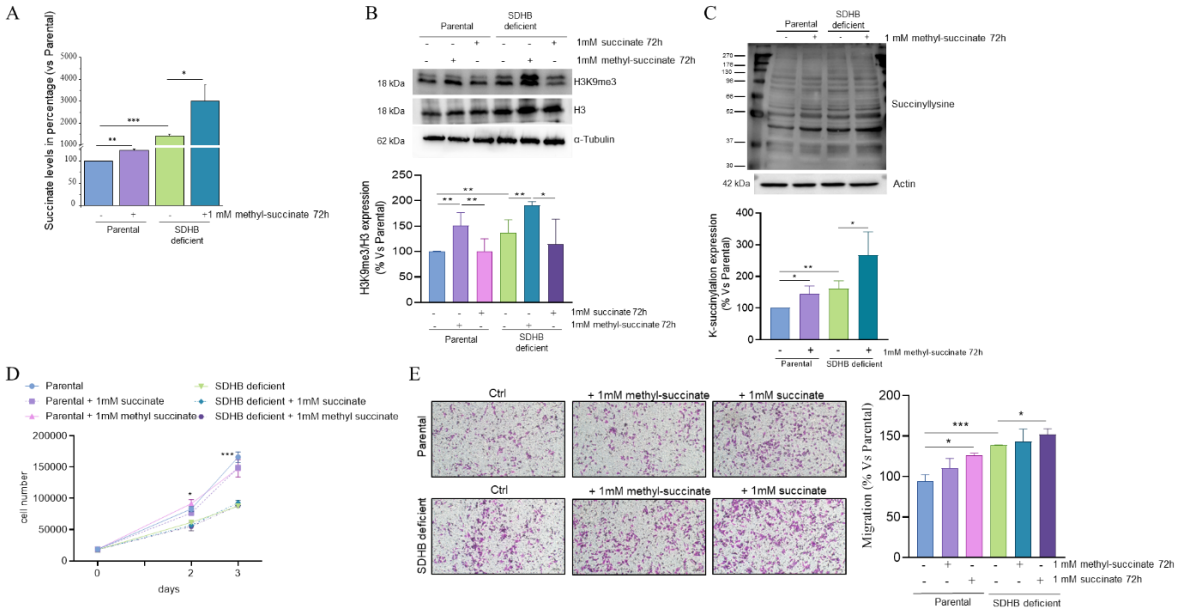

*Figure 20: Effects of intracellular and extracellular succinate on methylation, succinylation, proliferation and migration. (A) The bar graph shows the significant increase of the intracellular succinate assessed by GC/MS, in Parental and SDHB-deficient cells after 72h of methyl-succinate treatment, compared with their untreated counterparts. (B) Representative blots and densitometric evaluation showed the levels of H3k9me3 and H3 in Parental and SDHB-deficient cells after 72h of 1mM of methyl-succinate or succinate treatment. α-Tubulin was used as loading control. (C) Representative blots and densitometric evaluation showed the total levels of succinylated proteins in Parental and SDHB-deficient cells after 72h of 1mM of methyl-succinate. Actin was used as loading control. (D) Proliferation of Parental and SDHB deficient cells was monitored at different timepoints following administration of 1mM of methyl-succinate or 1mM of succinate. SDHB deficient cells proliferation was significantly lower compared to Parental cells, resulting significantly already after 2 days; proliferation of Parental and SDHB-deficient cells was not influenced after methyl-succinate nor succinate treatment. (E) Parental and SDHB deficient cell migration through 8 μm porous transwell membranes following 72h of 1mM of methyl-succinate and 1mM of succinate. Images are representative of migrating cells of three independent experiments, each performed in duplicate. Scale bar = 100 μm. Migration was normalized on total cell number and the quantification is reported as percentages. Bar graphs are derived from three independent experiment, ± S.D. (*P < 0.05, **P < 0.01, ***P < 0.001).*

4.2.3 SUCNR1 expression is higher in SDHB-deficient cells and binding of succinate activates ERK1/2 pathway.

We next investigated the expression of SUCNR1 in Parental and SDHB-deficient cells (Figure 21A). Western blot analysis showed that SDHB deficient cells express higher levels of SUCNR1 compared to Parental cells. Interestingly, only Parental cells significantly increased SUCNR1 expression after 1 mM of succinate treatment for 72 h. Methyl-succinate treatment for 72 h did not affect SUCNR1 expression. In order to investigate the association of SUCNR1 with the cognate G protein, Parental and SDH- deficient cells were stimulated with 1 mM succinate for 15 and 30 min, and we

observed an increase in ERK1/2 phosphorylation (Figure 21B) that suggested coupling with the Gq protein. Moreover, basal levels of ERK1/2 phosphorylation were significantly higher in SDHB-deficient cells compared to Parental cells. In a recent study, Lu and colleagues [153] showed that succinate binding to SUCNR1 increased migration by means of ERK1/2 activation and subsequent phosphorylation of DRP1. We hypothesized that the same effect could be present in our cells. This was the case, since interestingly, we also observed an increase in DRP1 phosphorylation at the same time points of succinate treatments (Figure 21B).

Since the 72-htreatment with succinate increased SUCNR1 level and since basal ERK1/2 phosphorylation was higher in SDHB-deficient cells, we next evaluated whether this condition could affect also ERK1/2 and DRP1 phosphorylation (Figure 21C). As expected, the phosphorylation level of both ERK1/2 and DRP1 in SDHB-deficient cells were already remarkably high; this may explain why, after treatment, we detected a significant increase only in phospho-DRP1. On the contrary, in Parental cells, chronic treatment with succinate caused increased level of phospho-DRP1.

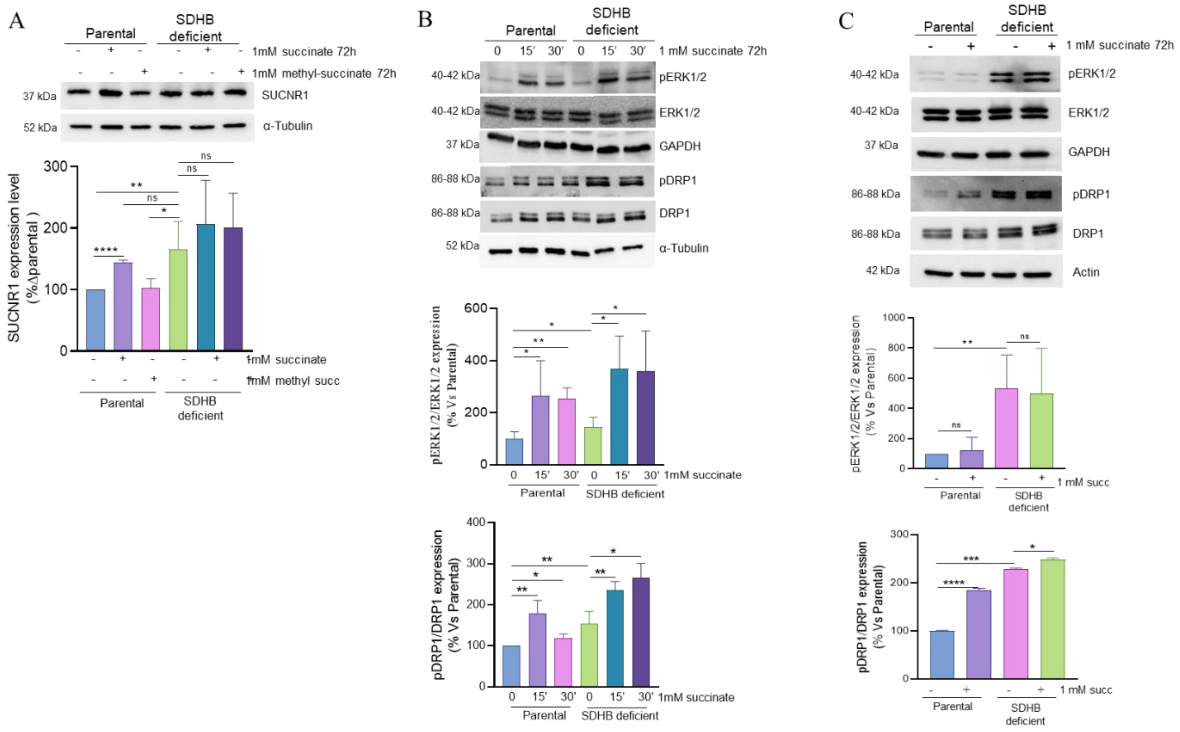

Figure 21: (A) Representative blots and densitometric evaluation of SUCNR1 expression following 72h of 1mM of methyl-succinate or 1mM of succinate treatment. Tubulin was used as loading control. (B) Representative blots and densitometric evaluation of ERK1/2, phospho-ERK1/2, DRP1 and phospho-DRP1 following 15, 30 minutes of 1mM succinate treatment. GAPDH and α-Tubulin were used as loading control. (C) Representative blots and densitometric evaluation of ERK1/2, phospho-ERK1/2, DRP1 and phospho-DRP1 expression following 72h of treatment with 1mM of extracellular succinate.

*GAPDH and Actin were used as loading control. Bar graphs are derived from three independent experiment, ± S.D. (*P < 0.05, **P < 0.01, ***P < 0.001, ****P < 0.0001).*

4.2.4 Inhibition of ERK1/2 reduces cell migration by decreasing phosphorylated DRP1 levels.

We first wanted to confirm the involvement of ERK1/2 phosphorylation in DRP1 activation, and then we evaluated the possible role of ERK1/2 in cell migration. In order to do it, we used the specific ERK1/2 inhibitor SCH772984. We tested different concentrations of SCH772984 to identify a specific dose that was able to inhibit ERK1/2 phosphorylation, while being non-toxic to cells, arriving at the concentration of 10nM. As shown in Figure 22A, this dose inhibited ERK1/2 phosphorylation, but did not impair cell proliferation, as demonstrated by the cell doubling time (Figure 22B). Western blot of ERK1/2 phosphorylation showed that by pre-treating our cell lines with SCH772984 for 1 h and then treating them with succinate for 15 min, the upregulation induced by succinate treatment was significantly reduced (Figure 22A). To evaluate the involvement of ERK1/2 activation in DRP1 phosphorylation, we assessed the levels of total and phosphorylated DRP1 in the presence of SCH772984 (Figure 22A). We observed that treatment with 10nM SCH772984 decreased DRP1 phosphorylation, even after succinate stimulation, suggesting that this decrease was due to the lack of ERK1/2 activity. Of note, a report on human mesenchymal stromal cells suggests that succinate promotes cell migration by SUCNR1-mediated Drp-1 phosphorylation [152]. We therefore hypothesised that this mechanism might also be involved in our cellular model. Indeed, we showed that pre-treatment with SCH772984 at 10nM was able to reduce cell migration in both cell lines compared to their untreated counterpart (Figure 22C). Interestingly, migration induced by succinate was significantly reduced following ERK1/2 inhibition. However, presence of extracellular succinate made the inhibitory effect of SCH772984 less efficient.

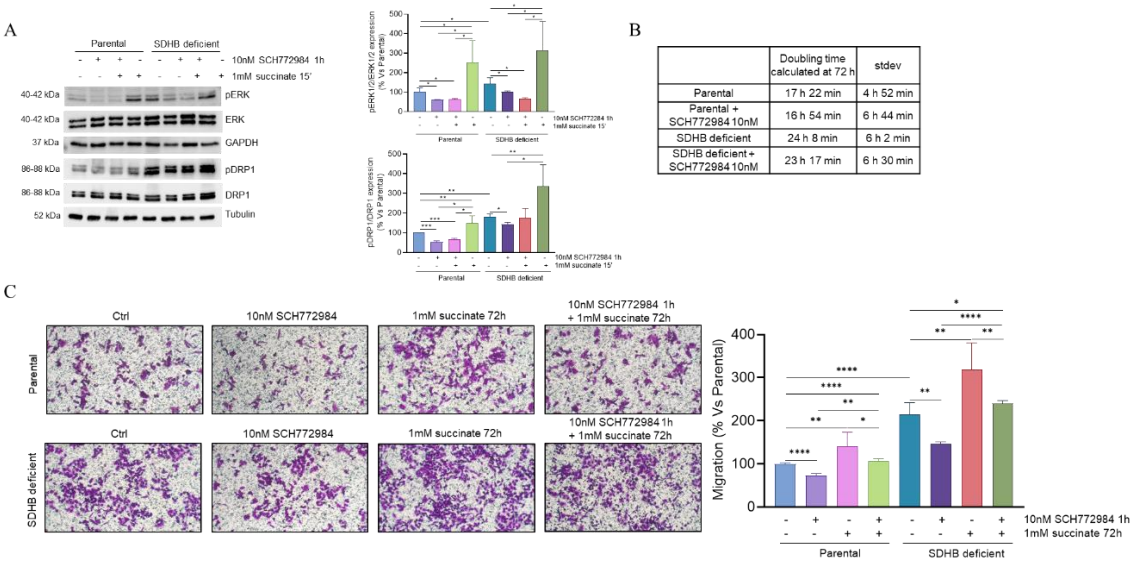

	Doubling time calculated at 72 h	stdev
Parental	17 h 22 min	4 h 52 min
Parental + SCH772984 10nM	16 h 54 min	6 h 44 min
SDHB deficient	24 h 8 min	6 h 2 min
SDHB deficient + SCH772984 10nM	23 h 17 min	6 h 30 min

*Figure 22: (A) Representative blots and densitometric evaluation of ERK1/2, phospho-ERK1/2, DRP1 and phospho-DRP1 at different conditions: pre-treated with SCH772984 for 1h and later treated with 1mM of succinate for 15 minutes, as controls we used both cells treated with succinate for 15 minutes or with SCH772984 for 1h. For basal expression we used untreated cells. (B) Doubling time of Parental and SDHB deficient cells treated or not with 10nM of SCH772984 calculated at 72h. (C) Parental and SDHB deficient cell were pre-treated with 1mM of succinate for 72h, then seeded for migration in the presence or absence of 10nM of SCH772984. Images are representative of migrating cells of three independent experiments, each performed in duplicate. Scale bar = 200 µm. Migration was normalized on total cell number. The quantification is reported as percentages. Bar graphs are derived from three independent experiment, ± S.D. (*P < 0.05, **P < 0.01, ***P < 0.001, ****P < 0.0001.).*

4.3 Results aim 3

4.3.1 SDHB-deficient cells show increases contacts between Mitochondria and the Nucleus.

In order to evaluate the distance and the number of Mito-Nuclear Contacts we analysed ultrathin transmission electron microscopy (TEM) section of Parental and SDHB-deficient cells (Figure 23A). The analysis showed a significant reduction in the distance between mitochondria and the nucleus (Figure 23B) alongside with an increase in the number of contact sites (Figure 23C) in SDHB-deficient cells compared to Parental ones.

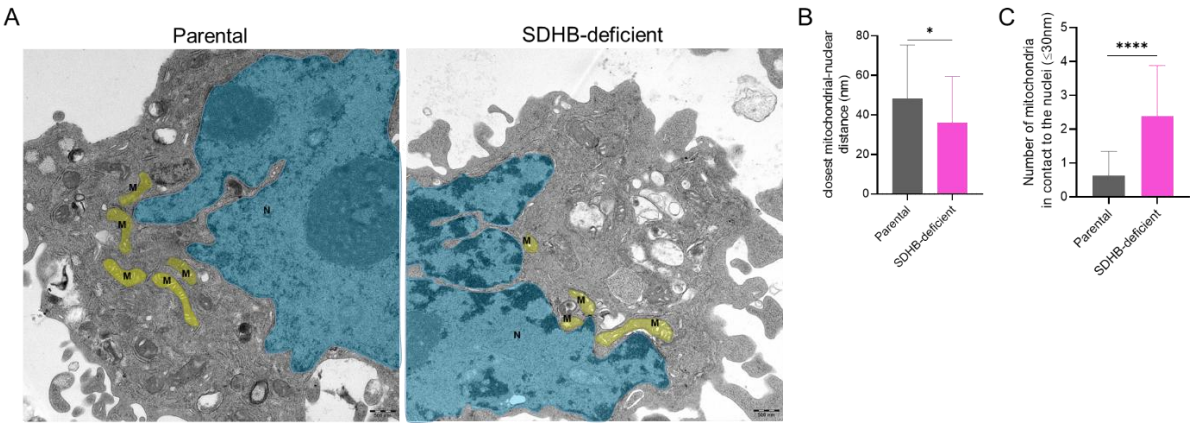

*Figure 23: Analysis of the distance between mitochondria and the nucleus. (A)The transmission electron micrography (TEM) highlight the mitochondria (M; yellow) and the nucleus (N; blue) hPheo1 Parental and SDHB-deficient cells. Scale Bar = 500nm. (B) Quantification of the distance between mitochondria and the nucleus in hPheo1 Parental and SDHB-deficient cells. (C) Histograms indicate the number of mitochondria in contact with the nucleus (less than 30 nm). *P ≤0.05; ****P ≤ 0.0001.*

4.3.2 SDHB-deficient cells displayed higher expression of TSPO in perinuclear area. We next performed a western blot to evaluate the expression levels of the different proteins involved in NAM such as the Protein Kinase A (PKA), acyl-CoA binding domain containing 3 (ACBD3), A-Kinase Anchor Protein 95 (AKAP95), Translocator Protein (TSPO) and the beta subunit of ATP synthase (ATPβ), used as housekeeping. We found that only TSPO expression significantly increased in SDHB-deficient cells (Figure 24A). In order to evaluate the localization of TSPO we than performed cell fractionation. Interestingly, perinuclear extraction highlighted higher levels of TSPO in the perinuclear area of SDHB-deficient cells (Figure 24B). Accordingly, with this result, immunofluorescence analysis showed increased levels of co-localization between TSPO and Lamin B1 in SDHB-deficient cells compared to Parental (Figure 24C).

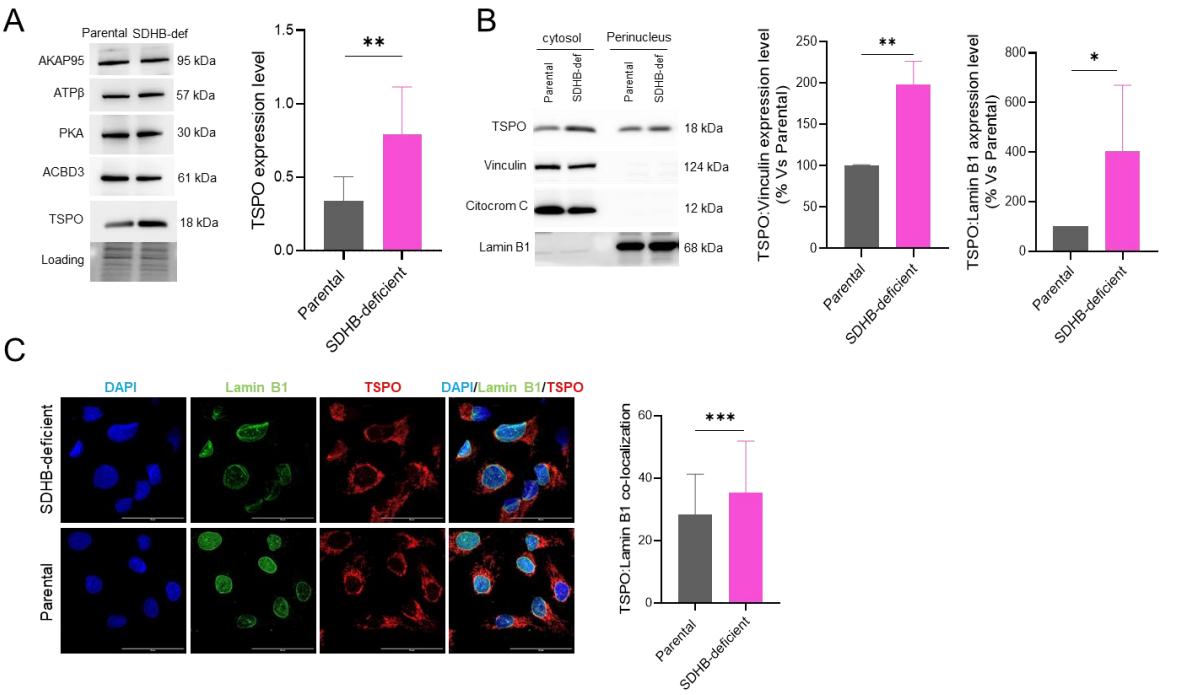

*Figure 24: Evaluation of the protein involve in Mito-Nuclear Contact Sites. (A) Western Blot analysis of NAM protein (B) Western blot analysis and the relative densitometric evaluation of TSPO in the cytosol and perinucleus of Parental and SDHB-deficient cells (C) Immunofluorescence and relative co-localization analysis of TSPO and Lamin B1 in hPheo1 Parental and SDHB-deficient cells. Scale bar = 50 μm (*P < 0.05; **P < 0.01; ****P < 0.0001).*

4.3.3 TSPO downregulation prevents NAM formation.

To corroborate TSPO essentiality in retaining the Mito-Nuclear Contacts, we down-regulated TSPO in both Parental and SDHB-deficient cells (Figure 25A) and then we performed Proximity-Labelling Assay (PLA). Thus, using this approach, we first confirmed a significant increase in the number of NAM in SDHB-deficient cells compared to Parental but we also observed a significant reduction in NAM formation following TSPO ablation (Figure 25B).

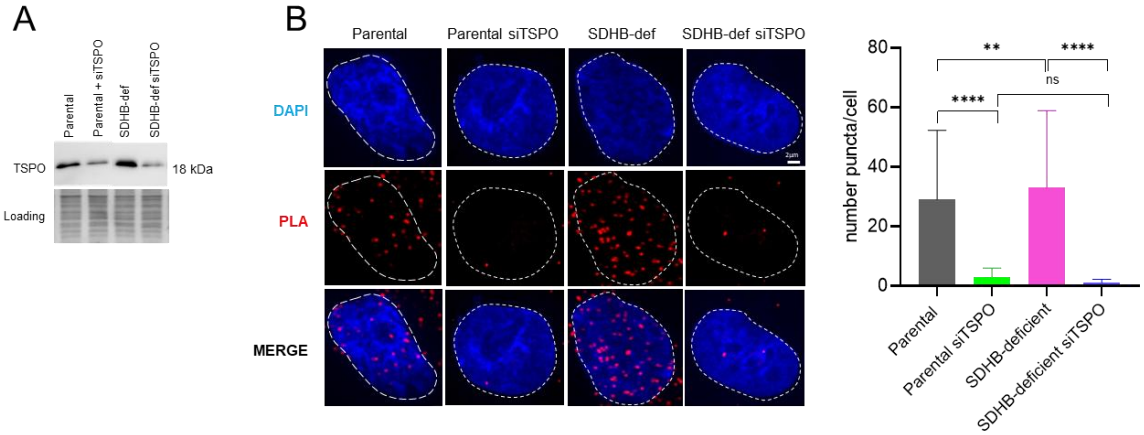

Figure 25: TSPO knockdown prevents NAM formation. (A) Western Blot showing the expression of TSPO following TSPO knockdown in Parental and SDHB-deficient cells. (B) Proximity ligation assay (PLA) and the relative average number of PLA dots per cell in Parental and SDHB-deficient cells

*following TSPO knockdown and incubated with anti-Lamin B1 and anti-TOMM20 antibodies; Nuclei are stained with DAPI; representative images show an increased number of PLA dots (red) in SDHB-deficient cells compared to Parental. TSPO knockdown significantly reduced the number of PLA dots. Scale bar = 2µm (**P < 0.01; ****P < 0.0001).*

4.3.4 Loss of SDHB impairs cellular redox-state.

We next evaluated mitochondrial ROS levels using MitoSOX: a fluorescent indicator dye used to specifically detect and measure superoxide within the mitochondria of live cells. In SDHB-deficient cell, we see a significant increase in redox probe oxidation-suggesting higher levels of mitochondrial superoxide in these cells compared to Parental ones (Figure 26A). Live-cell imaging using the mitochondria-targeted HyPer-mito sensor demonstrated a significant increase in mitochondrial hydrogen peroxide (H_2O_2) levels in SDHB-deficient cells compared to Parental, indicating elevated oxidative stress within the mitochondrial compartment (Figure 26B). Increased mitochondrial ROS production correlated with a significant increase in lipid peroxidation, demonstrated by fluorescence-based detection using the lipid peroxidation-sensitive probe C11-BODIPY 581/591 (Figure 26C). This result suggest that mitochondrial oxidative stress may contribute to membrane lipid damage in SDHB-deficient cells.

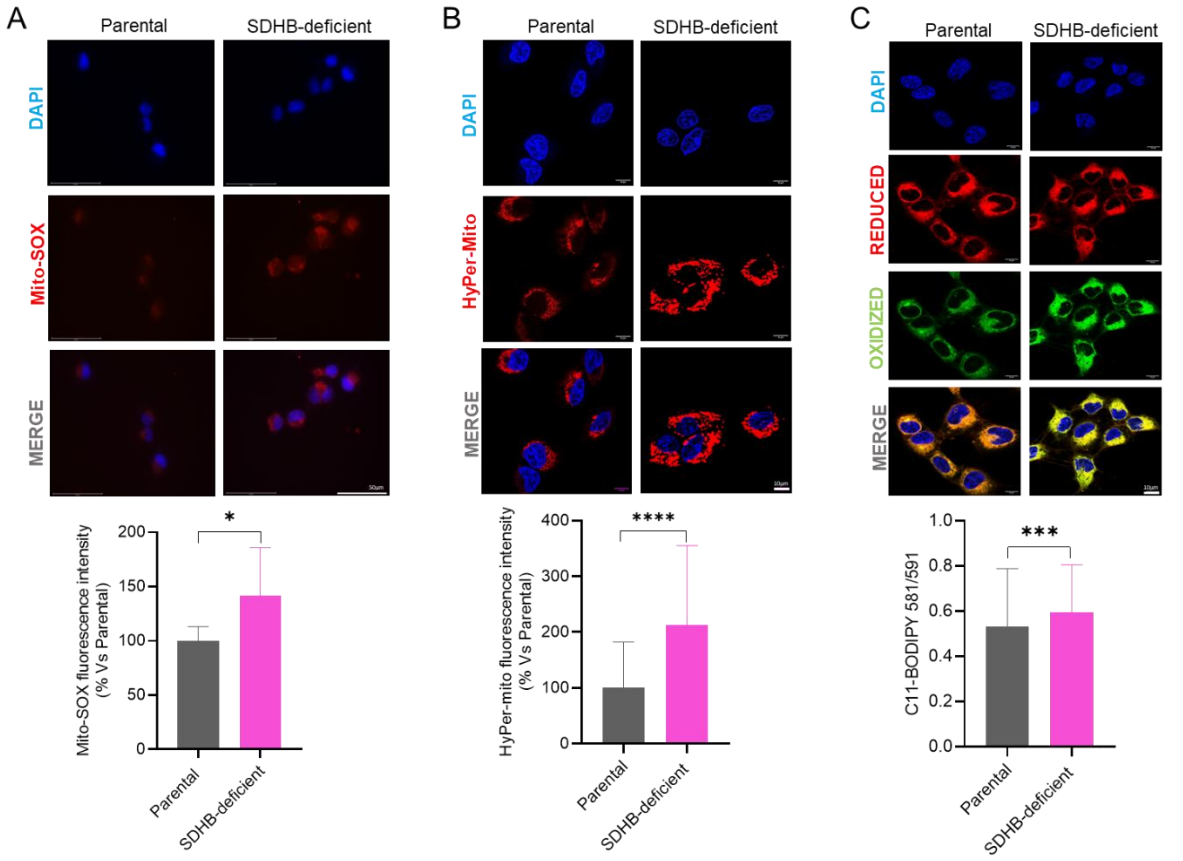

Figure 26: Loss of SDHB increases mitochondrial ROS production and lipid peroxidation. (A) Representative images of hPheo1 Parental and SDHB-deficient cells loaded with (A) Mito-SOX (B)

*HyPer-mito and (C) C11-BODIPY 581/591 and relative histograms analysis. Scale bar = 50μm and 10μm. *P<0.05; ***P<0.001; ****P<0.0001.*

4.3.5 Mitochondrial ROS levels significantly decrease when TSPO is silenced.

In order to evaluate the contribution of TSPO in mitochondrial ROS production, we knockdown TSPO and then we used the mitochondria-targeted HyPer-mito sensor to measured hydrogen peroxide levels. Notably, the knockdown of TSPO markedly reduced mitochondrial H_2O_2 accumulation in both cell lines (Figure 27A-B), suggesting a key role for this protein in regulating mitochondrial redox homeostasis.

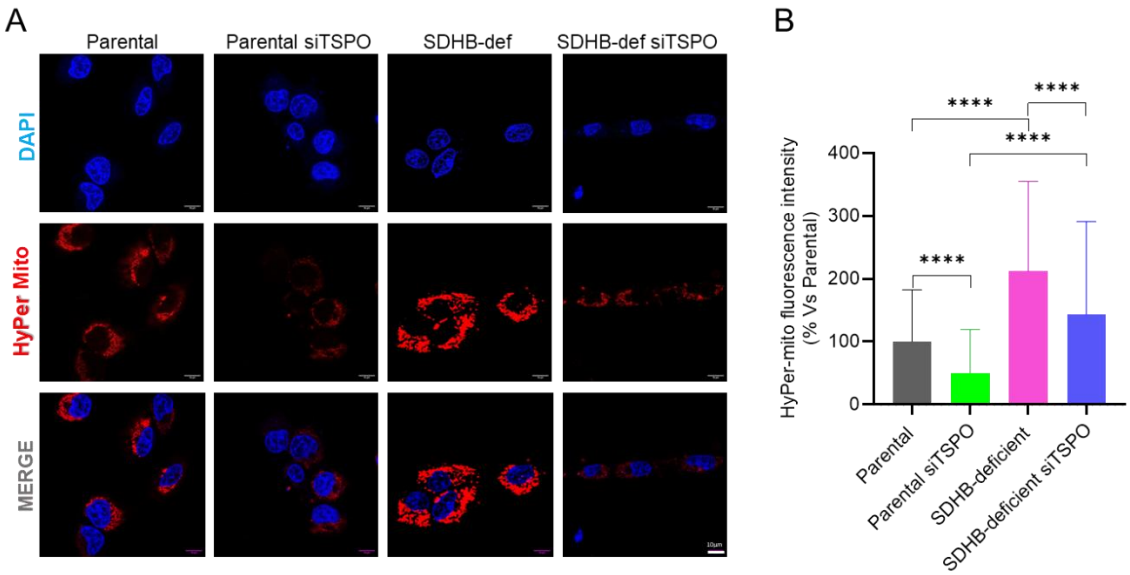

*Figure 27: Hydrogen Peroxide Levels decreases following TSPO knock-down. (A) Representative images of hPheo1 Parental and SDHB-deficient cells transfected with siRNA targeting TSPO or left untreated and loaded with HyPer-mito sensor. Scale Bar = 10μm (B) Relative histogram analysis (****P<0.0001).*

4.3.6 TSPO contributes to cellular proliferation and migration potential.

To further investigate the contribution of TSPO into two fundamental aspects of tumour growth and progression, we performed proliferation and migration experiments following TSPO knockdown in our tumour lines. The silencing of TSPO significantly reduces both proliferation (figure 28A) and migration (figure 28B) in both tumour cell lines, although the effects of the downregulation was not able to bring the two populations back to an equal proliferation and/or migration rate. Indeed, even after TSPO knockdown, Parental cell proliferation was still higher compared to SDHB-deficient cells while SDHB-deficient cells migration was greater than Parental.

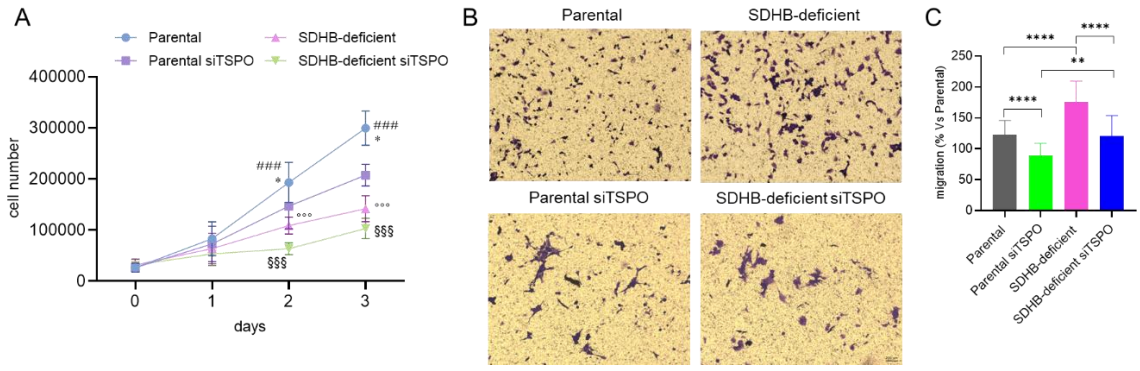

*Figure 28: Effects on cell proliferation and migration following TSPO knock-down. (A) Proliferation of hPheo1 Parental and SDHB-deficient cells control and silenced for TSPO was evaluated ad day 1,2 and 3. The knock-down of TSPO significantly decreased the proliferation of both tumour cells. Asterisks indicate the statistic of values between Parental and Parental siTSPO (*P<0.05); # indicate the statistical differences between Parental and SDHB-deficient (###P<0.001), ° indicate the statistical differences between SDHB-deficient and SDHB-deficient siTSPO (°°°P<0.001) while § indicate the statistical differences between Parental siTSPO and SDHB-deficient siTSPO (§§§ P< 0.001). (B) Migration of both Parental and SDHB-deficient following TSPO resulted statistically lower compared to each control condition. Scale bar = 200μm. Migration was normalized on total cell number. The graphs are derived from three independent experiment, ± S.D. The quantification is reported as percentages.*

4.3.7 Mitochondrial TSPO and Nuclear AKAP95 increases in human SDHx mutated primary tissue.

Based on the results obtained from cellular experiments, in which we observed increased NAM and TSPO expression of SDHB-deficient cells, we extended our analysis to Human Primary Tissue samples from Non-Pathogenic Variants (NPV) or SDHx-mutated PGLs patients to investigate whether this upregulation is also present in a more physiologically relevant and complex setting. However, electron microscope analysis of the distance between mitochondria and the nucleus was not feasible due to the significantly increased number of mitochondria, as can be clearly seen in Figure 29A, as this could potentially bias the interpretation of the results. Western blot analysis was conducted to assess the expression of NAM proteins (Figure 29B). Very interestingly, our results showed that the expression of PKA, AKAP95 as well as TSPO resulted statistically increased in SDHx-mutated tissue samples compared to NPV. On the contrary, ACBD3 expression was slightly higher but not statistically significant, thereby reinforcing the consistency between *in vitro* and in vivo findings.

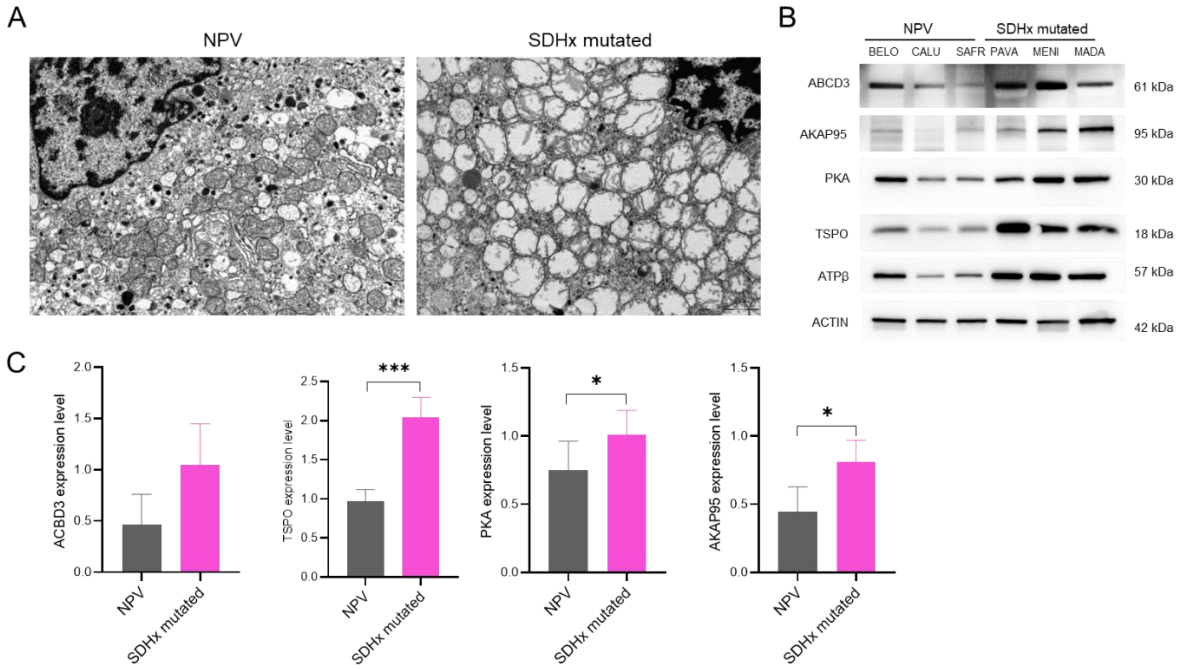

*Figure 29: Evaluation of the NAMs proteins in Human Primary Tissue from NPV or SDHx-mutated PGLs patients. (A) Transmission electron micrography (TEM) of representative NPV or SDHx-mutated PGLs tissue samples. Scale Bar = 2µm. (B) Western Blot analysis of NAM protein in NPV or SDHx-mutated tissue samples and (C) relative densitometric evaluation of ACBD3, TSPO, PKA and AKAP95 (*P<0.05; ***P<0.001).*

4.3 Results aim 4

4.4.1 SDHB-deficient cells do not affect HUVEC proliferation but increase migration.

In order to investigate the effect of HUVECs on proliferation of Parental and SDHB-deficient cells and *vice-versa*, we co-cultured our cell lines and counted at day one and three. Interestingly, we found that proliferation of Parental cells was not influenced by the presence of HUVECs while, on the contrary, proliferation of SDHB-deficient cells was significantly increased after three days of co-culture, as compared to their single-culture counterparts. In contrast, we observed that the growth of HUVECs was not influenced by the presence of hPheo1 tumour cells (either Parental or SDHB-deficient) (Figure 30A). We also studied the migration in two-dimension (2D) of HUVECs in the presence or absence of Parental and SDHB-deficient and *vice-versa*. We found that the migration of HUVECs was statistically upregulated only when co-cultured with SDHB-deficient cells (Figure 30B). We have previously shown that hPheo1 SDHB-deficient cells migratory capability is significantly higher compared to Parental ones. In fact, not surprisingly, we confirmed the increased migration ability of this cell lines. However, hPheo1 (either Parental or SDHB-deficient cells) co-cultured with HUVECs were not able to increase their migratory capacity compared to their single-culture counterparts (Figure 30C).

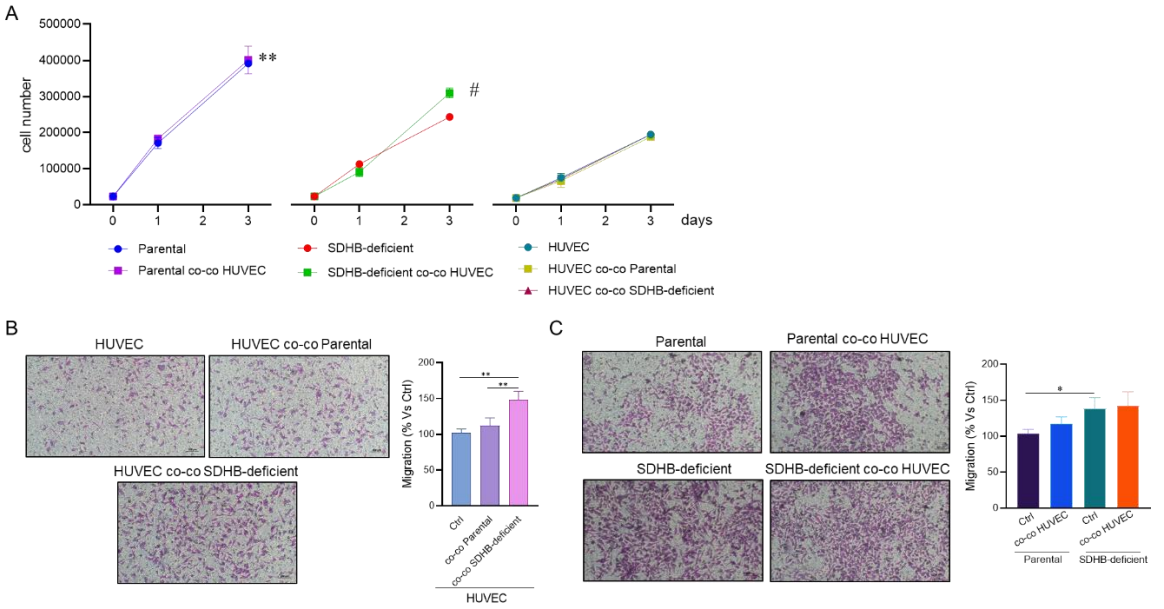

*Figure 30: Reciprocal effect of tumours cells and HUVEC cells on proliferation and migration. (A) Proliferation of Parental, SDHB-deficient and HUVEC cells was monitored at different timepoints in single and co-culture condition. SDHB deficient cells proliferation was significantly lower compared to Parental cells; only SDHB-deficient cells proliferation significantly increased by co-culture with HUVEC. The presence of both Parental and SDHB-deficient cells did not influence HUVEC proliferation. Asterisks indicate the statistic of values between Parental and SDHB deficient (**P < 0.01); hashtags indicate the statistical differences between SDHB-deficient and SDHB-deficient cell co-cultured with HUVECs #P < 0.05). (B) Migration of HUVEC cells significantly increased only when co-cultured with SDHB-deficient cells. (C) Migration of both Parental and SDHB-deficient cells was not influenced by co-culture with HUVECs, resulting not statistically significant compared each control. Scale bar = 100μm. Migration was normalized on total cell number. The quantification is reported as percentages. Bar graphs are derived from three independent experiment, ± S.D. (*P<0.05, **P<0.01).*

4.4.2 SDHB-deficient cells increased HUVEC permeabilization by reducing the expression of junction proteins.

The permeability of HUVECs was evaluated by analysing the passage of fluorescein isothiocyanate (FITC)-dextran, a marker of cell permeability, across the endothelium monolayer (Figure 31A). We found that only after 72h of co-culture with SDHB-deficient cells, the amount of FITC-dextran significantly increased, meaning that the permeability is increase. The stability of endothelial cells and vascular permeability is controlled by tight and adherent junctions. Therefore, when we evaluated the protein levels of tight junction Claudin-5 and adherent junction CD31 (PECAM), we found that the expression of both significantly decreased when HUVEC were co-cultured with SDHB-deficient cells (Figure 31B). Additionally, in the same experimental conditions, we confirm this result by Immunofluorescence staining of Claudin-5 (Figure 31C).

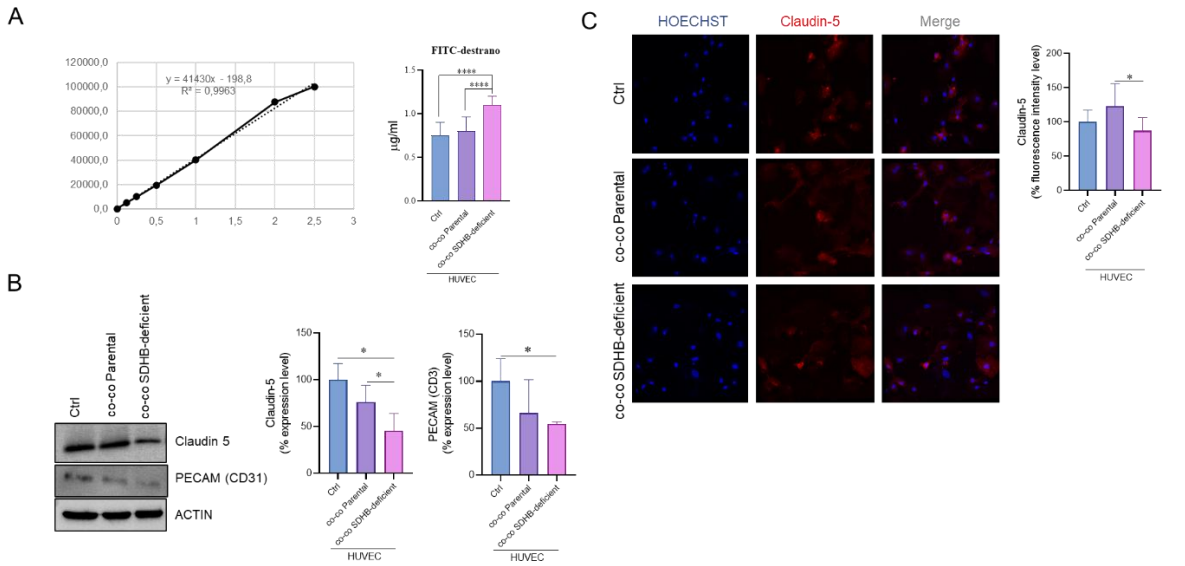

*Figure 31: Effect of tumour cells on permeabilization. (A) The endothelial permeability was decreased only after co-culture with SDHB-deficient cells. (B) Representative blots and densitometric evaluation of PECAM and Claudin-5 in HUVEC cells in single and co-culture with Parental and SDHB-deficient cells. (C) Immunofluorescence staining of Claudin-5 was examined by a confocal microscope in single and co-culture with Parental and SDHB-deficient cells. Scale bar = 200µm. The quantification is reported as percentages. Bar graphs are derived from three independent experiment, ± S.D. (*P < 0.05, ****P < 0.0001.).*

4.4.3 SDHB-deficient conditioned media increase *in vitro* Capillary-like Structures.

To assed the effect of tumour cells on angiogenesis, we used the capillary morphogenesis assay in which we resuspended HUVEC cells in complete EBM or in Parental or SDHB-deficient conditioned media (Figure 32A) and we quantify the formed capillary network after 6 h using different parameters, such as the number of nodes, junctions, meshes, segments and branches. Interestingly, the presence of SDHB-deficient conditioned media, was able to significantly increased all the parameters analysed. On the contrary, the Parental conditioned media were able to significantly increased only few parameters such as the number of nodes, meshes and branches (Figure 32B). To understand if these effects were caused by soluble factors or tumour EVs, we ultra-centrifuged conditioned media to separate supernatants from EVs. We repeated the experiment using a culture medium enriched with EVs (EVs secreted by Parental or SDHB-deficient and resuspended in EBM), and the supernatant counterparts (Figure 32C-D). Intriguingly, we found that EVs secreted by SDHB-deficient cells significantly enhanced tube formation, as their removal led to a marked reduction in the number of nodes, junctions, meshes, and segments in endothelial networks. In contrast, depletion of EVs from Parental cells resulted in a significant decrease only in the number of branches. These findings

corroborate the stronger angiogenic effects observed with full conditioned media from SDHB-deficient cells compared to Parental cells.

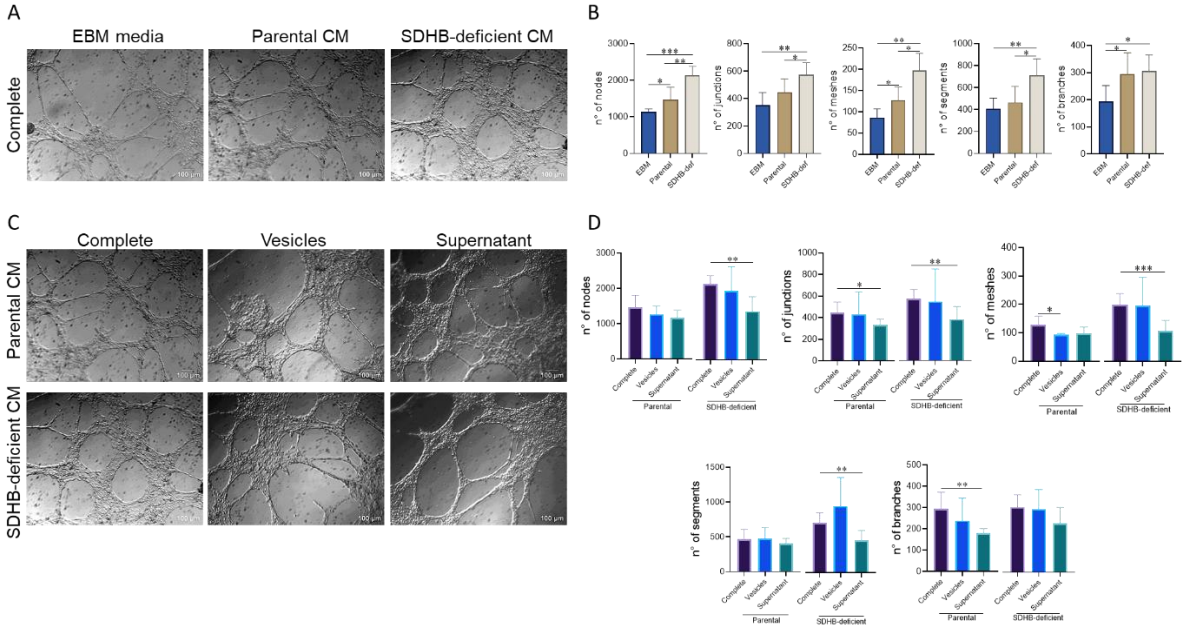

*Figure 32: Effect of tumour cells conditioned media on in vitro angiogenesis. Angiogenesis was measured by capillary morphogenesis assay at 6 h in HUVECs (A) Representative images of capillary morphogenesis of HUVECs in complete media and Parental or SDHB-deficient conditioned media. (B) Histograms represent the respective analysis of the number of nodes, junctions, meshes, segments, and branches. (C) Representative images of capillary morphogenesis obtained by resuspending HUVECs in Parental or SDHB-deficient complete, EVs enriched or supernatant media. Scale Bar = 100µm. (D) Histograms represent the respective analysis of the number of nodes, junctions, meshes, segments, and branches. Mean ± SD, n = 3. (*P<0.05, **P<0.01, ***P<0.001).*

4.4.4 Nanosight Analysis revealed that SDHB-deficient cells produce a larger amount of EVs compared to Parental.

We then studied the concentration (particles/ml) and size (nm) of EVs produced by both Parental and SDH-deficient conditioned culture media or EBM medium (Figure 33A). The relative analysis reported in figure 33B, showed that the size of EVs of both Parental (264.3 ± 5.2 nm) and SDHB-deficient (272.5 ± 5.9 nm) cells resulted statistically bigger compared to the size of vesicles of EBM medium (158.4 ± 8.9 nm). The number of vesicles (particles/ml) resulted significantly greater in Parental (1.16E+10 ± 6.69E+08) and SDHB-deficient (1.23E+10 ± 9.98E+08) compared to EBM (5.56E+09 ± 5.36E+08). However, it is worth noting, that the number of vesicles of SDHB-deficient media was statistically higher also compared to Parental ones.

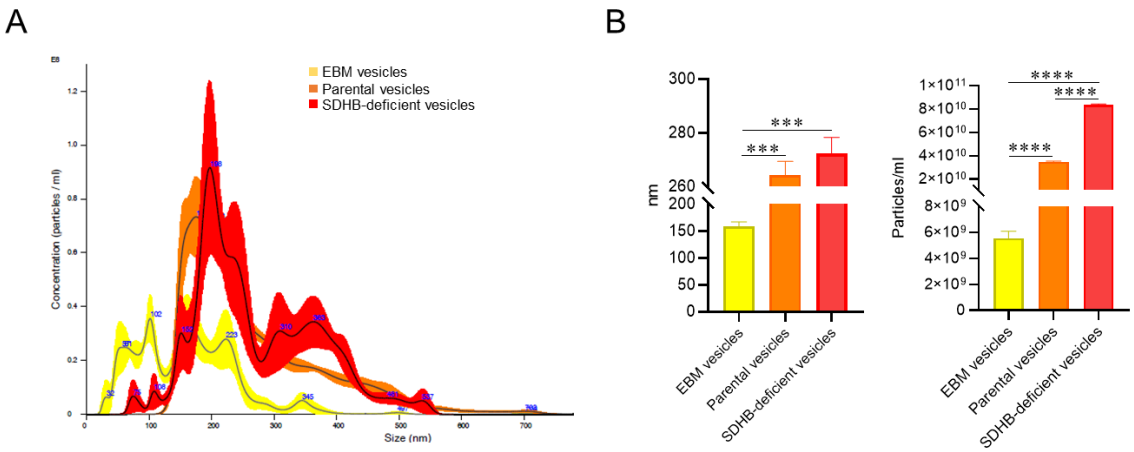

*Figure 33: (A) Graph of concentration/average size obtained from a Nanosight analysis that plots the average number of particles per millilitre as a function of their size in nanometres. (B) Histograms represent the analysis of EVs size reported in nm (left) and concentration reported in particles/ml (right). Mean ± SD, n = 3. (***P<0.001, ****P<0.0001.).*

4.4 Results aim 5

4.5.1 The characterization of human primary fibroblast cultures showed positivity to CAFs markers

We tested our human primary fibroblast cultures for specific molecular markers of fibroblasts and CAFs, including fibroblast-specific protein-1 (FSP1), alpha smooth muscle actin (α-SMA) and fibroblast activation protein (FAP). Immunofluorescence analysis showed positivity for both FSP1 and αSMA, confirming that our primary cultures were indeed enriched with fibroblasts. Furthermore, they showed positivity for FAP, a marker widely used to classify aggressive CAF subtypes (Figure 34).

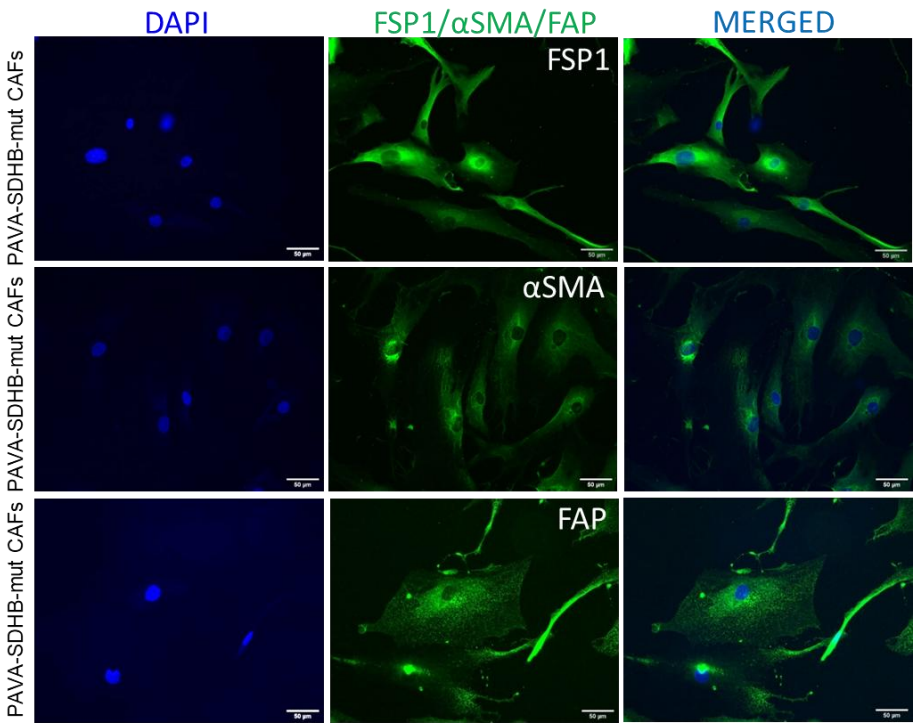

Figure 34: Characterization of Human Primary Fibroblasts. Immunofluorescence was applied to analyze the expression of Fibroblast Specific Protein-1 (FSP1), alpha-smooth muscle actin (α-SMA) and fibroblast activation protein (FAP) in primary culture fibroblasts. Scale bars = 50μm.

4.5.2 SDHB-mutated CAFs increases proliferation when co-cultured with hPheo1 cells.

We analysed the effect of CAFs on proliferation of Parental and SDHB-deficient cells and *vice-versa*. Interestingly, we found that proliferation of Parental cells was not influenced by the presence of both CAFs while, on the contrary, proliferation of SDHB-deficient cells significantly increased already after three days of co-culture with both BELO-NPV or PAVA SDHB-mutated CAFs, as compared to their single-culture counterparts (Figure 35A). In contrast, we observed that only the growth of PAVA SDHB-mutated CAFs was positively affected by the presence of hPheo1 tumour cells (either Parental or SDHB-deficient) (Figure 35B).

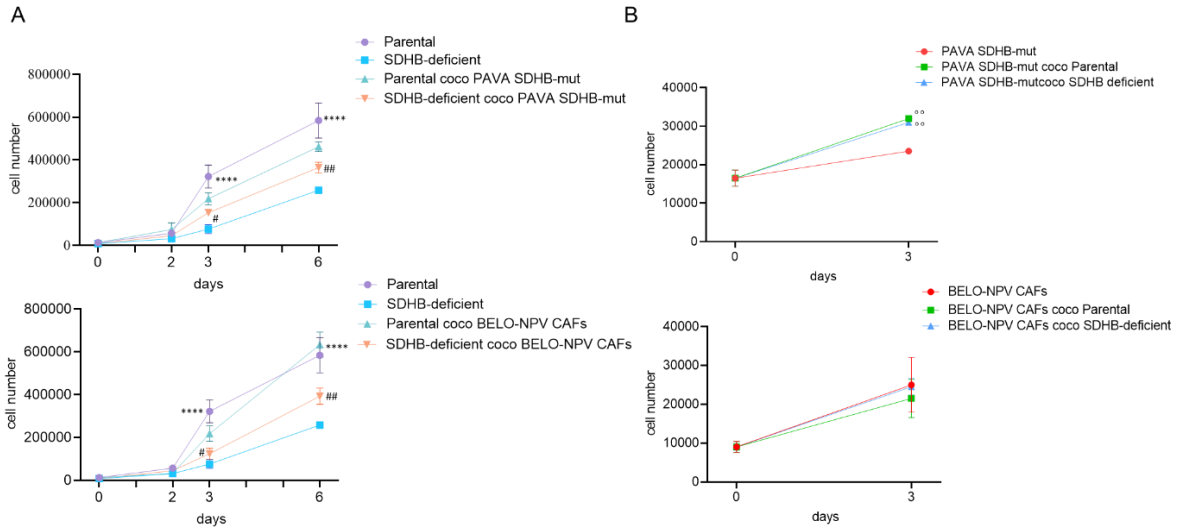

*Figure 35: Reciprocal effect of tumours cells and NPV or SDHB-mutated CAFs on proliferation. (A) Proliferation of Parental and SDHB-deficient cells in single and co-culture with PAVA-SDHB-mutated or BELO-NPV CAFs was monitored at different timepoints (2, 3 and 6 days). SDHB deficient cells proliferation was significantly lower compared to Parental cells; only SDHB-deficient cells proliferation significantly increased when co-cultured with both CAFs. (B) Proliferation of CAFs in single or co-culture with Parental or SDHB-deficient cells was followed after 3 days or culture. The presence of both Parental and SDHB-deficient cells significantly increased only PAVA SDHB-mutated CAFs proliferation but not BELO-NPV CAFs one. The quantification is reported as percentages. Bar graphs are derived from three independent experiment, ± S.D. Asterisks indicate the statistic of values between Parental and SDHB deficient (****P<0.0001); hashtags indicate the statistical differences between SDHB-deficient and SDHB-deficient cell co-cultured with CAFs $^{\#}P < 0.05$, $^{\#\#}P<0.01$) and dots indicate the statistical differences between CAFs and Parental or SDHB-deficient (°°P<0.01).*

4.5.3 SDHB-deficient cells increase CAFs migration.

We next studied the migration in two-dimension (2D) of CAFs in the presence or absence of Parental and SDHB-deficient. We found that, only when co-cultured with SDHB-deficient cells, CAFs migration was statistically upregulated (Figure 36A-B).

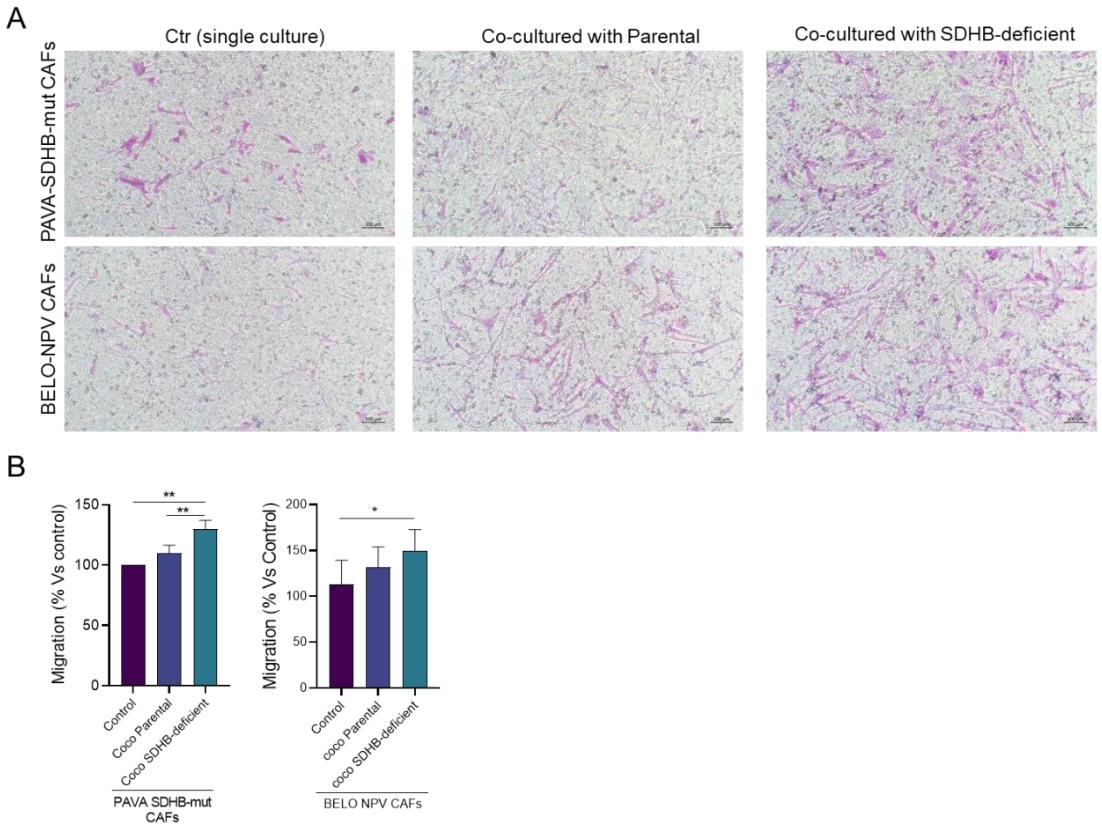

*Figure 36: Effect of tumours cells on NPV or SDHB-mutated CAFs migration. (A) Migration of HUVEC cells significantly increased only when co-cultured with SDHB-deficient cells. (C) Migration of both Parental and SDHB-deficient cells was not influenced by co-culture with HUVECs, resulting not statistically significant compared each control. Scale bar = 100μm. Migration was normalized on total cell number. The quantification is reported as percentages. Bar graphs are derived from three independent experiment, ± S.D. (*P<0.05, **P<0.01).*

4.5.4 SDHB-mutated CAFs positively influence hPheo1 migration.

The migratory capacity of Parental and SDHB-deficient was analysed in single culture or in co-culture with both PAVA SDHB-mutated or BELO-NPV CAFs. Our results showed that, only in the presence of PAVA SDHB-mutated CAFs, hPheo1 cell lines were able to increase their migratory capacity compared to their single-culture counterparts (Figure 37A). Indeed, when co-cultured with BELO-NPV CAFs, either Parental or SDHB-deficient cells, did not increased their migration ability (Figure 37B).

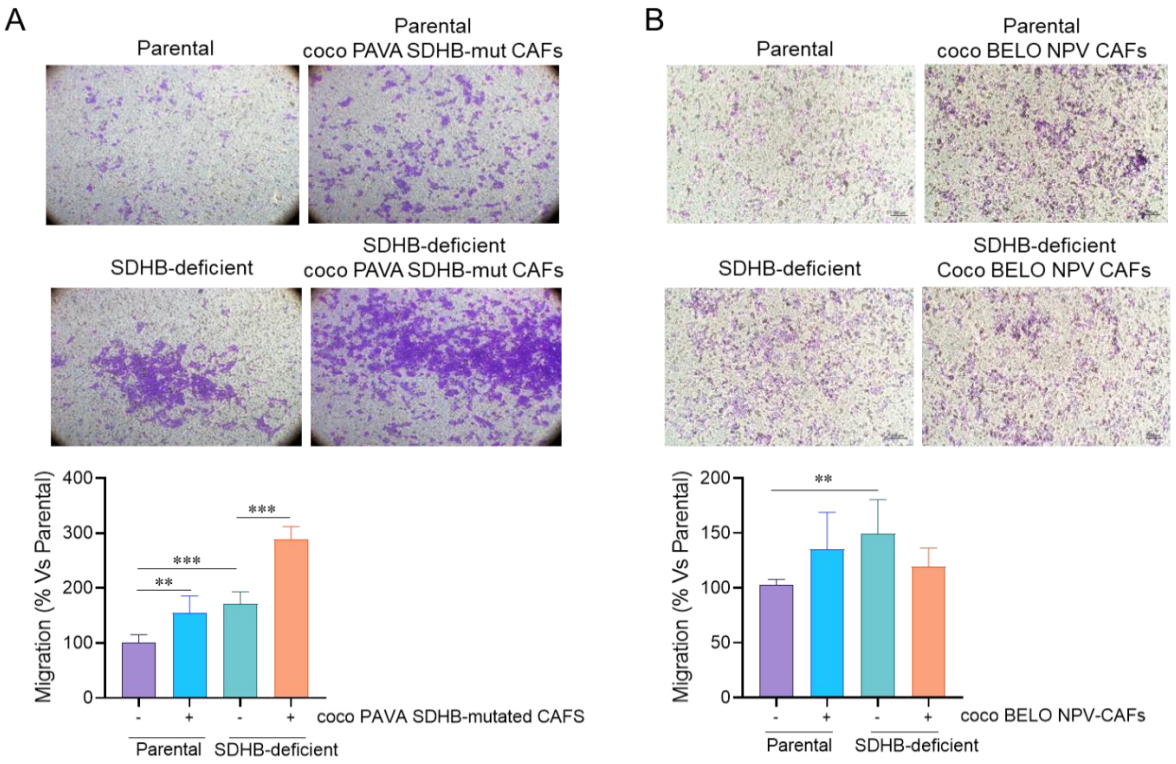

*Figure 37: Effect of NPV or SDHB-mutated CAFs on tumours cells migration. (A) Migration of Parental and SDHB-deficient cells migration resulted significantly increased in the presence of PAVA SDHB-mutated CAFs compared to their single-culture. (B) Migration of both Parental and SDHB-deficient cells was not influenced by co-culture with BELO NPV CAFs, resulting not statistically significant compared each control conditions. Scale bar = 100µm. Migration was normalized on total cell number. The quantification is reported as percentages. Bar graphs are derived from three independent experiment, ± S.D. (**P<0.01, ***P<0.001).*

4.5.5 SDHB-deficient spheroids show higher aggressiveness in the presence of SDHB-mutated CAFs.

To evaluate the aggressiveness induced by CAFs, we studied migration of SDHB-deficient spheroids labelled with mCherry by directly laying the spheroids itself on different monolayer of CAFs (NPV, SDHD-mutated or SDHB-mutated CAFs). Picture of spheroids were acquired at day 0 using a light microscope. At day 3, images were acquired under Leica Stellaris DMi8 confocal microscope. We detect a clear and significant detachment of tumour cells from spheroids invading the surrounding space in all conditions (Figure 38A), but we also observed that this migration was significantly different depending on CAFs phenotype. In particular, in the presence of SDHD-mutated CAFs, spheroids showed an intermediate trend in migration compared with NPV CAFs and SDHB-mutated CAFs. Indeed, the migration areas of SDHB-deficient spheroids with SDHD-mutated CAFs was higher compared with NPV CAFs, but lower compared with SDHB-mutated CAFs (Figure 38B).

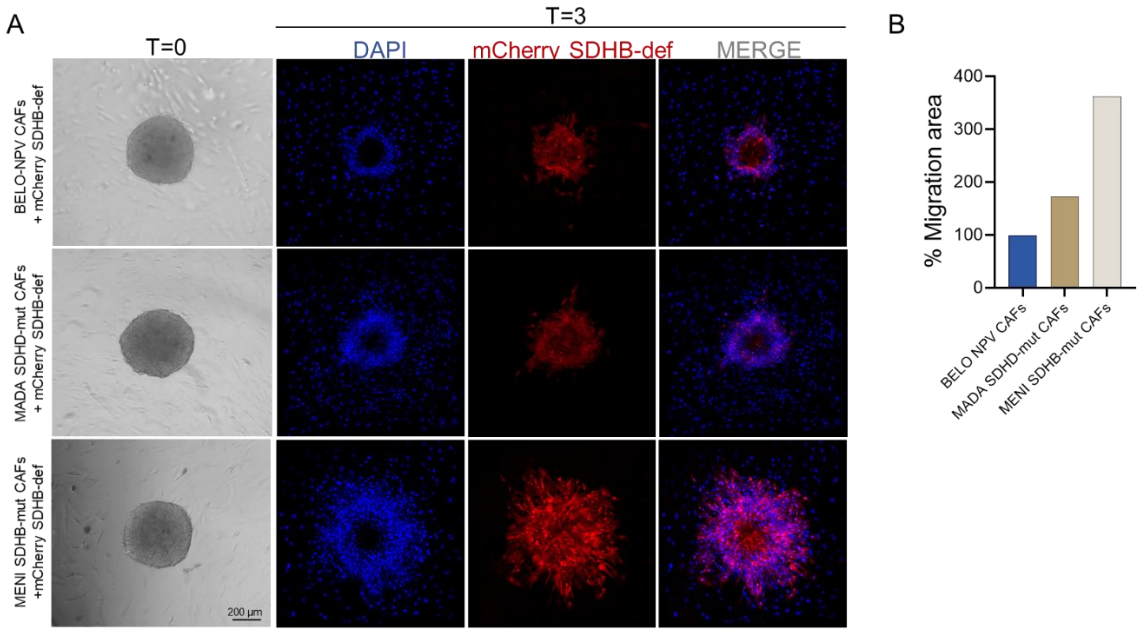

Figure 38: Effect of different CAFs on SDHB-deficient labelled with mCherry spheroids migration. (A) Representative images of spheroids laid on different CAFs at day 0. The migration capability was observed after 3 days. The presence CAFs induced an evident detachment of clusters of cells in the surrounding space. (B) The computation of the spheroids migratory areas was calculated as the difference between areas at day 0 and day 3. The migration process was evident with all CAFs. Nevertheless, the effect of the microenvironment was significantly more evident with SDHB-mutated CAFs compared with NPV CAFs. Migration with SDHD-mutated CAFs was found to be intermediate between that with NPV CAFs and SDHB-mutated CAFs.

4.5.6 CAFs transcriptional responses depend on both tumour and stromal genotype.

To assess how the genotype of fibroblasts and tumour cells affects global gene expression in the tumour microenvironment, we performed RNA-seq and generated volcano plots comparing various co-culture conditions. Specifically, BELO-NPV CAFs (BK) were co-cultured with either SDHB-deficient cells (BB) or Parental cells (BP), while PAVA SDHB-mutated CAFs (PK) were co-cultured with the same two cell lines (PB and PP, respectively).

The BB vs BK comparison (Figure 39B) revealed a substantial transcriptional shift, with 1,002 genes significantly upregulated and 602 downregulated (padj < 0.05, |log2FC| > 1), indicating that SDHB-deficient tumour cells induce broad gene expression changes in NPV CAFs. Similarly, in the BP vs BK comparison (Figure 39A), 729 genes were upregulated and 366 downregulated, suggesting that even Parental cells can modulate CAFs gene expression, though to a lesser extent than SDHB-deficient cells. This comparison between BP Vs BB (Figure 39C) revealed 165 significantly upregulated and 77 downregulated genes, indicating that the SDHB-deficient cells induced specific transcriptional changes in BELO NPV CAFs.

In SDHB-mutated CAFs (PK), co-culture with SDHB-deficient cells (PB) induced an even more pronounced response, with 1,151 genes upregulated and 834 downregulated compared to PK culture (Figure 39E). In contrast, co-culture with Parental cells (PP vs PK) led to 965 upregulated and 629 downregulated genes (Figure 39D). Notably, the PB vs PP comparison, directly contrasting the effect of tumour genotype on a constant fibroblast background, showed 295 genes upregulated and 292 downregulated, indicating that tumour cell genotype independently affects transcriptional reprogramming in co-culture (Figure 39F).

Comparing the two sets of results (BB vs BP and PB vs PP) highlights the combined effect of both tumour and CAFs genotypes: the presence of SDHB mutation in CAFs (PB vs PP) enhances the transcriptional remodelling driven by SDHB-deficient tumour cells compared to the effect observed in non-mutated fibroblasts (BB vs BP). These findings underscore the complex crosstalk within the tumour microenvironment, where both stromal and tumour genetic backgrounds shape gene expression programs that may influence tumour progression and microenvironment remodelling.

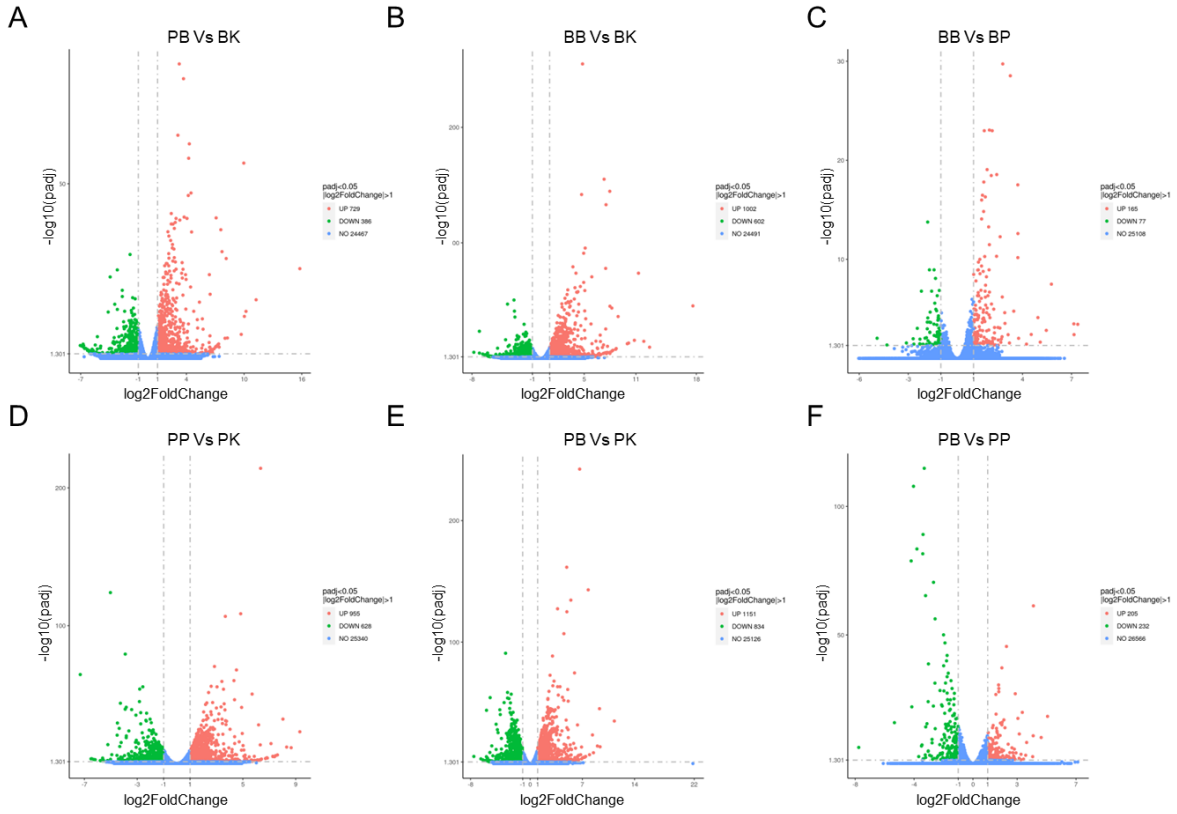

Figure 39: Volcano plots showing differentially expressed genes in CAFs carrying SDHB-mutation or Non-Pathogenic Variants, after 72h of co-culture with hPheo1 Parental or SDHB-deficient cells. Differential expression analysis was performed for three pairwise comparisons: BP vs BK (A), BB vs BK (B), and BB vs BP (C), PP vs PK (D), PB vs PK (E), and PB vs PP (F). Each point represents a gene, with the x-axis indicating the log_2 fold change in expression and the y-axis representing statistical

significance (-log_{10} adjusted p-value). Genes significantly upregulated ($log_2FC > 1$, padj < 0.05) are shown in red, downregulated genes ($log_2FC < -1$, padj < 0.05) in green, and non-significant genes in blue. CAFs show a stronger transcriptional response when co-cultured with SDHB-deficient cells (BB or PB) compared to either control (BK or PK) or Parental cells (BP or PP).

4.5.7 ECM Remodelling Gene Expression in CAFs Co-Cultured with SDHB-Deficient and Parental Tumour Cells

Given the observed differences in spheroid migration depending on CAFs genotype, we focused our analysis on genes involved in extracellular matrix (ECM) remodelling to better understand the molecular basis of this phenotypic variation. We identified genes commonly differentially expressed in CAFs co-cultured with either SDHB-deficient or Parental cells. Our analysis revealed a subset of matrix-associated genes that were consistently regulated across both co-culture conditions (Table 3-4). Notably, the number of matrix remodelling genes significantly altered in SDHB-mutated CAFs was slightly higher compared to Non-Pathogenic Variant (NPV) CAFs when co-cultured with SDHB-deficient or Parental cells. However, both CAFs genotype exhibited a conserved transcriptional response characterized by significant upregulation of key matrix components such as COL3A1, TNC, FBN1, LAMA1 and FBN1 which are crucial for collagen fibril formation, matrix assembly, and cell adhesion. Conversely, genes associated with matrix stabilization and organization, including VTN, MATN2, THBS3, and FBLN1, were consistently downregulated in both contexts. Additionally, CSPG4, a proteoglycan involved in matrix interactions and signalling, showed moderate upregulation across SDHB-mutated CAFs. These findings suggest that despite differences in CAFs genotype, the co-culture with tumour cells induces a shared ECM remodelling program that may contribute to alterations in matrix composition and tumour microenvironment remodelling, potentially influencing tumour cell migration and invasiveness observed in spheroid assays.

Gene	Regulation	Function in ECM
COL3A1	Up-regulated	Collagen fibril formation
TNC	Up-regulated	ECM glycoprotein, cell migration
FN1	Up-regulated	Cell adhesion, matrix assembly
LAMA1	Up-regulated	Basement membrane component
CSPG4	Up-regulated	Proteoglycan, matrix interaction
VTN	Down-regulated	Cell adhesion, matrix stabilization
MATN2	Down-regulated	ECM assembly and stabilization
THBS3	Down-regulated	ECM glycoprotein, cell-matrix adhesion
FBLN1	Down-regulated	ECM structural protein

Table 3: Common differentially expressed extracellular matrix remodelling genes in SDHB-mutated CAFs co-cultured with SDHB-Deficient or Parental Cells; COL3A1, Collagen Type III Alpha 1 Chain; TNC, Tenascin C; FN1, Fibronectin 1; LAMA1, Laminin Subunit Alpha 1; CSPG4, Chondroitin Sulfate Proteoglycan 4; VTN, Vitronectin; MATN2, Matrilin 2; THBS3, Thrombospondin 3; FBLN1, Fibulin 1

Gene	Regulation	Function in ECM
COL3A1	Up-regulated	Collagen fibril formation
FBN1	Up-regulated	ECM organization and integrity
TNC	Up-regulated	ECM glycoprotein, cell migration
MMP14	Up-regulated	Proteolytic degradation of ECM
THBS3	Down-regulated	ECM glycoprotein, cell-matrix adhesion

Table 4: Common differentially expressed extracellular matrix genes in Non-Pathogenic Variant (NPV) CAFs co-cultured with SDHB-Deficient or Parental Cells. COL3A1, Collagen Type III Alpha 1 Chain; TNC, Tenascin C; FBN1, Fibrillin 1; MMP14, Metallo-proteinase 14; THBS3, Thrombospondin 3;

5. Discussions

The following discussion has been published on Endocrine-related cancer. doi: 10.1530/ERC-23-0167.

5.1 Discussion aim 1 - electrophysiological properties of hPheo1

In the present study, we provide evidence that the loss of SDHB subunit affects electrophysiological features of human pheochromocytoma cells, which in turn leads to functional changes that can be related to an increase in their aggressiveness. Importantly, we also demonstrate for the first time that, *in vitro*, the enhanced migratory ability of SDHB-deficient cells was significantly inhibited by restoring their bioelectrical properties following glibenclamide treatment. It is known that transmembrane ion fluxes not only contribute to cell excitability but also play a noteworthy role in proliferation, cell cycle progression, and cell maturation and differentiation. Ion flows determine, for instance, the RMP, the voltage across the resting plasma membrane established by the balance of extracellular and intracellular ion concentrations. Such a balance is regulated by the activity of different ion channels, pumps and transporters located within the cell membrane that have specific ion selectivity and permeability. RMP is considered a fundamental regulator of cell behaviour in both excitable and non-excitable cells, modulating important cell functions such as proliferation and differentiation [206]. Thus, bioelectric properties can be useful markers for cell characterization because they are related to cell cycle progression, cell mitotic activity and differentiation. Interestingly, electrophysiological studies in several cancer cell types [207] have revealed depolarized membrane potential that favours cell proliferation: cancerous cells tend to have a depolarized RMP and are mitotically highly active. In contrast, more quiescent cells show more hyperpolarized membrane and show low mitotic activity [206]. In line with this observation, our results have actually documented that SDHB-deficient cells, which have a more negative membrane potential, exhibit a lower proliferative status compared to Parental cells. Another interesting finding is related to the analysis of passive properties. In particular, Cm, the electrical capacitance of cell membrane, is strictly connected to the membrane composition consisting of phospholipid bilayer with which various proteins are ‘associated’. Therefore, the overall Cm of a cell is a value directly proportional to the membrane surface area and the dielectric properties of the membrane. For this reason, Cm is usually considered an index related to the

cell surface. A thorough evaluation of this parameter could be used as an alternative marker for assessing cell proliferation for a wide field of applications, including cancer research. In this regard, Prakash and Abshire [208] employed integrated capacitance sensors for monitoring the growth of anchorage-dependent cells from breast cancer and observed an increased Cm value in response to cell adhesion that is usually followed by elevated proliferation. According to these observations, our experimental results revealed significantly lower Cm values in SDHB-deficient cells compared to Parental, which were indeed less adherent and featured lower proliferation. Interestingly, analysis of the ion currents in Parental cells revealed the occurrence of outward K+ currents and an I–V relation typical of voltage-dependent currents [200]. In contrast, analysis of SDHB-deficient cells showed that they feature greater mean amplitude and lack of voltage threshold. Of note, this larger outward current agrees with the significantly more hyperpolarized RMP observed in SDHB-deficient cells compared to Parental cells. The voltage dependence of this current, estimated by the I–V plot analysis, resembled that reported for currents flowing through ATP-sensitive potassium channels (KATP) [201], which are considered electrical transducers of the metabolic state of a cell by coupling cellular metabolism to the membrane potential [209]. Since SDHB-deficient cells showed reduced intracellular ATP content due to impaired SDH activity that is expected to trigger KATP channel activation, we performed experiments using the KATP channel inhibitor glibenclamide [201]. We indeed observed that glibenclamide significantly reduced the outward current, indicating a substantial implication of KATP current in the overall outward current. Noteworthy, the ion current recorded in the presence of glibenclamide, when KATP channels are blocked, showed a voltage threshold not statistically significant to that seen in Parental cells, suggesting that KATP channels are primarily activated in SDHB-deficient cells. Moreover, glibenclamide addition to SDHB-deficient cells determined a substantial recovery also of the passive properties showing similar values to those observed in Parental cells. As expected, the Rm value following the use of the channel blocker was definitely increased. In fact, channel blockers normally reduce the membrane conductance since they inhibit ion fluxes through those channels open in the resting cell that contribute to keep the membrane resistance low [210]. Although KATP channels are expressed on the cell surface membranes, several studies reported their presence also on mitochondria [211, 212]. This may not be surprising, since mitochondria are the major producers of ATP and the main

users of O2, mKATP channels are strategically located to sense changes in metabolite amount [213, 214]. However, despite the possible presence of KATP channels on the mitochondrial membrane (mKATP channels) in our cell model, the whole cell patch clamp technique applied in our study likely consents us to record phenomena occurring on the plasma lemma or, eventually, on membrane systems in continuity with it, not comprising events occurring on internal organelles. Based on this observation, we may reasonably suppose that glibenclamide effects observed on electrophysiological records are those on plasma membrane KATP channels. It is unclear if glibenclamide addition might affect KATP, but even if it could do it, this effect may not be observable in our current recordings. In this regard, Country and Jonz, by the whole-cell patch-clamp recordings, found that plasma membrane currents were not influenced by mKATP channel drugs in isolated goldfish retinal horizontal cells [213]. Further evidences for a role of KATP channels in SDHB-deficient cells' behaviour comes from experiments in which the addition of ATP, which is expected to have an inhibitory effect on KATP channels, also caused passive properties normalization of SDHB-deficient cells. At the same time, the outward current time course and the I–V plot related to experiments carried out under this condition indeed resembled the pattern of Parental cells, showing not statistically significant differences compared to them. This indicates that SDHB-deficient cells feature K+ channel activation similar to their Parental counterparts when the ATP content is restored, underlining the role of the metabolic condition in determining peculiar bioelectrical properties. Interestingly, since our results showed no differences in Kir6.1 expression, it is reasonable to conclude that the differences observed in electrophysiological recordings of outward K+ currents are related only to different functional activation of KATP channels and not to changes in their expression levels. It is known that tumour cells show a shift from oxidative phosphorylation to aerobic glycolysis even in the presence of oxygen, a phenomenon known as Warburg effect [215]. In addition to the lower ATP concentrations, SDHB-deficient cells showed increased intracellular lactate production followed by a reduced culture media pH compared with Parental cells. These results could be explained by the fact that cancer cells, typified by higher expression of regulators such as monocarboxylate transporters (MCTs), can mobilize lactic acid to the extracellular environment, whereby maintaining the intracellular pH homeostasis while decreasing the extracellular pH, as found for SDHB-deficient cells.

Furthermore, SDHB-deficient cells showed a lower proliferation rate compared to Parental cells. These results are in line with our data previously obtained on MTT cells silenced for SDHB [185], where we observed a lower proliferation rate. The association between deletion of SDHB and low proliferation has been demonstrated also for breast cancer [216]. From an ultrastructural point of view, using electron microscopy, we showed that SDHB depletion resulted in enlarged mitochondria and poorly organized internal cristae. This observation is consistent, albeit to a lesser extent, with the earlier report by Douwes Dekker and colleagues that SDHD-linked tumours have swollen mitochondria with loss of cristae [217]. Loriot and colleagues observed that EMT was activated in human metastatic SDHB-mutated PGLs [218]. Few years later, the same research group showed that in SDHB knockout mouse chromaffin cells occurred a molecular reprogramming compatible with the activation of EMT process [219]. More recently, Tabebi and colleagues [199] observed an upregulation of several genes involved in EMT in a SDHB knockout model of hPheo1. In accordance, we show that SDHB deficiency in hPheo1 cells leads to a transcriptional upregulation of Twist1, Snai1/2 and Vimentin. Remarkably, Tabebi et al. also found a significant increase in the percentage of trypsin sensitive cells due to SDHB loss, that is in agreement with our results. The association between trypsin sensitivity and migration is very limited; however, Zhu and colleagues [220] described this correlation in three different cancer cell lines, the MB49, the EJ and the SKOV3. Depletion of SDHB altered adhesion properties of the extracellular matrix by increasing trypsin sensitivity, by decreasing adhesion capacity and by inducing the acquisition of an EMT phenotype, therefore promoting a more malignant profile [219, 221, 222]. In this work, we showed that SDHB-deficient cells proliferate less than Parental cells but migrate significantly more, supporting their more aggressive phenotype. This result not only is consistent with what was found in SDHB knockout mouse chromaffin cells [219] but also with our previous data obtained with another chromaffin cell model, the MTT cells. In fact, in this cell line, we observed a higher migratory trend in single cultured MTT SDHB-silenced spheroids compared with single cultured MTT Wt spheroids [198]. Furthermore, when spheroids were co-cultured with cancer associated fibroblast (CAFs), despite we observed a massive migration induction, the number of the cells was smaller compared to their single cultured counterpart [192], supporting our hypothesis that the high motility is inversely related to cell proliferation and vice versa. Indeed, the addition of glibenclamide

significantly promoted proliferation and adhesion but significantly reduced migration and trypsin sensitivity of these cells. One of the strengths of this study is that hPheo1 cells and their SDHB-deficient counterparts [157, 188] are the only available human pheochromocytoma cells, which makes them a plausible candidate to increase our understanding of the fundamental mechanisms involved in oncogenesis and tumour development of PGLs. The main feature of pheochromocytomas and sympathetic paragangliomas is the release of catecholamines such as epinephrine, norepinephrine or dopamine [3]. However, characterization of hPheo1 cells showed that even if genes associated with catecholamine synthesis were highly expressed in the tumour tissue of origin, most of them were downregulated in hPheo1 cells. Consequently, one of the limits of this work is linked to the impossibility of studying the currents involved in catecholamine secretion. Despite the lack of hormone production, we provide here novel insights into the role of SDH that, by altering the metabolic characteristics of human pheochromocytoma cells, modulates their bioelectric properties which, in turn, affect some functional features and increase their aggressiveness. However, these functional alterations can be restored to some extent when the bioelectrical ones are recovered. Bioelectric signalling in cancer and particularly in metastasis is a growing field of study, which has demonstrated the importance in many of the key mechanisms of metastasis [223]. It is worth noting that all data presented here support the hypothesis that glibenclamide may exert significant anti-tumour activity in PGLs by inhibiting KATP channels [224]. In this regard, early studies have reported that glibenclamide could actually inhibit progression in many other cancers such as bladder carcinoma [225], prostate [226] and liver [227]. Moreover, in recent years, it has been demonstrated that glibenclamide can suppress cell invasion and migration in a human ovarian clear cell carcinoma ES-2 cells by blocking KATP channels [228]. Further experiments should be performed to support our data, especially in vivo studies and the use of selective drugs targeting KATP channels will be of interest. Taken together, our results highlight the importance of focusing also on cancer cell electrophysiological profile in order to eventually provide new approaches to targeting metastatic disease.

5.2 Discussion aim 2 - succinate role as an oncometabolite

In this paper, we shed light on the role of extracellular succinate and its receptor in modulating molecular processes that lead to the more aggressive phenotype of SDHB-deficient hPheo1 cells. We demonstrated that the binding of succinate with

SUCNR1 activates ERK1/2, that in turn induces DRP1 phosphorylation promoting migration. The activation of this pathway suggests that SUCNR1 is possibly coupled with Gq protein. Moreover, we also demonstrated that this pathway is not the only mechanism involved in this phenomenon.

Paragangliomas are rare neuroendocrine tumours arising from chromaffin cells with a strong hereditary basis. One of the susceptibility genes involved in the aetiology of these tumours is succinate dehydrogenase (SDH), whose mutations lead to aberrant accumulation of succinate. In addition, mutation in SDHB specifically predisposes to a more aggressive phenotype. Succinate is an intermediate in the tricarboxylic acid (TCA) cycle, and has emerged as a significant oncometabolite implicated in tumourigenesis: under pathological conditions such as hypoxia or mitochondrial dysfunction, succinate accumulates and exerts diverse effects on cancer progression [229]. One key mechanism involves the activation of succinate receptor 1 (SUCNR1, also known as GPR91), a G-protein-coupled receptor expressed in different tissues and tumour microenvironments [230]. SUCNR1 activation by extracellular succinate promotes pro-inflammatory signalling, angiogenesis, and cellular proliferation via pathways such as ERK1/2 and PI3K/Akt, and by HIF-1α stabilization. Recent studies also indicate that SUCNR1 signalling may modulate immune cell recruitment and polarization, further supporting a pro-tumourigenic milieu. Moreover, intracellular succinate can inhibit α-ketoglutarate-dependent dioxygenases, including prolyl-hydroxylases and histone demethylases, thereby altering epigenetic and hypoxic responses that favour cancer cell survival and metastasis [142].

Since in paragangliomas the role of succinate is not completely clear, which is the case in particular for its receptor SUCNR1, we studied both the effect of intracellular succinate accumulation and the role of extracellular succinate binding to SUCNR1 in two human pheochromocytoma sub-lines, Parental and SDHB-deficient cells. We used two forms of succinate, one permeable to cell membranes, which allowed us to increase its intracellular levels and study the effects of its accumulation, and one non-permeable, which acts via its membrane receptor SUCNR1.

Our results confirmed that intracellular succinate accumulation is able to induce a hyper-methylated and hyper-succinylated phenotype in our cell models. Using GC-MS, we showed that only the treatment with methyl-succinate increased intracellular succinate levels and was able to induce hyper-methylation in both cell lines compared to the untreated counterparts. Similarly, protein succinylation levels were significantly

increased by methyl-succinate treatment, compared to untreated cells. These results are in agreement with those previously observed, that inactivation of SDH causes the inhibition of α-ketoglutarate dependent dioxygenases, including histone demethylases, leading to an increase of H3K9me3 as reported by Letouzé and colleagues [25]. In addition, in RCC with decreased SDHD or SDHB expression, accumulation of succinate was reported to enhance cancer cell invasion and metastasis by increasing DNA 5-methylcytosine (5mC) and suppressing 5-hydroxymethylcytosine (5-hmC) by inhibition of TET-2, resulting in global DNA methylation [231].

We then evaluated effects of both succinates on cell proliferation and migration. We confirmed that SDHB-deficient growth is slower, but migration is higher compared to Parental cells [204]. With regard to proliferation, we found no statistical difference in the proliferation rate following treatment with either methylated or unmethylated succinate, which suggests that succinate is not involved in this process. Remarkably, only unmethylated succinate increased cell migration of both sub-lines, indicating that migration is controlled by the interaction between extracellular succinate and its receptor SUCNR1. Intriguingly, in SDHB-deficient cells, the protein expression level of the succinate receptor was higher compared to Parental cells. Besides, only in Parental cells the expression of SUCNR1 significantly increased after succinate treatment probably because in SDHB-deficient cells its expression is already high. We did not observe any difference in the expression of the succinate receptor upon methyl-succinate treatment. These data demonstrate that only the pathways activated by extracellular succinate and SUCNR1 regulate its expression. However, the molecular mechanisms by which this occurs have yet to be identified. Overall, our results agree with recent evidence: for instance, in immune cells, activation of SUCNR1 increases migration to sites of tissue damage or infection, thus contributing to the orchestration of inflammatory responses [159]. In the tumour microenvironment, high levels of succinate can stimulate SUCNR1 and promote epithelial-mesenchymal transition (EMT), matrix remodelling and tumour cell invasion, facilitating metastasis [158, 160].

SUCNR1 can be coupled with different G proteins, activating distinct intracellular signalling, depending on the cell type. In a recent study conducted on cardiomyocytes, Lu and colleagues [153] showed that succinate activates SUCNR1, initiating a signalling cascade that result in ERK1/2 phosphorylation. In addition,

different studies have identified ERK1/2 [152, 232, 233] as an activator of DRP1 regulating mitochondrial fission by promoting DRP1 phosphorylation. Interestingly, several studies reported that mitochondrial fission promotes cancer cell migration and invasion of diverse cancers including breast, hepatocellular and thyroid cancer [234-236]. In line with these results, we found higher expression of phosphorylated ERK1/2 and DRP1 in SDHB-deficient compared to Parental cells. Furthermore, succinate treatment for 15 or 30 min resulted in increase of ERK1/2 and DRP1 phosphorylation in both sub-lines. This implies that one of the possible succinate-SUCNR1 axis acts via Gq protein activation. On the other hand, longer stimulations with succinate, where we also observed upregulation of SUCNR1 in Parental cells, did not lead to increased ERK1/2 phosphorylation. On the contrary, DRP1 phosphorylation was found upregulated in both cell lines under identical experimental conditions. This effect may be explained by tighter regulation of ERK1/2 phosphorylation than that of DRP1, possibly since ERK1/2 is upstream of the central signalling cascade, the MAPK pathway, which controls a wide range of essential cellular processes. DRP1 phosphorylation, which drives mitochondrial fission, is a significantly slower process than other intracellular signaling pathways. This provides a mechanistic basis for a more precise and tightly regulated control of ERK1/2 phosphorylation activity rather than DRP1 phosphorylation. Consequently, ERK1/2 activity is subject to multiple levels of regulation, including sequential activation by RAF and MEK, positive and negative feedback loops, crosstalk with other pathways and precise spatial and temporal control (e.g. nuclear translocation) [237]. This allows highly sensitive and context-specific modulation of ERK1/2 activity. In contrast, DRP1 is a downstream effector that plays a more specialised role: regulation of mitochondrial fission. Its phosphorylation is controlled by a more restricted set of kinases, including ERK1/2 itself, as well as CDK1, PKA and CaMKII. Although ERK1/2 signalling has been considered an epitome of cell proliferation, it is now clear that deregulation of this pathway is linked to many other aspects of the tumour phenotype. Indeed, depending on the particular cell type, ERK1/2 signalling can regulate different processes such as differentiation, migration, angiogenesis and chromatin remodelling [238, 239]. Since in our cell models, ERK1/2 activation did not correlate with increased proliferation rate, we hypothesised that this pathway may be involved in cell migration. To test our hypothesis, we used a specific inhibitor of ERK1/2, SCH772984. This agent at 10 nM inhibited phosphorylation of ERK1/2 even after succinate stimulation,

without affecting proliferation or inducing cell death. We found that pharmacological inhibition of ERK1/2 was able to prevent DRP1 phosphorylation, indicating that also in our cells, DRP1 is a downstream target of ERK1/2. We showed that stimulation with succinate led to increased cell migration, but its effect was markedly reduced upon inhibition of ERK1/2 signalling. However, even in the presence of SCH772984, the effect of succinate was still significantly higher compared to control cells. These results suggest that although ERK1/2-mediated activation of DRP1 appears to be a critical step in hPheo1 cell migration, this pathway is not the only one involved in this process, meaning that there are additional signalling pathways involved in migration that are activated by binding of succinate to SUCNR1. Overall, our results show that increased SUCNR1 expression in SDHB-deficient cells is associated with ERK1/2-mediated activation of DRP1 and that this pathway is partially responsible for increased cell migration. Although our results uncovered the mechanism underlying the cell migration induced by succinate-SUCNR1 in part only, to the best of our knowledge, this is the only evidence concerning the functional effects of this interaction in human pheochromocytoma cells. It will be of interest for future studies to evaluate other pathways regulated by the succinate-SUCNR1 axis. We believe that understanding the role of the succinate-SUCNR1 axis in PGLs, particularly in SDHx-mutated tumours, will help identify pathways involved in key processes of tumour growth and spread.

5.3 Discussion aim 3 - mitochondria interaction with the nucleus

Here, we demonstrate that mitochondria establish direct contact sites with the nucleus in human pheochromocytoma cell lines, and identify the Translocator Protein (TSPO) as a key regulator in the formation of nucleus-associated mitochondria (NAMs). Moreover, we show a strong correlation between *in vitro* and *in vivo* findings, supporting the physiological relevance of our observations.

The mitochondria are essential organelles in eukaryotic cells, often referred to as the "powerhouses" of the cell because they generate most of the cell's supply of ATP Adenosine Triphosphate (ATP), the main energy currency. However, their role goes far beyond just energy production. Indeed, mitochondria actively participate in the reprogramming of mammalian cells [240, 241]. It is well established that mitochondria interact with the endoplasmic reticulum (ER) [242], however, in response to endogenous or exogenous perturbations, they retro-communicate with the nucleus to drive the transcription of genes. This pathway of signalling is known as the

mitochondrial retrograde response (MRR). The physical coupling between mitochondria and the nucleus has been reported as Nucleus-associated Mitochondria (NAM) [166]. The Translocator Protein (TSPO), located on the outer mitochondrial membrane, plays a critical role in regulating mitochondrial function, including cholesterol transport, apoptosis, and reactive oxygen species (ROS) signalling. Recent evidence suggests that TSPO is also involved in the formation of physical and functional contact sites between mitochondria and the nucleus [166]. Indeed, TSPO showed to be essential in this process, by acting as a scaffold or signalling hub that recruits or organizes molecular machinery required for tethering mitochondria to the nuclear envelope.

Given that SDHB-mutations lead to mitochondrial disfunction and metabolic alteration, in this part of our work we aimed to better understand how TSPO contributes to NAM formation and whether this mitochondrial–nuclear communication plays a role in the pathogenesis of these tumours.

We reported that the distance between mitochondria and the nucleus is significantly different between our two cell lines: when compared with Parental, SDHB-deficient cells showed a considerable decrease in the distance alongside with a significant increase in the number of contact sites. It is very interesting to note that the level of TSPO expression was found to be upregulated SDHB-deficient cells. Furthermore, perinuclear extraction and imaging technique, showed infiltrates of TSPO in the perinuclear region establish a constitutive space of occupancy by mitochondria, which is indicative of physical interaction. In addition, a higher number of proximal puncta was recorded by PLA in SDHB-deficient cells, leading us to hypothesise that TSPO may play a predominant role in contact formation in our cell lines. Indeed, TSPO silencing significantly reduced the number of proximal puncta recorded by PLA in both cell lines.

While originally studied for its role in cholesterol transport and steroidogenesis, emerging evidence shows that TSPO plays a broader role in mitochondrial function, ROS signalling and proliferation/invasion.

Loss-of-function mutation in SDHB impair electron flow in Complex II, thus leading to electron leakage and resulting in partial reduction of oxygen to form ROS. We showed that hPheo1 SDHB-deficient cells displayed higher levels of both mitochondrial superoxide (O_2^-) and hydrogen peroxide (H_2O_2) when compared to Parental. Moreover, ROS-induced lipid peroxidation was also confirmed by the lipid

peroxidation-sensitive probe C11-BODIPY 581/591. Our data are in line with previous results by Goncalves and colleagues [243] in which showed increased mitochondrial ROS and lipid peroxidation levels in imCC SDHB-/- cells. Interestingly, the mitochondrial remodelling around the nucleus could therefore crucially influence the signalling of ROS, which are also acknowledged factors in the retrograde response [240, 244] produced in excess by defective mitochondria over-expressing TSPO. Indeed, mitochondrial ROS levels significantly decrease when TSPO is down-regulated.

In the context of proliferation/migration, TSPO over-expression showed to drive proliferation and cancer progression in different cell model such as muscle cells, Breast Cancer cells, and rat glioma cells [245-247]. In our cell models TSPO contributes to both proliferation and migration: indeed, TSPO silencing significantly reduces both proliferation and migration in tumour cell lines, although the effects of the down-regulation were not able to bring the two populations back to an equal proliferation and/or migration rate. Indeed, even after TSPO knockdown, the proliferation of Parental cell was still higher compared to SDHB-deficient while SDHB-deficient cells migration was greater than Parental.

To validate the results obtained from our cell models and further investigate the role of TSPO and NAMs in a more physiologically relevant context, we aimed to analyse by western blot the expression of NAMs protein in Human Primary tissue samples from PGLs patients carrying Non-Pathogenic Variants (NPVs) or SDHx-mutations. Although the increased number of mitochondria made it difficult to perform an analysis of the mitochondrial-nuclear distance using electron microscopy, we nevertheless observed increased expression of the mitochondrial protein TSPO in SDHx-mutated tissues compared to NPVs. However, it is very interesting to note that the expression of nuclear AKAP95 was also upregulated, supporting the hypothesis of increased mitochondrial-nuclear communication and thus reinforcing the consistency between *in vitro* and *in vivo* results. Overall, these results make TSPO a potential biomarker for cancer and a therapeutic target in various diseases. These findings deepen our understanding of a fundamental process and detail the physical and metabolic coupling between mitochondria and the nucleus in human pheochromocytoma cells and tissues.

In conclusion, the ability of mitochondrial to communicate and send signals back to the nucleus ensures that mitochondrial performance is aligned with cellular demands,

stress conditions, and environmental changes. Disruption of this communication can lead to a range of disfunction, making the study of mitochondrial-nuclear interaction a key area in biomedical research. Understanding and potentially manipulating this communication holds promise for therapeutic interventions in metabolic, neurodegenerative, age-related diseases as well as cancer.

5.4 Discussion aim 4 - crosstalk between hPheo1 and endothelial cells

In this work we demonstrated that SDHB-deficient cells are capable not only of recruiting endothelial cells but also of increasing their permeability. Of note, we found that SDHB-deficient significantly induced the formation of capillary structures in HUVECs, compared to Parental ones, and that this effect was mainly due to EVs production.

The composition of the TME varies between tumour types, but hallmark features include immune cells, stromal cells, blood vessels, and extracellular matrix (ECM). Early in tumour growth, a dynamic and reciprocal relationship develops between cancer cells and the components of the TME to support cancer cell survival, local invasion and metastatic dissemination. To overcome a hypoxic and acidic microenvironment, the TME coordinate a program that promotes the formation of new blood vessels, a process known as neo-angiogenesis, in order to restore oxygen/nutrient supply, remove metabolic waste and lead to metastasis. Metastasis is a multistep process that involves translocation of cancer cells from the primary TME to distant locations. Tumour cells must first escape the primary tumour site and enter the vasculature in a process known as intravasation. During intravasation, tumour cells adhere to endothelial cells and this interaction changes the endothelial barrier and allows tumour cells to migrate.

In the context of tumour development, EVs are indeed gaining recognition as significant contributors to angiogenesis. They represent a heterogeneous collection of lipid bilayer-enclosed particles, actively synthesized and secreted by a myriad of cell types under normal or pathological conditions into the extracellular milieu. Cancer-derived EV cargo varies depending on cancer type and stage. This cargo may include a diverse range of nucleic acids, proteins, and lipids that can be a source of pro-tumourigenic and anti-tumourigenic signaling molecules [248].

Since Paragangliomas are known to be well vascularized tumours, we decided to focus the attention not only on the reciprocal effect among the two human pheochromocytoma cell lines (hPheo1), Parental or deficient for the SDHB subunit,

and the Human Umbilical Vein Endothelial Cell (HUVEC) line, on proliferation, migration, permeabilization and *in vitro* angiogenetic structures, but also the role of EVs as possible mediators of these processes.

Our results on proliferation showed that only SDHB-deficient cells, but not Parental, were able to increase their proliferation when co-cultured with HUVECs. On the contrary, HUVECs proliferation was not affected by either Parental or SDHB-deficient cells. Regarding migration, only SDHB-deficient cells significantly increased HUVECs migratory capacity, compared to single culture. On the contrary, the presence of HUVECs did not affect tumour cells migration. Taken together these results suggest that, when co-cultured with HUVECs, SDHB-deficient cells are able not only to proliferate more but also to recruit endothelial cells.

We next investigated whether endothelial monolayer permeability changes or not in the presence of tumour cells. Surprisingly, our results showed that the permeability to FITC-Dextran significantly increased when HUVECs were co-cultured only with SDHB-deficient cells. As we already mention, an important role of endothelial cells is to provide protective barriers to the various organs from their surroundings and help maintaining homeostasis [249, 250]. These protective barriers are categorized as Tight Junctions (TJs), Adherens Junctions (AJs), and Desmosomes.

In line with results on permeability, we observed a significant reduction of the protein expression levels of Tight Junction Claudin-5 and Adherens Junction CD31 (PECAM) in HUVECs co-cultured with SDHB-deficient cells. Claudin-5 is a key component of TJs in endothelial cells, acting as a key regulator of barrier permeability by forming paracellular pores that prevent unwanted molecules from passing through. When Claudin-5 is lost, the tight junctions become discontinuous, increasing paracellular permeability [251]. CD31 plays a crucial role in regulating endothelial junctional integrity, influencing events such as the maintenance of barrier function, endothelial cell survival, and regulating the migration of cells. It has been showed that Loss of CD31 lead to loosened adherens junctions and increased permeability in retinal cancer cell [252]. The importance of EVs has been uncovered also in a very interesting work by Wang and colleagues, where they showed that EVs can disrupt the endothelial barrier to promote the trans-endothelial migration of gastric cancer cells [253]. In addition, they also found that EVs were also able to reduce the expression of VE-cadherin, which maintains the integrity of endothelial junctions.

To study angiogenesis *in vitro*, we employed the capillary formation assay, which revealed the critical role of EVs, as their removal from the culture medium significantly impaired angiogenic structures, with a more pronounced effect observed for EVs derived from SDHB-deficient cells compared to those from parental cells.

Furthermore, the characterization of tumour-derived EVs demonstrated that, when normalized to the same number of cells, SDHB-deficient cells generated a markedly higher abundance of EVs compared to those derived from Parental cells, underscoring a potential link between SDHB deficiency and enhanced vesicular output, which may contribute to the altered tumour microenvironment; notably, both SDHB-deficient and Parental EVs exhibited a broad spectrum of sizes, reflecting their heterogeneity, and this observation prompts critical questions about the functional implications of such variability; therefore, future investigations are imperative to elucidate whether these size differences correlate with distinct cargo compositions - encompassing proteins, nucleic acids, lipids, and metabolites - that could differentially regulate key biological processes.

Overall, our *in vitro* results showed that SDHB-deficient cells are able to modify the surrounding microenvironment in such a way as to make it more suitable for tumour spread. In fact, they are able to recruit endothelial cells and, at the same time, thanks to their presence, SDHB-deficient cells are able to increase their own proliferation. Furthermore, SDHB-deficient cells increased both endothelial permeability and the number of vessels. In particular, vessel formation is due to the production of tumour EVs, which are not only produced in significantly greater numbers compared to Parental cells, but also have a different metabolic content. For these reasons, it will be interesting to conduct further studies to better understand also the lipid, the genetic and the protein content of these EVs. In conclusion, studying cancer EVs is crucial because they serve as key communicators in cancer progression, making them valuable biomarkers for early diagnosis and prognosis, and potential targets for developing new therapies and drug delivery systems. These tiny, cell-derived particles carry molecules like RNA and proteins that provide snapshots of tumour activity, allowing for non-invasive monitoring through liquid biopsies, and can even be engineered to deliver drugs directly to cancer cells or to re-engage the immune system against the tumour. We strongly believe that EVs influence and are influenced by the tumour microenvironment, and understanding their interactions helps in developing effective therapies.

5.5 Discussion aim 5 - hPheo1 communication with the stroma

In the last part of this project, we focused on another important population of the tumour microenvironment: fibroblasts. Fibroblasts are known to play a key role in cancer, mainly through their transformation into cancer-associated fibroblasts (CAFs), which significantly influence tumour onset, progression, metastasis and also resistance to therapy.

In order to better understand the role of CAFs in PGLs and thanks to our collaboration with Careggi Hospital, we were able to isolate fibroblasts from the peritumoural fat of patients with NPV or SDHx-mutated PGL who underwent surgery. After isolation, our cultures were tested and found to be positive for specific markers typically expressed by fibroblasts and CAFs. These include: smooth muscle alpha-actinin (αSMA), a key fibroblast intermediate filament protein that may indicate the presence of myofibroblasts; fibroblast-specific protein 1 (FSP1), also known as S100A4, a calcium-binding cytoplasmic protein expressed primarily in fibroblasts of various organs, which serves as a reliable marker for the identification of fibroblasts; and fibroblast activation protein (FAP), a cell surface protein expressed by cancer-associated fibroblasts.

It is well known that PGL aggressiveness depends on which susceptibility gene is mutated. It is particularly interesting that tumours mutated for genes encoding for the different subunits of the same enzyme, such as the SDH, show a completely different ability to spread and metastasize. Indeed, tumours mutated for SDHC or SDHD are usually benign, whereas those mutated for SDHB are very often malignant [254]. Since SDHB-mutated PGL are more aggressive than those mutated in other susceptibility genes, our results on migration confirm and support what has been stated in the literature. Given that our patient cohort harbored germline mutations in key susceptibility genes, we hypothesized that the heterogeneous genetic profiles of other cell populations within the tumor microenvironment, such as stromal cells, could exert differential modulatory effects on the metabolic and functional characteristics of tumor cells. Intrinsic genetic alterations in tumor cells could, in turn, reciprocally influence the adaptive responses and phenotypic plasticity of this surrounding population, thus contributing to the overall tumor heterogeneity and progression observed in these inherited syndromes.

In this study, we investigated the effect of primary human fibroblasts derived from patients with PGL with NPV or SDHx mutations on hPheo1 cell lines and vice versa.

To our knowledge, this is the only research conducted on primary cells derived from PGL tumours that demonstrates an important contribution of CAFs, especially those with SDHx mutations. In particular, we found that only the proliferation of SDHB-deficient hPheo1 cells was significantly increased when co-cultured with primary fibroblasts, compared to their respective single culture, regardless of their genotype. In contrast, Parental cells were not affected by the presence of fibroblasts in terms of proliferation. Similarly, only the growth of SDHB-mutated CAFs significantly increased when co-cultured with tumour cells. In contrast, the proliferative capacity of NPV CAFs in co-culture with both tumour lines did not change compared to single culture. We then observed that CAF migration significantly increased only when co-cultured with hPheo1 SDHB-deficient cells, regardless of their genotype. As for CAFs-induced tumour cell migration, we surprisingly found that migration increased only when co-cultured with SDHB-mutated CAFs, both in Parental and SDHB-deficient cells. From these initial results, we can conclude that the interaction between CAFs and tumour cells is finely determined by the cell genotype. In fact, SDHB-deficient cells proved to be more sensitive than Parental cells, in terms of proliferation, in the presence of CAFs. In addition, cell genotype also played a key role in migration, since only SDHB-mutated CAFs were able to increased tumour cell migration.

It is widely accepted that transformed cells, growing in a monolayer on plastic dishes, have little in common with the complex 3D multicellular organization found in living organisms. Awareness of this discrepancy has led to studies intended to find more appropriate cellular models to better represent the in vivo scenario. These models include long-known multicellular spheroids, which seems to represent the best compromise. In fact, they can be easily standardized, and yet, they provide enough complexity, such as 3D geometry, to represent relevant aspects of human tumours [255]. In addition, the use of spheroids also gives the possibility to better investigate other features, such as cell-cell interactions.

For all these reasons, we attempted to switch from a 2D culture to a 3D culture to study the effects of CAFs on spheroids migration. In so doing, SDHB-deficient cells were first transfected with mCherry, then spheroids were induced and subsequently placed on a monolayer of CAFs (NPV, SDHD or SDHB-mutated).

Interestingly, we observed an increase in spheroid migration induced by all CAFs, but the effect was more pronounced with SDHB-mutated CAFs than with NPV CAFs. Surprisingly, SDHD-mutated CAFs induced migration that was intermediate between

that induced by NPV CAFs and SDHB-mutated CAFs. Overall, we demonstrated that SDHB-deficient spheroids showed different functional response to the pro-migration drivers produced by NPV or SDHx-mutated CAFs.

Our results on spheroids migration, highlighted the relevance of the TME contribution to the aggressiveness of SDHB-deficient cells, and confirming that tumour stroma cells are a promising therapeutic target for cancer treatment.

RNA-seq analysis revealed that co-culture with hPheo1 tumour cells markedly reprograms CAFs transcriptional profiles, and that this reprogramming is modulated not only by tumour cells genotype but also by the CAFs genotype itself. The stronger response induced by SDHB-deficient cells, and the enhanced responsiveness of SDHB-mutated CAFs, highlighted a complex and potentially synergistic crosstalk shaped by mitochondrial/metabolic dysfunction. Indeed, our results showed that both Parental and SDHB-deficient cells can induce robust transcriptional changes in CAFs, but that SDHB-deficient tumour cells provoke a larger number of differentially expressed genes. This is consistent with the literature that metabolic stress or oncometabolite accumulation in SDHB-mutated cells amplifies their ability to influence the microenvironment. Mechanistically, loss of SDH activity leads to accumulation of succinate, which can inhibit α-ketoglutarate–dependent dioxygenases (including prolyl hydroxylases and histone/DNA demethylases) and thereby promote a pseudo-hypoxic, epigenetically altered state (e.g. via HIF stabilization) that may enhance secretion of paracrine factors or metabolic signals [256, 257]. In fact, extracellular succinate has been implicated in driving metastasis and remodelling in several cancers [258]. Thus, CAFs exposed to SDHB-deficient cells may receive stronger or qualitatively different signals (e.g. hypoxia-inducible factors, reactive oxygen species, cytokines) compared to Parental cells. A particularly striking aspect of our findings is that SDHB-mutated CAFs responded more strongly to tumour co-culture (i.e. more DEGs) than NPV CAFs. This suggests that stromal mitochondrial dysfunction primes or sensitizes fibroblasts to tumour-derived signals, altering their baseline state and capacity for reprogramming.

We hypothesised that SDHB-mutated CAFs are already under metabolic stress or have an altered redox balance, a modified epigenetic landscape, or altered basal signalling, making them more sensitive to external perturbations. In this “pre-activated” or more labile state, tumour-derived metabolic or cytokine signals could more easily alter transcriptional balance, leading to exaggerated changes.

This concept is consistent with the literature demonstrating that stromal heterogeneity and metabolic state influence CAF behaviour. For example, CAFs are not a uniform population but comprise subtypes with variable metabolic linkages and epigenetic states that influence tumour metabolism and response to therapy [259]. In tumours such as pancreatic ductal adenocarcinoma, CAF subtypes (myCAF, iCAF, apCAF) differ not only in their secretory phenotype but also in their metabolic interactions with tumour cells [260].

Because we observed consistent differential gene sets in the pairwise comparisons of tumour genotypes (i.e. BB vs BP and PB vs PP), we infer that SDHB-deficient cells exerts a robust influence regardless of stromal background. However, the magnitude of the response and number of DEGs depends on whether fibroblasts themselves harbour a mutation. This highlights context-dependent interference, in which the stromal genotype modulates the amplitude and possibly the quality of tumour-induced signals.

Focusing on extracellular matrix (ECM)-related genes, our analysis revealed that both SDHB-mutated and NPV CAFs, upon co-culture with SDHB-deficient or Parental cells, undergo conserved transcriptional remodelling of key matrix components. In particular, COL3A1, TNC, FN1, LAMA1 and FBN1 were consistently upregulated, while matrix stabilizers including VTN, MATN2, THBS3, and FBLN1 were downregulated. Additionally, the proteoglycan CSPG4 showed moderate upregulation in SDHB-mutated CAFs, suggesting a role in modulating cell-matrix interactions. The upregulation of fibrillar collagens and adhesion molecules aligns with previous reports that increased collagen deposition and tenascin-C expression contribute to ECM stiffening and promote tumour cell invasion and metastasis [261, 262]. For instance, COL3A1 is one of the major components of the stromal matrix and its overexpression correlates with enhanced tumour aggressiveness and poor prognosis in various cancers [3]. Tenascin-C (TNC) is a well-characterized ECM glycoprotein involved in matrix remodelling and cellular migration, known to be elevated in tumour microenvironments and linked to metastatic potential [263]. Conversely, the downregulation of matrix stabilizing proteins such as vitronectin (VTN) and fibulin-1 (FBLN1) may reflect dynamic ECM remodelling favouring a more permissive environment for tumour progression. VTN, a multifunctional adhesive glycoprotein, mediates cell attachment and inhibits proteolysis, and its reduced expression could lead to ECM disorganization facilitating cancer cell dissemination

[264]. Similarly, decreased fibulin-1 has been implicated in disrupted matrix architecture and increased tumour cell motility [265]. The observed modulation of CSPG4, a chondroitin sulfate proteoglycan, is noteworthy given its role in matrix remodelling and cell signalling that promotes cancer cell migration and survival [266]. Its upregulation may contribute to the altered tumour-stroma crosstalk observed in our co-culture system.

Importantly, these transcriptional changes in ECM-related genes correlate with our phenotypic observations of altered spheroid migration depending on fibroblast genotype, suggesting that fibroblast-driven ECM remodelling significantly impacts tumour cell behaviour. These results support the concept that the tumour microenvironment, shaped by both stromal and tumour genotypes, dynamically regulates matrix composition to influence tumour progression [267].

In light of our findings and the growing body of evidence suggesting that the biomechanical properties of the ECM, particularly its stiffness, play a pivotal role in dictating the migratory behaviour of tumour cells by modulating cytoskeletal dynamics and integrin-mediated signalling pathways, it would be highly informative to investigate how ECM stiffness influences the type of migration - whether amoeboid, characterized by rounded, protease-independent movement, or mesenchymal, marked by elongated, protease-dependent invasion - in our spheroids. These studies could reveal critical insights into how matrix rigidity shapes the metastatic potential and invasive strategies of these cells.

Mechanistically, these ECM changes may be driven by signalling pathways such as TGF-β and hypoxia-inducible factors, which are known to regulate CAF activation and ECM remodelling in cancers [268]. Further studies are warranted to delineate these pathways in the context of SDHB mutation. While our findings provide insight into ECM transcriptional dynamics, validation at the protein level and functional assays such as matrix stiffness measurements and invasion studies will be critical to fully understand the biological impact. Moreover, targeting ECM remodelling pathways may represent a therapeutic avenue to disrupt tumour-stroma interactions and inhibit cancer progression.

6. Bibliography

1. Lam, A.K., *Update on Adrenal Tumours in 2017 World Health Organization (WHO) of Endocrine Tumours.* Endocr Pathol, 2017. **28**(3): p. 213-227.
2. Mete, O., et al., *Overview of the 2022 WHO Classification of Paragangliomas and Pheochromocytomas.* Endocr Pathol, 2022. **33**(1): p. 90-114.
3. Lenders, J.W.M., et al., *Genetics, diagnosis, management and future directions of research of phaeochromocytoma and paraganglioma: a position statement and consensus of the Working Group on Endocrine Hypertension of the European Society of Hypertension.* J Hypertens, 2020. **38**(8): p. 1443-1456.
4. Berends, A.M.A., et al., *Incidence of pheochromocytoma and sympathetic paraganglioma in the Netherlands: A nationwide study and systematic review.* Eur J Intern Med, 2018. **51**: p. 68-73.
5. Buffet, A., et al., *An overview of 20 years of genetic studies in pheochromocytoma and paraganglioma.* Best Pract Res Clin Endocrinol Metab, 2020. **34**(2): p. 101416.
6. Mercado-Asis, L.B., et al., *PHEOCHROMOCYTOMA: A GENETIC AND DIAGNOSTIC UPDATE.* Endocr Pract, 2018. **24**(1): p. 78-90.
7. Lenders, J.W., et al., *Pheochromocytoma and paraganglioma: an endocrine society clinical practice guideline.* J Clin Endocrinol Metab, 2014. **99**(6): p. 1915-42.
8. Leung, A.A., et al., *Epidemiology of pheochromocytoma and paraganglioma: population-based cohort study.* Eur J Endocrinol, 2021. **184**(1): p. 19-28.
9. Ebbehoj, A., et al., *Incidence and Clinical Presentation of Pheochromocytoma and Sympathetic Paraganglioma: A Population-based Study.* J Clin Endocrinol Metab, 2021. **106**(5): p. e2251-e2261.
10. Aygun, N. and M. Uludag, *Pheochromocytoma and Paraganglioma: From Epidemiology to Clinical Findings.* Sisli Etfal Hastan Tip Bul, 2020. **54**(2): p. 159-168.
11. Berends, A.M.A., et al., *Intricacies of the Molecular Machinery of Catecholamine Biosynthesis and Secretion by Chromaffin Cells of the Normal Adrenal Medulla and in Pheochromocytoma and Paraganglioma.* Cancers (Basel), 2019. **11**(8).
12. Fishbein, L., *Pheochromocytoma and Paraganglioma: Genetics, Diagnosis, and Treatment.* Hematol Oncol Clin North Am, 2016. **30**(1): p. 135-50.
13. Boedeker, C.C., G.J. Ridder, and J. Schipper, *Paragangliomas of the head and neck: diagnosis and treatment.* Fam Cancer, 2005. **4**(1): p. 55-9.
14. Katabathina, V.S., et al., *Genetics and imaging of pheochromocytomas and paragangliomas: current update.* Abdom Radiol (NY), 2020. **45**(4): p. 928-944.
15. Constantinescu, G., et al., *Silent pheochromocytoma and paraganglioma: Systematic review and proposed definitions for standardized terminology.* Front Endocrinol (Lausanne), 2022. **13**: p. 1021420.
16. Eisenhofer, G., et al., *Pheochromocytoma catecholamine phenotypes and prediction of tumor size and location by use of plasma free metanephrines.* Clin Chem, 2005. **51**(4): p. 735-44.
17. Eisenhofer, G., et al., *Catecholamine metabolomic and secretory phenotypes in phaeochromocytoma.* Endocr Relat Cancer, 2011. **18**(1): p. 97-111.
18. Jiang, J., et al., *Sino-European Differences in the Genetic Landscape and Clinical Presentation of Pheochromocytoma and Paraganglioma.* J Clin Endocrinol Metab, 2020. **105**(10).
19. Gieldon, L., et al., *Optimizing Genetic Workup in Pheochromocytoma and Paraganglioma by Integrating Diagnostic and Research Approaches.* Cancers (Basel), 2019. **11**(6).
20. Luchetti, A., et al., *Profiling of somatic mutations in phaeochromocytoma and paraganglioma by targeted next generation sequencing analysis.* Int J Endocrinol, 2015. **2015**: p. 138573.
21. Burnichon, N., et al., *Integrative genomic analysis reveals somatic mutations in pheochromocytoma and paraganglioma.* Hum Mol Genet, 2011. **20**(20): p. 3974-85.
22. Jochmanova, I. and K. Pacak, *Genomic Landscape of Pheochromocytoma and Paraganglioma.* Trends Cancer, 2018. **4**(1): p. 6-9.
23. Fishbein, L., et al., *Comprehensive Molecular Characterization of Pheochromocytoma and Paraganglioma.* Cancer Cell, 2017. **31**(2): p. 181-193.

24. Crona, J., D. Taïeb, and K. Pacak, *New Perspectives on Pheochromocytoma and Paraganglioma: Toward a Molecular Classification.* Endocr Rev, 2017. **38**(6): p. 489-515.
25. Letouzé, E., et al., *SDH mutations establish a hypermethylator phenotype in paraganglioma.* Cancer Cell, 2013. **23**(6): p. 739-52.
26. Pang, Y., et al., *A novel splicing site IRP1 somatic mutation in a patient with pheochromocytoma and JAK2.* BMC Cancer, 2018. **18**(1): p. 286.
27. Bezawork-Geleta, A., et al., *Mitochondrial Complex II: At the Crossroads.* Trends Biochem Sci, 2017. **42**(4): p. 312-325.
28. Selak, M.A., et al., *Succinate links TCA cycle dysfunction to oncogenesis by inhibiting HIF-alpha prolyl hydroxylase.* Cancer Cell, 2005. **7**(1): p. 77-85.
29. Bechmann, N., et al., *HIF2α supports pro-metastatic behavior in pheochromocytomas/paragangliomas.* Endocr Relat Cancer, 2020. **27**(11): p. 625-640.
30. Jochmanová, I., et al., *Hypoxia-inducible factor signaling in pheochromocytoma: turning the rudder in the right direction.* J Natl Cancer Inst, 2013. **105**(17): p. 1270-83.
31. Wang, K., et al., *Pre-clinical phaeochromocytoma and paraganglioma models: Cell lines, animal models, and a human primary culture model.* Best Pract Res Clin Endocrinol Metab, 2024. **38**(6): p. 101913.
32. Lenders, J.W., et al., *Phaeochromocytoma.* Lancet, 2005. **366**(9486): p. 665-75.
33. Kopetschke, R., et al., *Frequent incidental discovery of phaeochromocytoma: data from a German cohort of 201 phaeochromocytoma.* Eur J Endocrinol, 2009. **161**(2): p. 355-61.
34. Nölting, S., et al., *Personalized Management of Pheochromocytoma and Paraganglioma.* Endocr Rev, 2022. **43**(2): p. 199-239.
35. McCrary, H.C., et al., *Characterization of Malignant Head and Neck Paragangliomas at a Single Institution Across Multiple Decades.* JAMA Otolaryngol Head Neck Surg, 2019. **145**(7): p. 641-646.
36. Eisenhofer, G., et al., *Plasma metanephrines are markers of pheochromocytoma produced by catechol-O-methyltransferase within tumors.* J Clin Endocrinol Metab, 1998. **83**(6): p. 2175-85.
37. Boyle, J.G., et al., *Comparison of diagnostic accuracy of urinary free metanephrines, vanillyl mandelic Acid, and catecholamines and plasma catecholamines for diagnosis of pheochromocytoma.* J Clin Endocrinol Metab, 2007. **92**(12): p. 4602-8.
38. Eisenhofer, G. and M. Peitzsch, *Laboratory evaluation of pheochromocytoma and paraganglioma.* Clin Chem, 2014. **60**(12): p. 1486-99.
39. de Jong, W.H., et al., *Dietary influences on plasma and urinary metanephrines: implications for diagnosis of catecholamine-producing tumors.* J Clin Endocrinol Metab, 2009. **94**(8): p. 2841-9.
40. Deutschbein, T., et al., *Influence of various confounding variables and storage conditions on metanephrine and normetanephrine levels in plasma.* Clin Endocrinol (Oxf), 2010. **73**(2): p. 153-60.
41. Lenders, J.W., et al., *Is supine rest necessary before blood sampling for plasma metanephrines?* Clin Chem, 2007. **53**(2): p. 352-4.
42. Osinga, T.E., et al., *Mass spectrometric quantification of salivary metanephrines-A study in healthy subjects.* Clin Biochem, 2016. **49**(13-14): p. 983-8.
43. Taïeb, D., et al., *European Association of Nuclear Medicine Practice Guideline/Society of Nuclear Medicine and Molecular Imaging Procedure Standard 2019 for radionuclide imaging of phaeochromocytoma and paraganglioma.* Eur J Nucl Med Mol Imaging, 2019. **46**(10): p. 2112-2137.
44. Nölting, S., et al., *Current Management of Pheochromocytoma/Paraganglioma: A Guide for the Practicing Clinician in the Era of Precision Medicine.* Cancers (Basel), 2019. **11**(10).
45. Sbardella, E. and A.B. Grossman, *Pheochromocytoma: An approach to diagnosis.* Best Pract Res Clin Endocrinol Metab, 2020. **34**(2): p. 101346.
46. Carrasquillo, J.A., et al., *Imaging of Pheochromocytoma and Paraganglioma.* J Nucl Med, 2021. **62**(8): p. 1033-1042.
47. Treglia, G., et al., *Diagnostic performance of 18F-dihydroxyphenylalanine positron emission tomography in patients with paraganglioma: a meta-analysis.* Eur J Nucl Med Mol Imaging, 2012. **39**(7): p. 1144-53.

48. Nockel, P., et al., *Preoperative genetic testing in pheochromocytomas and paragangliomas influences the surgical approach and the extent of adrenal surgery.* Surgery, 2018. **163**(1): p. 191-196.
49. Neumann, H.P.H., et al., *Comparison of Pheochromocytoma-Specific Morbidity and Mortality Among Adults With Bilateral Pheochromocytomas Undergoing Total Adrenalectomy vs Cortical-Sparing Adrenalectomy.* JAMA Netw Open, 2019. **2**(8): p. e198898.
50. Castinetti, F., et al., *Outcomes of adrenal-sparing surgery or total adrenalectomy in phaeochromocytoma associated with multiple endocrine neoplasia type 2: an international retrospective population-based study.* Lancet Oncol, 2014. **15**(6): p. 648-55.
51. Fishbein, L., et al., *mutation carriers with malignant pheochromocytoma respond better to CVD.* Endocr Relat Cancer, 2017. **24**(8): p. L51-L55.
52. Niemeijer, N.D., et al., *Chemotherapy with cyclophosphamide, vincristine and dacarbazine for malignant paraganglioma and pheochromocytoma: systematic review and meta-analysis.* Clin Endocrinol (Oxf), 2014. **81**(5): p. 642-51.
53. Granberg, D., C.C. Juhlin, and H. Falhammar, *Metastatic Pheochromocytomas and Abdominal Paragangliomas.* J Clin Endocrinol Metab, 2021. **106**(5): p. e1937-e1952.
54. Ribeiro Franco, P.I., et al., *Tumor microenvironment components: Allies of cancer progression.* Pathol Res Pract, 2020. **216**(1): p. 152729.
55. Hanahan, D. and R.A. Weinberg, *Hallmarks of cancer: the next generation.* Cell, 2011. **144**(5): p. 646-74.
56. Shoucair, I., et al., *The Role of Cancer-Associated Fibroblasts and Extracellular Vesicles in Tumorigenesis.* Int J Mol Sci, 2020. **21**(18).
57. Gao, X., et al., *Histopathological Analysis of Tumor Microenvironment and Angiogenesis in Pheochromocytoma.* Front Endocrinol (Lausanne), 2020. **11**: p. 587779.
58. Bhowmick, N.A., E.G. Neilson, and H.L. Moses, *Stromal fibroblasts in cancer initiation and progression.* Nature, 2004. **432**(7015): p. 332-7.
59. Biffi, G., et al., *IL1-Induced JAK/STAT Signaling Is Antagonized by TGFβ to Shape CAF Heterogeneity in Pancreatic Ductal Adenocarcinoma.* Cancer Discov, 2019. **9**(2): p. 282-301.
60. Albrengues, J., et al., *Epigenetic switch drives the conversion of fibroblasts into proinvasive cancer-associated fibroblasts.* Nat Commun, 2015. **6**: p. 10204.
61. Liu, T., et al., *Cancer-associated fibroblasts: an emerging target of anti-cancer immunotherapy.* J Hematol Oncol, 2019. **12**(1): p. 86.
62. Cirri, P. and P. Chiarugi, *Cancer associated fibroblasts: the dark side of the coin.* Am J Cancer Res, 2011. **1**(4): p. 482-97.
63. Webber, J., et al., *Cancer exosomes trigger fibroblast to myofibroblast differentiation.* Cancer Res, 2010. **70**(23): p. 9621-30.
64. Chowdhury, R., et al., *Cancer exosomes trigger mesenchymal stem cell differentiation into pro-angiogenic and pro-invasive myofibroblasts.* Oncotarget, 2015. **6**(2): p. 715-31.
65. Fang, T., et al., *Tumor-derived exosomal miR-1247-3p induces cancer-associated fibroblast activation to foster lung metastasis of liver cancer.* Nat Commun, 2018. **9**(1): p. 191.
66. Witkiewicz, A.K., et al., *An absence of stromal caveolin-1 expression predicts early tumor recurrence and poor clinical outcome in human breast cancers.* Am J Pathol, 2009. **174**(6): p. 2023-34.
67. Sloan, E.K., et al., *Stromal cell expression of caveolin-1 predicts outcome in breast cancer.* Am J Pathol, 2009. **174**(6): p. 2035-43.
68. Capparelli, C., et al., *CTGF drives autophagy, glycolysis and senescence in cancer-associated fibroblasts via HIF1 activation, metabolically promoting tumor growth.* Cell Cycle, 2012. **11**(12): p. 2272-84.
69. Vallabhaneni, K.C., H. Haller, and I. Dumler, *Vascular smooth muscle cells initiate proliferation of mesenchymal stem cells by mitochondrial transfer via tunneling nanotubes.* Stem Cells Dev, 2012. **21**(17): p. 3104-13.
70. Guan, F., et al., *Mitochondrial transfer in tunneling nanotubes-a new target for cancer therapy.* J Exp Clin Cancer Res, 2024. **43**(1): p. 147.

71. LeBleu, V.S. and R. Kalluri, *A peek into cancer-associated fibroblasts: origins, functions and translational impact.* Dis Model Mech, 2018. **11**(4).
72. Chen, Y., K.M. McAndrews, and R. Kalluri, *Clinical and therapeutic relevance of cancer-associated fibroblasts.* Nat Rev Clin Oncol, 2021. **18**(12): p. 792-804.
73. Orimo, A., et al., *Stromal fibroblasts present in invasive human breast carcinomas promote tumor growth and angiogenesis through elevated SDF-1/CXCL12 secretion.* Cell, 2005. **121**(3): p. 335-48.
74. Gorchs, L., et al., *Cancer-associated fibroblasts from lung tumors maintain their immunosuppressive abilities after high-dose irradiation.* Front Oncol, 2015. **5**: p. 87.
75. Weinberg, F., et al., *Mitochondrial metabolism and ROS generation are essential for Kras-mediated tumorigenicity.* Proc Natl Acad Sci U S A, 2010. **107**(19): p. 8788-93.
76. Gupta, S., A. Roy, and B.S. Dwarakanath, *Metabolic Cooperation and Competition in the Tumor Microenvironment: Implications for Therapy.* Front Oncol, 2017. **7**: p. 68.
77. Carmeliet, P. and R.K. Jain, *Angiogenesis in cancer and other diseases.* Nature, 2000. **407**(6801): p. 249-57.
78. Papetti, M. and I.M. Herman, *Mechanisms of normal and tumor-derived angiogenesis.* Am J Physiol Cell Physiol, 2002. **282**(5): p. C947-70.
79. Huang, M., et al., *New insights into antiangiogenic therapy resistance in cancer: Mechanisms and therapeutic aspects.* Drug Resist Updat, 2022. **64**: p. 100849.
80. Park, S.A., et al., *Structure and function of vascular endothelial growth factor and its receptor system.* BMB Rep, 2018. **51**(2): p. 73-78.
81. Claesson-Welsh, L. and M. Welsh, *VEGFA and tumour angiogenesis.* J Intern Med, 2013. **273**(2): p. 114-27.
82. Abhinand, C.S., et al., *VEGF-A/VEGFR2 signaling network in endothelial cells relevant to angiogenesis.* J Cell Commun Signal, 2016. **10**(4): p. 347-354.
83. Siveen, K.S., et al., *Vascular Endothelial Growth Factor (VEGF) Signaling in Tumour Vascularization: Potential and Challenges.* Curr Vasc Pharmacol, 2017. **15**(4): p. 339-351.
84. Melegh, Z. and S. Oltean, *Targeting Angiogenesis in Prostate Cancer.* Int J Mol Sci, 2019. **20**(11).
85. Drogat, B., et al., *Acute L-glutamine deprivation compromises VEGF-a upregulation in A549/8 human carcinoma cells.* J Cell Physiol, 2007. **212**(2): p. 463-72.
86. Cao, X., et al., *Glycogen synthase kinase GSK3α promotes tumorigenesis by activating HIF1/VEGFA signaling pathway in NSCLC tumor.* Cell Commun Signal, 2022. **20**(1): p. 32.
87. Xie, H., et al., *Endothelin-1 down-regulated vascular endothelial growth factor A is involved in trichloroethene-induced kidney injury.* Toxicol Ind Health, 2022. **38**(5): p. 287-298.
88. Huang, Q., et al., *[The poor prognosis is correlated with the high expression of vascular endothelial growth factor (VEGF) and low expression of thrombospondin 1 (TSP-1) in patients with breast cancer].* Xi Bao Yu Fen Zi Mian Yi Xue Za Zhi, 2019. **35**(9): p. 828-831.
89. Presta, M., et al., *Fibroblast growth factor/fibroblast growth factor receptor system in angiogenesis.* Cytokine Growth Factor Rev, 2005. **16**(2): p. 159-78.
90. Seghezzi, G., et al., *Fibroblast growth factor-2 (FGF-2) induces vascular endothelial growth factor (VEGF) expression in the endothelial cells of forming capillaries: an autocrine mechanism contributing to angiogenesis.* J Cell Biol, 1998. **141**(7): p. 1659-73.
91. Augustin, H.G., et al., *Control of vascular morphogenesis and homeostasis through the angiopoietin-Tie system.* Nat Rev Mol Cell Biol, 2009. **10**(3): p. 165-77.
92. Suri, C., et al., *Requisite role of angiopoietin-1, a ligand for the TIE2 receptor, during embryonic angiogenesis.* Cell, 1996. **87**(7): p. 1171-80.
93. Maisonpierre, P.C., et al., *Angiopoietin-2, a natural antagonist for Tie2 that disrupts in vivo angiogenesis.* Science, 1997. **277**(5322): p. 55-60.
94. Huang, H., et al., *Targeting the ANGPT-TIE2 pathway in malignancy.* Nat Rev Cancer, 2010. **10**(8): p. 575-85.
95. Krzyszczyk, P., et al., *The Role of Macrophages in Acute and Chronic Wound Healing and Interventions to Promote Pro-wound Healing Phenotypes.* Front Physiol, 2018. **9**: p. 419.

96. Wynn, T.A., A. Chawla, and J.W. Pollard, *Macrophage biology in development, homeostasis and disease.* Nature, 2013. **496**(7446): p. 445-55.
97. Orecchioni, M., et al., *Macrophage Polarization: Different Gene Signatures in M1(LPS+) vs. Classically and M2(LPS-) vs. Alternatively Activated Macrophages.* Front Immunol, 2019. **10**: p. 1084.
98. Martinez, F.O. and S. Gordon, *The M1 and M2 paradigm of macrophage activation: time for reassessment.* F1000Prime Rep, 2014. **6**: p. 13.
99. Kim, S.Y. and M.G. Nair, *Macrophages in wound healing: activation and plasticity.* Immunol Cell Biol, 2019. **97**(3): p. 258-267.
100. Wang, H., et al., *The Impact of the Tumor Microenvironment on Macrophage Polarization in Cancer Metastatic Progression.* Int J Mol Sci, 2021. **22**(12).
101. Wei, Y., et al., *The local immune landscape determines tumor PD-L1 heterogeneity and sensitivity to therapy.* J Clin Invest, 2019. **129**(8): p. 3347-3360.
102. Zhang, Y., et al., *High-infiltration of tumor-associated macrophages predicts unfavorable clinical outcome for node-negative breast cancer.* PLoS One, 2013. **8**(9): p. e76147.
103. Xue, Y., et al., *Tumor-infiltrating M2 macrophages driven by specific genomic alterations are associated with prognosis in bladder cancer.* Oncol Rep, 2019. **42**(2): p. 581-594.
104. Kumar, A.T., et al., *Prognostic Significance of Tumor-Associated Macrophage Content in Head and Neck Squamous Cell Carcinoma: A Meta-Analysis.* Front Oncol, 2019. **9**: p. 656.
105. Nishie, A., et al., *Macrophage infiltration and heme oxygenase-1 expression correlate with angiogenesis in human gliomas.* Clin Cancer Res, 1999. **5**(5): p. 1107-13.
106. Torisu, H., et al., *Macrophage infiltration correlates with tumor stage and angiogenesis in human malignant melanoma: possible involvement of TNFalpha and IL-1alpha.* Int J Cancer, 2000. **85**(2): p. 182-8.
107. Cao, J., et al., *Prognostic role of tumour-associated macrophages and macrophage scavenger receptor 1 in prostate cancer: a systematic review and meta-analysis.* Oncotarget, 2017. **8**(47): p. 83261-83269.
108. Oriuchi, N., S. Sugawara, and T. Shiga, *Positron Emission Tomography for Response Evaluation in Microenvironment-Targeted Anti-Cancer Therapy.* Biomedicines, 2020. **8**(9).
109. Brassart-Pasco, S., et al., *Tumor Microenvironment: Extracellular Matrix Alterations Influence Tumor Progression.* Front Oncol, 2020. **10**: p. 397.
110. Frantz, C., K.M. Stewart, and V.M. Weaver, *The extracellular matrix at a glance.* J Cell Sci, 2010. **123**(Pt 24): p. 4195-200.
111. Hynes, R.O., *The extracellular matrix: not just pretty fibrils.* Science, 2009. **326**(5957): p. 1216-9.
112. Henke, E., R. Nandigama, and S. Ergün, *Extracellular Matrix in the Tumor Microenvironment and Its Impact on Cancer Therapy.* Front Mol Biosci, 2019. **6**: p. 160.
113. McCarthy, J.B., D. El-Ashry, and E.A. Turley, *Hyaluronan, Cancer-Associated Fibroblasts and the Tumor Microenvironment in Malignant Progression.* Front Cell Dev Biol, 2018. **6**: p. 48.
114. Naito, Y., et al., *How cancer cells dictate their microenvironment: present roles of extracellular vesicles.* Cell Mol Life Sci, 2017. **74**(4): p. 697-713.
115. Peinado, H., et al., *Melanoma exosomes educate bone marrow progenitor cells toward a pro-metastatic phenotype through MET.* Nat Med, 2012. **18**(6): p. 883-91.
116. Kosaka, N., et al., *Neutral sphingomyelinase 2 (nSMase2)-dependent exosomal transfer of angiogenic microRNAs regulate cancer cell metastasis.* J Biol Chem, 2013. **288**(15): p. 10849-59.
117. Yokoi, A., et al., *Malignant extracellular vesicles carrying MMP1 mRNA facilitate peritoneal dissemination in ovarian cancer.* Nat Commun, 2017. **8**: p. 14470.
118. Tominaga, N., et al., *Brain metastatic cancer cells release microRNA-181c-containing extracellular vesicles capable of destructing blood-brain barrier.* Nat Commun, 2015. **6**: p. 6716.
119. Wei, F., et al., *Exosomes derived from gemcitabine-resistant cells transfer malignant phenotypic traits via delivery of miRNA-222-3p.* Mol Cancer, 2017. **16**(1): p. 132.
120. Naito, Y., et al., *Cancer extracellular vesicles contribute to stromal heterogeneity by inducing chemokines in cancer-associated fibroblasts.* Oncogene, 2019. **38**(28): p. 5566-5579.

121. Cocucci, E. and J. Meldolesi, *Ectosomes and exosomes: shedding the confusion between extracellular vesicles.* Trends Cell Biol, 2015. **25**(6): p. 364-72.
122. Cocucci, E., G. Racchetti, and J. Meldolesi, *Shedding microvesicles: artefacts no more.* Trends Cell Biol, 2009. **19**(2): p. 43-51.
123. Stridsberg, M., et al., *Prostasomes are neuroendocrine-like vesicles in human semen.* Prostate, 1996. **29**(5): p. 287-95.
124. Yáñez-Mó, M., et al., *Biological properties of extracellular vesicles and their physiological functions.* J Extracell Vesicles, 2015. **4**: p. 27066.
125. Yoshioka, Y., et al., *Comparative marker analysis of extracellular vesicles in different human cancer types.* J Extracell Vesicles, 2013. **2**.
126. Escola, J.M., et al., *Selective enrichment of tetraspan proteins on the internal vesicles of multivesicular endosomes and on exosomes secreted by human B-lymphocytes.* J Biol Chem, 1998. **273**(32): p. 20121-7.
127. Agrahari, V., et al., *Extracellular Microvesicles as New Industrial Therapeutic Frontiers.* Trends Biotechnol, 2019. **37**(7): p. 707-729.
128. Bettegowda, C., et al., *Detection of circulating tumor DNA in early- and late-stage human malignancies.* Sci Transl Med, 2014. **6**(224): p. 224ra24.
129. Minciacchi, V.R., M.R. Freeman, and D. Di Vizio, *Extracellular vesicles in cancer: exosomes, microvesicles and the emerging role of large oncosomes.* Semin Cell Dev Biol, 2015. **40**: p. 41-51.
130. Akers, J.C., et al., *Biogenesis of extracellular vesicles (EV): exosomes, microvesicles, retrovirus-like vesicles, and apoptotic bodies.* J Neurooncol, 2013. **113**(1): p. 1-11.
131. Kerr, J.F., A.H. Wyllie, and A.R. Currie, *Apoptosis: a basic biological phenomenon with wide-ranging implications in tissue kinetics.* Br J Cancer, 1972. **26**(4): p. 239-57.
132. Crescitelli, R., et al., *Distinct RNA profiles in subpopulations of extracellular vesicles: apoptotic bodies, microvesicles and exosomes.* J Extracell Vesicles, 2013. **2**.
133. Turiák, L., et al., *Proteomic characterization of thymocyte-derived microvesicles and apoptotic bodies in BALB/c mice.* J Proteomics, 2011. **74**(10): p. 2025-33.
134. Wu, D., et al., *Apoptotic release of histones from nucleosomes.* J Biol Chem, 2002. **277**(14): p. 12001-8.
135. Utleg, A.G., et al., *Proteomic analysis of human prostasomes.* Prostate, 2003. **56**(2): p. 150-61.
136. Urabe, F., et al., *Extracellular vesicles as biomarkers and therapeutic targets for cancer.* Am J Physiol Cell Physiol, 2020. **318**(1): p. C29-C39.
137. Guo, Q. and C. Jiang, *Delivery strategies for macromolecular drugs in cancer therapy.* Acta Pharm Sin B, 2020. **10**(6): p. 979-986.
138. Liu, J., et al., *The biology, function, and applications of exosomes in cancer.* Acta Pharm Sin B, 2021. **11**(9): p. 2783-2797.
139. Krock, B.L., N. Skuli, and M.C. Simon, *Hypoxia-induced angiogenesis: good and evil.* Genes Cancer, 2011. **2**(12): p. 1117-33.
140. Pollard, P.J., et al., *Accumulation of Krebs cycle intermediates and over-expression of HIF1alpha in tumours which result from germline FH and SDH mutations.* Hum Mol Genet, 2005. **14**(15): p. 2231-9.
141. Richter, S., et al., *Krebs cycle metabolite profiling for identification and stratification of pheochromocytomas/paragangliomas due to succinate dehydrogenase deficiency.* J Clin Endocrinol Metab, 2014. **99**(10): p. 3903-11.
142. Xiao, M., et al., *Inhibition of α-KG-dependent histone and DNA demethylases by fumarate and succinate that are accumulated in mutations of FH and SDH tumor suppressors.* Genes Dev, 2012. **26**(12): p. 1326-38.
143. Cervera, A.M., et al., *Inhibition of succinate dehydrogenase dysregulates histone modification in mammalian cells.* Mol Cancer, 2009. **8**: p. 89.
144. Hoekstra, A.S., et al., *Inactivation of SDH and FH cause loss of 5hmC and increased H3K9me3 in paraganglioma/pheochromocytoma and smooth muscle tumors.* Oncotarget, 2015. **6**(36): p. 38777-88.

145. Killian, J.K., et al., *Succinate dehydrogenase mutation underlies global epigenomic divergence in gastrointestinal stromal tumor.* Cancer Discov, 2013. **3**(6): p. 648-57.
146. He, W., et al., *Citric acid cycle intermediates as ligands for orphan G-protein-coupled receptors.* Nature, 2004. **429**(6988): p. 188-93.
147. Rubic, T., et al., *Triggering the succinate receptor GPR91 on dendritic cells enhances immunity.* Nat Immunol, 2008. **9**(11): p. 1261-9.
148. Aguiar, C.J., et al., *Succinate modulates Ca(2+) transient and cardiomyocyte viability through PKA-dependent pathway.* Cell Calcium, 2010. **47**(1): p. 37-46.
149. Correa, P.R., et al., *Succinate is a paracrine signal for liver damage.* J Hepatol, 2007. **47**(2): p. 262-9.
150. Regard, J.B., I.T. Sato, and S.R. Coughlin, *Anatomical profiling of G protein-coupled receptor expression.* Cell, 2008. **135**(3): p. 561-71.
151. Ariza, A.C., P.M. Deen, and J.H. Robben, *The succinate receptor as a novel therapeutic target for oxidative and metabolic stress-related conditions.* Front Endocrinol (Lausanne), 2012. **3**: p. 22.
152. Ko, S.H., et al., *Succinate promotes stem cell migration through the GPR91-dependent regulation of DRP1-mediated mitochondrial fission.* Sci Rep, 2017. **7**(1): p. 12582.
153. Lu, Y.T., et al., *Succinate induces aberrant mitochondrial fission in cardiomyocytes through GPR91 signaling.* Cell Death Dis, 2018. **9**(6): p. 672.
154. Mu, X., et al., *Oncometabolite succinate promotes angiogenesis by upregulating VEGF expression through GPR91-mediated STAT3 and ERK activation.* Oncotarget, 2017. **8**(8): p. 13174-13185.
155. Park, S.Y., et al., *Succinate induces hepatic fibrogenesis by promoting activation, proliferation, and migration, and inhibiting apoptosis of hepatic stellate cells.* Biochem Biophys Res Commun, 2018. **496**(2): p. 673-678.
156. Cervera, A.M., et al., *Cells silenced for SDHB expression display characteristic features of the tumor phenotype.* Cancer Res, 2008. **68**(11): p. 4058-67.
157. Matlac, D.M., et al., *Succinate Mediates Tumorigenic Effects.* Front Endocrinol (Lausanne), 2021. **12**: p. 589451.
158. Wu, J.Y., et al., *Cancer-Derived Succinate Promotes Macrophage Polarization and Cancer Metastasis via Succinate Receptor.* Mol Cell, 2020. **77**(2): p. 213-227.e5.
159. Littlewood-Evans, A., et al., *GPR91 senses extracellular succinate released from inflammatory macrophages and exacerbates rheumatoid arthritis.* J Exp Med, 2016. **213**(9): p. 1655-62.
160. Mills, E. and L.A. O'Neill, *Succinate: a metabolic signal in inflammation.* Trends Cell Biol, 2014. **24**(5): p. 313-20.
161. Prinz, W.A., *Bridging the gap: membrane contact sites in signaling, metabolism, and organelle dynamics.* J Cell Biol, 2014. **205**(6): p. 759-69.
162. Phillips, M.J. and G.K. Voeltz, *Structure and function of ER membrane contact sites with other organelles.* Nat Rev Mol Cell Biol, 2016. **17**(2): p. 69-82.
163. Fan, H. and Y. Tan, *Lipid Droplet-Mitochondria Contacts in Health and Disease.* Int J Mol Sci, 2024. **25**(13).
164. Wong, Y.C., D. Ysselstein, and D. Krainc, *Mitochondria-lysosome contacts regulate mitochondrial fission via RAB7 GTP hydrolysis.* Nature, 2018. **554**(7692): p. 382-386.
165. Shai, N., et al., *Systematic mapping of contact sites reveals tethers and a function for the peroxisome-mitochondria contact.* Nat Commun, 2018. **9**(1): p. 1761.
166. Desai, R., et al., *Mitochondria form contact sites with the nucleus to couple prosurvival retrograde response.* Sci Adv, 2020. **6**(51).
167. Gatliff, J., et al., *A role for TSPO in mitochondrial Ca.* Cell Death Dis, 2017. **8**(6): p. e2896.
168. Frison, M., et al., *The translocator protein (TSPO) is prodromal to mitophagy loss in neurotoxicity.* Mol Psychiatry, 2021. **26**(7): p. 2721-2739.
169. Tu, L.N., et al., *Translocator Protein (TSPO) Affects Mitochondrial Fatty Acid Oxidation in Steroidogenic Cells.* Endocrinology, 2016. **157**(3): p. 1110-21.
170. Fairbrother-Browne, A., et al., *Mitochondrial-nuclear cross-talk in the human brain is modulated by cell type and perturbed in neurodegenerative disease.* Commun Biol, 2021. **4**(1): p. 1262.

171. Peruzzo, R., et al., *Mitochondrial Metabolism, Contact Sites and Cellular Calcium Signaling: Implications for Tumorigenesis.* Cancers (Basel), 2020. **12**(9).
172. Bustos, G., et al., *The ER-mitochondria Ca.* Int Rev Cell Mol Biol, 2021. **363**: p. 49-121.
173. Ray, B., et al., *Mitochondrial and Organellar Crosstalk in Parkinson's Disease.* ASN Neuro, 2021. **13**: p. 17590914211028364.
174. Greene, L.A. and A.S. Tischler, *Establishment of a noradrenergic clonal line of rat adrenal pheochromocytoma cells which respond to nerve growth factor.* Proc Natl Acad Sci U S A, 1976. **73**(7): p. 2424-8.
175. Tischler, A.S., et al., *Glucocorticoids increase catecholamine synthesis and storage in PC12 pheochromocytoma cell cultures.* J Neurochem, 1983. **40**(2): p. 364-70.
176. Tischler, A.S. and L.A. Greene, *Nerve growth factor-induced process formation by cultured rat pheochromocytoma cells.* Nature, 1975. **258**(5533): p. 341-2.
177. Greene, L.A. and G. Rein, *Release, storage and uptake of catecholamines by a clonal cell line of nerve growth factor (NGF) responsive pheo-chromocytoma cells.* Brain Res, 1977. **129**(2): p. 247-63.
178. Hopewell, R. and E.B. Ziff, *The nerve growth factor-responsive PC12 cell line does not express the Myc dimerization partner Max.* Mol Cell Biol, 1995. **15**(7): p. 3470-8.
179. Jacks, T., et al., *Tumour predisposition in mice heterozygous for a targeted mutation in Nf1.* Nat Genet, 1994. **7**(3): p. 353-61.
180. Tischler, A.S., et al., *Characterization of Pheochromocytomas in a Mouse Strain with a Targeted Disruptive Mutation of the Neurofibromatosis Gene Nf1.* Endocr Pathol, 1995. **6**(4): p. 323-335.
181. Tischler, A.S., J.F. Powers, and J. Alroy, *Animal models of pheochromocytoma.* Histol Histopathol, 2004. **19**(3): p. 883-95.
182. Martiniova, L., et al., *Characterization of an animal model of aggressive metastatic pheochromocytoma linked to a specific gene signature.* Clin Exp Metastasis, 2009. **26**(3): p. 239-50.
183. Gimenez-Roqueplo, A.P., et al., *Mutations in the SDHB gene are associated with extra-adrenal and/or malignant phaeochromocytomas.* Cancer Res, 2003. **63**(17): p. 5615-21.
184. Amar, L., et al., *Succinate dehydrogenase B gene mutations predict survival in patients with malignant pheochromocytomas or paragangliomas.* J Clin Endocrinol Metab, 2007. **92**(10): p. 3822-8.
185. Richter, S., et al., *Primary fibroblast co-culture stimulates growth and metabolism in Sdhb-impaired mouse pheochromocytoma MTT cells.* Cell Tissue Res, 2018. **374**(3): p. 473-485.
186. Morin, A., et al., *TET-Mediated Hypermethylation Primes SDH-Deficient Cells for HIF2α-Driven Mesenchymal Transition.* Cell Rep, 2020. **30**(13): p. 4551-4566.e7.
187. Powers, J.F., et al., *A xenograft and cell line model of SDH-deficient pheochromocytoma derived from Sdhb+/- rats.* Endocr Relat Cancer, 2020. **27**(6): p. 337-354.
188. Ghayee, H.K., et al., *Progenitor cell line (hPheo1) derived from a human pheochromocytoma tumor.* PLoS One, 2013. **8**(6): p. e65624.
189. Rai, S.K., et al., *Targeting pheochromocytoma/paraganglioma with polyamine inhibitors.* Metabolism, 2020. **110**: p. 154297.
190. Rapizzi, E., et al., *Succinate dehydrogenase subunit B mutations modify human neuroblastoma cell metabolism and proliferation.* Horm Cancer, 2014. **5**(3): p. 174-84.
191. Rapizzi, E., et al., *Role of microenvironment on neuroblastoma SK-N-AS SDHB-silenced cell metabolism and function.* Endocr Relat Cancer, 2015. **22**(3): p. 409-17.
192. Martinelli, S., et al., *SDHB and SDHD silenced pheochromocytoma spheroids respond differently to tumour microenvironment and their aggressiveness is inhibited by impairing stroma metabolism.* Mol Cell Endocrinol, 2022. **547**: p. 111594.
193. Livak, K.J. and T.D. Schmittgen, *Analysis of relative gene expression data using real-time quantitative PCR and the 2(-Delta Delta C(T)) Method.* Methods, 2001. **25**(4): p. 402-8.
194. Rossitti, H.M., et al., *Activation of RAS Signalling is Associated with Altered Cell Adhesion in Phaeochromocytoma.* Int J Mol Sci, 2020. **21**(21).
195. Luciani, P., et al., *Exendin-4 induces cell adhesion and differentiation and counteracts the invasive potential of human neuroblastoma cells.* PLoS One, 2013. **8**(8): p. e71716.

196. Di Franco, A., et al., *Searching for Classical Brown Fat in Humans: Development of a Novel Human Fetal Brown Stem Cell Model.* Stem Cells, 2016. **34**(6): p. 1679-91.
197. Squecco, R., et al., *Platelet-Rich Plasma Modulates Gap Junction Functionality and Connexin 43 and 26 Expression During TGF-β1-Induced Fibroblast to Myofibroblast Transition: Clues for Counteracting Fibrosis.* Cells, 2020. **9**(5).
198. D'Antongiovanni, V., et al., *The microenvironment induces collective migration in.* Endocr Relat Cancer, 2017. **24**(10): p. 555-564.
199. Tabebi, M., et al., *Loss of SDHB Induces a Metabolic Switch in the hPheo1 Cell Line toward Enhanced OXPHOS.* Int J Mol Sci, 2022. **23**(1).
200. Rhie, D.J., et al., *Somatostatin potentiates voltage-dependent K+ and Ca2+ channel expression induced by nerve growth factor in PC12 cells.* Brain Res Dev Brain Res, 1999. **112**(2): p. 267-74.
201. Shi, X., et al., *Role of ATP-sensitive potassium channels and inflammatory response of basilar artery smooth muscle cells in subarachnoid hemorrhage of rabbit and immune-modulation by shikonin.* Food Chem Toxicol, 2019. **134**: p. 110804.
202. Proks, P., H. de Wet, and F.M. Ashcroft, *Activation of the K(ATP) channel by Mg-nucleotide interaction with SUR1.* J Gen Physiol, 2010. **136**(4): p. 389-405.
203. Morata-Tarifa, C., et al., *Low adherent cancer cell subpopulations are enriched in tumorigenic and metastatic epithelial-to-mesenchymal transition-induced cancer stem-like cells.* Sci Rep, 2016. **6**: p. 18772.
204. Amore, F., et al., *The aggressiveness of succinate dehydrogenase subunit B-deficient chromaffin cells is reduced when their bioelectrical properties are restored by glibenclamide.* Endocr Relat Cancer, 2023. **30**(10).
205. Zhang, Z., et al., *Identification of lysine succinylation as a new post-translational modification.* Nat Chem Biol, 2011. **7**(1): p. 58-63.
206. Sundelacruz, S., M. Levin, and D.L. Kaplan, *Role of membrane potential in the regulation of cell proliferation and differentiation.* Stem Cell Rev Rep, 2009. **5**(3): p. 231-46.
207. Yang, M. and W.J. Brackenbury, *Membrane potential and cancer progression.* Front Physiol, 2013. **4**: p. 185.
208. Prakash, S.B. and P. Abshire, *Tracking cancer cell proliferation on a CMOS capacitance sensor chip.* Biosens Bioelectron, 2008. **23**(10): p. 1449-57.
209. Nichols, C.G., *KATP channels as molecular sensors of cellular metabolism.* Nature, 2006. **440**(7083): p. 470-6.
210. Ostroumov, A., M. Simonetti, and A. Nistri, *Cystic fibrosis transmembrane conductance regulator modulates synaptic chloride homeostasis in motoneurons of the rat spinal cord during neonatal development.* Dev Neurobiol, 2011. **71**(3): p. 253-68.
211. Busija, D.W., et al., *Targeting mitochondrial ATP-sensitive potassium channels--a novel approach to neuroprotection.* Brain Res Brain Res Rev, 2004. **46**(3): p. 282-94.
212. Zhao, S., M. Wang, and Z. Ma, *Therapeutic potential of ATP-sensitive potassium channels in Parkinson's disease.* Brain Res Bull, 2021. **169**: p. 1-7.
213. Country, M.W. and M.G. Jonz, *Mitochondrial KATP channels stabilize intracellular Ca2+ during hypoxia in retinal horizontal cells of goldfish (Carassius auratus).* J Exp Biol, 2021. **224**(18).
214. Maqoud, F., et al., *ATP-sensitive Potassium Channel Subunits in Neuroinflammation: Novel Drug Targets in Neurodegenerative Disorders.* CNS Neurol Disord Drug Targets, 2022. **21**(2): p. 130-149.
215. Warburg, O., F. Wind, and E. Negelein, *THE METABOLISM OF TUMORS IN THE BODY.* J Gen Physiol, 1927. **8**(6): p. 519-30.
216. Bezawork-Geleta, A., et al., *The Assembly Factor SDHAF2 Is Dispensable for Flavination of the Catalytic Subunit of Mitochondrial Complex II in Breast Cancer Cells.* J Biol Chem, 2016. **291**(41): p. 21414-21420.
217. Douwes Dekker, P.B., et al., *SDHD mutations in head and neck paragangliomas result in destabilization of complex II in the mitochondrial respiratory chain with loss of enzymatic activity and abnormal mitochondrial morphology.* J Pathol, 2003. **201**(3): p. 480-6.

218. Loriot, C., et al., *Epithelial to mesenchymal transition is activated in metastatic pheochromocytomas and paragangliomas caused by SDHB gene mutations.* J Clin Endocrinol Metab, 2012. **97**(6): p. E954-62.
219. Loriot, C., et al., *Deciphering the molecular basis of invasiveness in Sdhb-deficient cells.* Oncotarget, 2015. **6**(32): p. 32955-65.
220. Zhu, Y.T., et al., *A modified method by differential adhesion and serum-free culture medium for enrichment of cancer stem cells.* J Cancer Res Ther, 2018. **14**(Supplement): p. S421-S426.
221. Walia, V. and R.C. Elble, *Enrichment for breast cancer cells with stem/progenitor properties by differential adhesion.* Stem Cells Dev, 2010. **19**(8): p. 1175-82.
222. Pastushenko, I. and C. Blanpain, *EMT Transition States during Tumor Progression and Metastasis.* Trends Cell Biol, 2019. **29**(3): p. 212-226.
223. Payne, S.L., et al., *Potassium channel-driven bioelectric signalling regulates metastasis in triple-negative breast cancer.* EBioMedicine, 2022. **75**: p. 103767.
224. Gao, R., T. Yang, and W. Xu, *Enemies or weapons in hands: investigational anti-diabetic drug glibenclamide and cancer risk.* Expert Opin Investig Drugs, 2017. **26**(7): p. 853-864.
225. Wondergem, R., et al., *Membrane potassium channels and human bladder tumor cells: II. Growth properties.* J Membr Biol, 1998. **161**(3): p. 257-62.
226. Abdul, M. and N. Hoosein, *Expression and activity of potassium ion channels in human prostate cancer.* Cancer Lett, 2002. **186**(1): p. 99-105.
227. Malhi, H., et al., *KATP channels regulate mitogenically induced proliferation in primary rat hepatocytes and human liver cell lines. Implications for liver growth control and potential therapeutic targeting.* J Biol Chem, 2000. **275**(34): p. 26050-7.
228. Yasukagawa, T., et al., *Suppression of cellular invasion by glybenclamide through inhibited secretion of platelet-derived growth factor in ovarian clear cell carcinoma ES-2 cells.* FEBS Lett, 2012. **586**(10): p. 1504-9.
229. Eijkelenkamp, K., et al., *Clinical implications of the oncometabolite succinate in SDHx-mutation carriers.* Clin Genet, 2020. **97**(1): p. 39-53.
230. Gilissen, J., et al., *Insight into SUCNR1 (GPR91) structure and function.* Pharmacol Ther, 2016. **159**: p. 56-65.
231. Aggarwal, R.K., et al., *Functional succinate dehydrogenase deficiency is a common adverse feature of clear cell renal cancer.* Proc Natl Acad Sci U S A, 2021. **118**(39).
232. Prieto, J., et al., *Early ERK1/2 activation promotes DRP1-dependent mitochondrial fission necessary for cell reprogramming.* Nat Commun, 2016. **7**: p. 11124.
233. Huang, C.Y., et al., *Inhibition of ERK-Drp1 signaling and mitochondria fragmentation alleviates IGF-IIR-induced mitochondria dysfunction during heart failure.* J Mol Cell Cardiol, 2018. **122**: p. 58-68.
234. Zhao, J., et al., *Mitochondrial dynamics regulates migration and invasion of breast cancer cells.* Oncogene, 2013. **32**(40): p. 4814-24.
235. Ferreira-da-Silva, A., et al., *Mitochondrial dynamics protein Drp1 is overexpressed in oncocytic thyroid tumors and regulates cancer cell migration.* PLoS One, 2015. **10**(3): p. e0122308.
236. Sun, X., et al., *Mitochondrial fission promotes cell migration by Ca.* Liver Int, 2018. **38**(7): p. 1263-1272.
237. Kashatus, J.A., et al., *Erk2 phosphorylation of Drp1 promotes mitochondrial fission and MAPK-driven tumor growth.* Mol Cell, 2015. **57**(3): p. 537-51.
238. Dunn, K.L., et al., *The Ras-MAPK signal transduction pathway, cancer and chromatin remodeling.* Biochem Cell Biol, 2005. **83**(1): p. 1-14.
239. Yoon, S. and R. Seger, *The extracellular signal-regulated kinase: multiple substrates regulate diverse cellular functions.* Growth Factors, 2006. **24**(1): p. 21-44.
240. Quirós, P.M., A. Mottis, and J. Auwerx, *Mitonuclear communication in homeostasis and stress.* Nat Rev Mol Cell Biol, 2016. **17**(4): p. 213-26.
241. Butow, R.A. and N.G. Avadhani, *Mitochondrial signaling: the retrograde response.* Mol Cell, 2004. **14**(1): p. 1-15.

242. Csordás, G., D. Weaver, and G. Hajnóczky, *Endoplasmic Reticulum-Mitochondrial Contactology: Structure and Signaling Functions.* Trends Cell Biol, 2018. **28**(7): p. 523-540.
243. Goncalves, J., et al., *Loss of SDHB Promotes Dysregulated Iron Homeostasis, Oxidative Stress, and Sensitivity to Ascorbate.* Cancer Res, 2021. **81**(13): p. 3480-3494.
244. Formentini, L., et al., *The mitochondrial ATPase inhibitory factor 1 triggers a ROS-mediated retrograde prosurvival and proliferative response.* Mol Cell, 2012. **45**(6): p. 731-42.
245. Wu, L.P., et al., *TSPO ligands prevent the proliferation of vascular smooth muscle cells and attenuate neointima formation through AMPK activation.* Acta Pharmacol Sin, 2020. **41**(1): p. 34-46.
246. Zhang, D., et al., *Mitochondrial TSPO Promotes Hepatocellular Carcinoma Progression through Ferroptosis Inhibition and Immune Evasion.* Adv Sci (Weinh), 2023. **10**(15): p. e2206669.
247. Rechichi, M., et al., *TSPO over-expression increases motility, transmigration and proliferation properties of C6 rat glioma cells.* Biochim Biophys Acta, 2008. **1782**(2): p. 118-25.
248. Malkin, E.Z. and S.V. Bratman, *Bioactive DNA from extracellular vesicles and particles.* Cell Death Dis, 2020. **11**(7): p. 584.
249. Gibson, M.C. and N. Perrimon, *Apicobasal polarization: epithelial form and function.* Curr Opin Cell Biol, 2003. **15**(6): p. 747-52.
250. Marchiando, A.M., W.V. Graham, and J.R. Turner, *Epithelial barriers in homeostasis and disease.* Annu Rev Pathol, 2010. **5**: p. 119-44.
251. Kakogiannos, N., et al., *JAM-A Acts via C/EBP-α to Promote Claudin-5 Expression and Enhance Endothelial Barrier Function.* Circ Res, 2020. **127**(8): p. 1056-1073.
252. Eshaq, R.S. and N.R. Harris, *Hyperglycemia-induced ubiquitination and degradation of β-catenin with the loss of platelet endothelial cell adhesion molecule-1 in retinal endothelial cells.* Microcirculation, 2020. **27**(2): p. e12596.
253. Wang, M., et al., *Gastric cancer cell-derived extracellular vesicles disrupt endothelial integrity and promote metastasis.* Cancer Lett, 2022. **545**: p. 215827.
254. Timmers, H.J., et al., *Clinical presentations, biochemical phenotypes, and genotype-phenotype correlations in patients with succinate dehydrogenase subunit B-associated pheochromocytomas and paragangliomas.* J Clin Endocrinol Metab, 2007. **92**(3): p. 779-86.
255. Weiswald, L.B., D. Bellet, and V. Dangles-Marie, *Spherical cancer models in tumor biology.* Neoplasia, 2015. **17**(1): p. 1-15.
256. Chatoff, A., et al., *Metabolic Effects of Succinate Dehydrogenase Loss in Cancer.* J Cell Physiol, 2025. **240**(7): p. e70066.
257. Al Khazal, F.J., et al., *Similar deficiencies, different outcomes: succinate dehydrogenase loss in adrenal medulla vs. fibroblast cell culture models of paraganglioma.* Cancer Metab, 2024. **12**(1): p. 39.
258. Kuo, C.C., J.Y. Wu, and K.K. Wu, *Cancer-derived extracellular succinate: a driver of cancer metastasis.* J Biomed Sci, 2022. **29**(1): p. 93.
259. Xia, B., et al., *The metabolic crosstalk of cancer-associated fibroblasts and tumor cells: Recent advances and future perspectives.* Biochim Biophys Acta Rev Cancer, 2024. **1879**(6): p. 189190.
260. Peiffer, R., et al., *Cancer-Associated Fibroblast Diversity Shapes Tumor Metabolism in Pancreatic Cancer.* Cancers (Basel), 2022. **15**(1).
261. Levental, K.R., et al., *Matrix crosslinking forces tumor progression by enhancing integrin signaling.* Cell, 2009. **139**(5): p. 891-906.
262. Midwood, K.S. and G. Orend, *The role of tenascin-C in tissue injury and tumorigenesis.* J Cell Commun Signal, 2009. **3**(3-4): p. 287-310.
263. Oskarsson, T., *Extracellular matrix components in breast cancer progression and metastasis.* Breast, 2013. **22 Suppl 2**: p. S66-72.
264. Lin, Y., et al., *Vitronectin promotes proliferation and metastasis of cervical cancer cells via the epithelial-mesenchymal transition.* Front Oncol, 2024. **14**: p. 1466264.
265. Argraves, W.S., et al., *Fibulins: physiological and disease perspectives.* EMBO Rep, 2003. **4**(12): p. 1127-31.

266. Zhang, H., et al., *Immunotherapeutic Targeting of NG2/CSPG4 in Solid Organ Cancers.* Vaccines (Basel), 2022. **10**(7).
267. Hanahan, D. and L.M. Coussens, *Accessories to the crime: functions of cells recruited to the tumor microenvironment.* Cancer Cell, 2012. **21**(3): p. 309-22.
268. Kalluri, R., *The biology and function of fibroblasts in cancer.* Nat Rev Cancer, 2016. **16**(9): p. 582-98.